Functional defects and molecular mechanisms of Left Ventricular NonCompaction (LVNC) in Nkx2.5 mutant mice

Thi Hong Minh Nguyen

AIX-MARSEILLE UNIVERSITY

FACULTY OF SCIENCES

DOCTORAL SCHOOL OF LIFE SCIENCES AND HEALTH

TAGC-UMR 1090

IBDM-UMR 7288

DOCTORAL THESIS

GENOMICS AND BIOINFORMATICS

Functional defects and molecular mechanisms of Left Ventricular NonCompaction (LVNC) in *Nkx2.5* mutant mice

by

Minh T.H. NGUYEN

Defended on 19/09/2016 in front of jury members:

Pr. Régis COSTELLO	President
Dr. Stéphanie BARRERE-LEMAIRE	Reporter
Dr. Flavien CHARPENTIER	Reporter
Dr. Joël NARGEOT	Examiner
Dr. Nathalie LALEVEE	Supervisor
Dr. Lucile MIQUEROL	Co-supervisor

AIX-MARSEILLE UNIVERSITÉ

FACULTÉ DES SCIENCES

ECOLE DOCTORALE DES SCIENCES DE LA VIE ET DE LA SANTE

TAGC-UMR 1090

IBDM-URM 7288

THÈSE DE DOCTORAT

GÉNOMIQUE ET BIOINFORMATIQUE

Défauts fonctionnels et mécanismes moléculaires associés à la Non Compaction du Ventricule Gauche (LVNC) chez des souris mutantes pour *Nkx2.5*

Par

Minh T.H. Nguyen

Soutenue le 19/09/2016 devant le jury :

Pr. Régis COSTELLO	Président
Dr. Stéphanie BARRERE-LEMAIRE	Rapportrice
Dr. Flavien CHARPENTIER	Rapporteur
Dr. Joël NARGEOT	Examinateur
Dr. Nathalie LALEVEE	Directrice de thèse
Dr. Lucile MIQUEROL	Co-directrice de thèse

SUMMARY

The heart is the first organ that forms and functions in the developing vertebrate embryo. It functions as a pump leading to blood circulation throughout the whole body. The cardiac conduction system is a group of specialized cardiomyocytes that initiate and propagate electrical impulses in order to coordinate heart contractions. The transcription factor *Nkx2.5* is present early in the embryonic heart (at around E7.5) and is still expressed throughout the developing and adult heart. It also plays a role in maintaining the normal function of the cardiac conduction system. Conditional deletions of *Nkx2.5* gene cause disturbance in heart development and cardiomyopathy in the mouse. Furthermore *Nkx2.5* mutations have been found in patients with left ventricular non-compaction (LVNC).

LVNC is a rare cardiomyopathy, characterized by hypertrabeculation and deep trabecular recesses in the left ventricle. This genetic disorder, associated with several mutations, exhibits clinical, morphological and functional heterogeneity. The main complications are heart failure, systemic embolic events and malignant arrhythmias. It is still unclear whether LVNC results from a defect occurring during cardiac development. One hypothesis to consider is that the severity of LVNC depends on which embryonic stage the arrest of myocardial compaction occurs.

Our aim was to study the pathological evolution of LVNC by characterizing functional defects and identifying molecular mechanisms in mouse models with abnormal ventricular trabeculae development.

To establish a LVNC mouse model, we generated specific *Nkx2.5* conditional knockout by applying the Flox/loxP system inducible by tamoxifen injection to activate Cre recombination. This leads to the deletion of *Nkx2.5* allele in atria and trabecular derived cardiomyocytes at embryonic stages when trabeculae arise (at around E10), or start to compact (at around E14), or at neonatal stages (after birth) when the heart is almost finish compaction step.

To quantify the degree of non–compaction and the subendocardial and interstitial fibrosis, we carried out immunofluorescence analyses on left ventricular sections. Functional

analyses show defects in ECG recordings with increased PR and QRS durations. This phenotype worsens with age with bundle branch blocks and a diminution in the ejection fraction at 6 months following deletion at E10.5/11.5 but not E13.5/14.5, consistent with a more pronounced phenotype after deletion at the earlier developmental stage.

Microarray comparison of the transcriptomes of 6 month-old mice with different LVNC levels induced by *Nkx2.5* deletion at the two timepoints, revealed differences in ventricular gene expression between the two groups, predominantly in pathways involved in calcium signaling, blood vessel development and immune or inflammatory processes. Deregulated expression of numerous genes playing a crucial role in cardiac cell activity or cardiomyocyte differentiation correlates with the different phenotypes observed in these mutant mice.

To sum up, we were successful in generating several LVNC mouse models by the conditional deletion of *Nkx2.5* transcription factor in atria and trabecular derived cardiomyocytes. These mouse models are suitable for studying LVNC pathology. We also confirmed the hypothesis that the severity of LVNC depends on stages when disturbances in the trabecular development occur. Hypertrabeculation, cardiac conduction defects, decreased ejection fraction, and existence of fibrosis are robustly observed following deletion at E10.5/11.5 meaning that the deletion at early stage of trabecular development causes the most severe pathological phenotype of LVNC. There had been just a few publications showing inflammation in LVNC heart, which could be a very good finding for future researches.

RESUME

Le cœur est le premier organe à se former et à fonctionner lors du développement embryonnaire. Il s'agit d'une pompe qui permet au sang de circuler dans tout l'organisme. Le système de conduction cardiaque est constitué d'un groupe de cardiomyocytes spécialisés qui initie et propage les impulsions électriques afin de coordonner les contractions cardiaques. Le facteur de transcription *Nkx2.5* est présent dans le cœur dès E7.5 et reste exprimé durant tout le développement et dans le cœur adulte. Il joue également un rôle dans le maintien de la fonction du système de conduction cardiaque. Des délétions conditionnelles du gène *Nkx2.5* induisent des perturbations durant le développement du cœur et des cardiomyopathies chez la souris. De plus, des mutations de *Nkx2.5* ont été trouvées chez des patients atteints de LVNC (left ventricular non-compaction).

La LVNC est une cardiomyopathie rare, caractérisée par une hypertrabéculation et de profonds replis du ventricule gauche. Cette maladie génétique, associée à de nombreuses mutations, présente une hétérogénéité fonctionnelle, morphologique et clinique. Les principales complications sont la défaillance cardiaque, l'embolie systémique et des arythmies sévères. A ce jour, nous ne savons toujours pas si la LVNC résulte d'un défaut se produisant durant le développement cardiaque et si sa gravité dépend du stade embryonnaire auquel l'arrêt de la compaction se produit.

Notre objectif a été d'étudier l'évolution pathologique de la LVNC en caractérisant les défauts fonctionnels et en identifiant les mécanismes moléculaires dans des modèles de souris présentant un développement anormal des trabécules ventriculaires.

Pour établir un modèle de LVNC, nous avons généré des souris KO conditionnel pour *Nkx2.5* grâce au système Flox/loxP inductible par injection de tamoxifène qui active la recombinaison Cre. Nous avons ainsi supprimé l'allèle *Nkx2.5* dans l'oreillette et les cardiomyocytes dérivant des trabécules. Nous avons choisi de sipprimé *Nkx2.5* au stade embryonnaire E10 quand le trabécule s'accroît, au stade E14 quand il se compacte, ou juste après la naissance quand le cœur a terminé son processus de compaction.

Afin de quantifier le degré de non-compaction et la fibrose interstitielle et subendocardique, nous avons analysé des sections ventriculaires gauches par immunofluorescence. Au niveau fonctionnel, les ECG montrent une augmentation des intervalles PR et QRS qui conduisent avec l'âge à des blocs de branches, accompagnés à 6 mois d'une diminution de la fraction d'éjection observable uniquement après la délétion à E10.

En comparant les transcriptomes réalisés sur des souris âgées de 6 mois dans lesquelles la délétion de *Nkx2.5* a été réalisée à E10 et à E13, nous avons révélé des différences importantes de l'expression des gènes ventriculaires, particulièrement dans les voies impliquées dans la signalisation calcique, le développement des vaisseaux sanguins, et les processus immunitaires et inflammatoires. L'expression modifiée de gènes jouant un rôle crucial dans l'activité des cellules cardiaques ou la différenciation des cardiomyocytes est parfaitement corrélée avec les différents phénotypes observés dans ces souris mutantes.

En résumé, nous avons réussi à générer différents modèles de LVNC, dans lesquelles nous avons pu étudier cette pathologie, en supprimant le facteur de transcription *Nkx2.5* dans les oreillettes et les cardiomyocytes dérivés des trabécules. Nous avons également confirmé que la sévérité de la LVNC dépend du stade de développement du trabécule auquel le défaut se produit. Peu de publications décrivent à ce jour les mécanismes responsables de l'état inflammatoire observé dans la LVNC, nos résultats sont donc prometteurs pour de futures recherches dans cette voie.

ACKNOWLEDGEMENTS

Look back the time during the 3 years of my thesis, I would like to thank to those people who help me a lot to make my thesis possible and help me to improve my knowledge. They made me feel full of motivation and helped me resolve the difficulties during my thesis.

First of all, I deepest thank to my supervisors Dr. Nathalie LALEVEE at TAGC/INSERM U1090 and Dr. Lucile MIQUEROL at IBDM/CNRS who guided and taught me throughout all my thesis duration. They brought me to the light of science from twilight, and showed me the way to think logistic as a scientist. From deepest of my heart, I thank them for all their kind help and effort to put me into the right way to expand my vision for a better carrier in the near future. I myself can feel the progression year by year under their advices.

I would like to express my great thanks to Caroline CHOQUET who is Lucile's PhD student at IBDM/CNRS for all her kindness in helping me during my work here. We had a great time working together not only as a colleague but also as a good friend.

I sincerely thank to Magali TORRES, a research engineer at TAGC for useful guidance me in experiment since the beginning of my study here.

I acknowledge my gratitude to Professor Pascal RIHET and Dr. Aurelie BERGON at TAGC/INSERM U1090 for the support to make me a better understanding in Biostatistics and teaching me analyzing data.

I also thank to Yasmin LABIAD who is a PhD student, and Andreas ZANZONI who is a post-doc at TAGC for their help in analyzing microarray experiments.

I offer my sincere thanks to all members of my thesis jury. Thanks to Professor Régis COSTELLO for accepting to become president of the jury. Thanks to Dr. Stéphanie BARRERE-LEMAIRE and Dr. Flavien CHARPENTIER for becoming reporters of the thesis. Thanks to Dr. Joël NARGEOT for becoming an examiner in my thesis jury. I thank you all for correcting and evaluating my thesis.

I am also thankful to Dr. Catherine NGUYEN, director of TAGC/INSERM U1090 and all members in TAGC laboratory for the support to my thesis and make me unforgettable time in my studying here.

I thank to Robert KELLY, team leader and all team Kelly's members at IBDM/CNRS for the support to make my thesis possible.

I am grateful thanks to Vietnamese and French government, especially the Vietnam International Education Development (VIED) and University of Science and Technology of Hanoi (USTH) for offering me this fellowship and giving me a good chance to study in France. I also thank to Campus France who take care of my living as well as studying here.

I warmly thank my friends, both Vietnamese and foreigner for sharing memorable time together. They treat me well and cheer me up with unforgettable memory.

Finally, I honestly thank to my husband, my parents, and my relatives for their love and mentality support. They always encourage me and pray for the happiness in my life.

TABLE OF CONTENTS

PRINCIPAL ABBREVIATIONS

AV	Atrioventricular
Bmp10	Bone Morphogenetic Protein 10
CCS	Cardiac conduction system
Comp	Compaction
Cx40	Gap Junction Protein Alpha 5 (Gja5)
Cx43	Gap Junction Protein Alpha 1 (Gja1)
ECG	Electrocardiography
Hcn4	Hyperpolarization Activated Cyclic Nucleotide Gated Potassium Channel 4
LV	Left ventricle
LVNC	Left ventricular noncompaction
MRI	Magnetic resonance imaging
Myh7	Myosin, Heavy Chain 7, Cardiac Muscle, Beta
Nkx2.5	NK2 Homeobox 5
RV	Right ventricle
SA	Sinoatrial
Scn5a	Sodium Voltage-Gated Channel Alpha Subunit 5
Tbx5	T-Box 5
Tnnt2	Troponin T2, Cardiac Type
Trab	Trabeculation
VCS	Ventricular conduction system

LIST OF FIGURES

Introduction

Results

Results part 1

LIST OF TABLES

Introdution

Materials and methods

Results

Results part 1.

Results part 2.

PART I. INTRODUCTION

CHAPTER 1. HEART FUNCTION AND DEVELOPMENT

1.1. Embryonic heart development

The heart is the first organ to form and function in the developing vertebrate embryo. From primitive streak, cells migrate from the upper layer undergoing gastrulation process to form the three germ layers, including the ectoderm, the endoderm, and the mesoderm. Mesodermal layer contains the cells that are destined to form the heart (Moorman et al., 2003). The heart is composed of cells from the primary heart field, which gives rise to the left ventricle (LV) and a part of the left and right atria, and the second heart field, which contributes to the formation of the right ventricle (RV), and the left and right atria. At the beginning, the heart is just a single tube then passing several steps to form a four-chamber heart. The sequence of early heart morphogenesis events is common to all vertebrate species, including heart tube formation, rightward looping, heart tube elongation by addition of progenitor cells from adjacent pharyngeal mesoderm, followed by cardiac chamber, cushion, and valve morphogenesis (Miquerol and Kelly, 2013).

Initially, in mouse heart, cardiac crescent which is formed by mesodermal derivatives and cardiac precursor cells appears at Embryonic day (E) 7.5 (Miquerol and Kelly, 2013; Nandi and Mishra, 2015). Then cardiac crescent fuses to form a primary heart tube at E8.5, followed by the elongation of the tube by addition of second heart field cells and the looping heart at E9.5. Four-chamber heart starts to form at E10.5 and changes to fit as mature heart from E14.5 with numerous temporal events, including "ballooning" of chamber myocardium, the emergence of trabeculations, the generation of the compact myocardium, and the formation of the interventricular septum (Nandi and Mishra, 2015; Risebro and Riley, 2006) (Figure 1). If there is any disturbance occurring on any step of early embryonic development, it will lead to different consequences of cardiac abnormalities.

When we look closer at the formation of the cardiac chamber, from the stage of looping, the primary heart tube is divided into atrial and ventricular components, which are separated by atrioventricular canal. The complex overlapping expression patterns of T-box containing transcription factors, including *Tbx20*, *Tbx5*, *Tbx2*, and *Tbx3*, regulates proliferative differences of the cardiac chamber formation (Miquerol and Kelly, 2013). The primary myocardial walls of the heart are also formed at this stage (Moorman et al., 2003). There are

two distinct components of the cardiomyocytes, including working and conductive cardiomyocytes responsible for contraction or electrical activity, respectively (Sedmera and McQuinn, 2008). Of course, the heart is made up of not only cardiomyocytes but also other cell types, including endocardium, cardiac fibroblasts, epicardium, smooth muscle, and endothelials (Doetschman and Azhar, 2012).

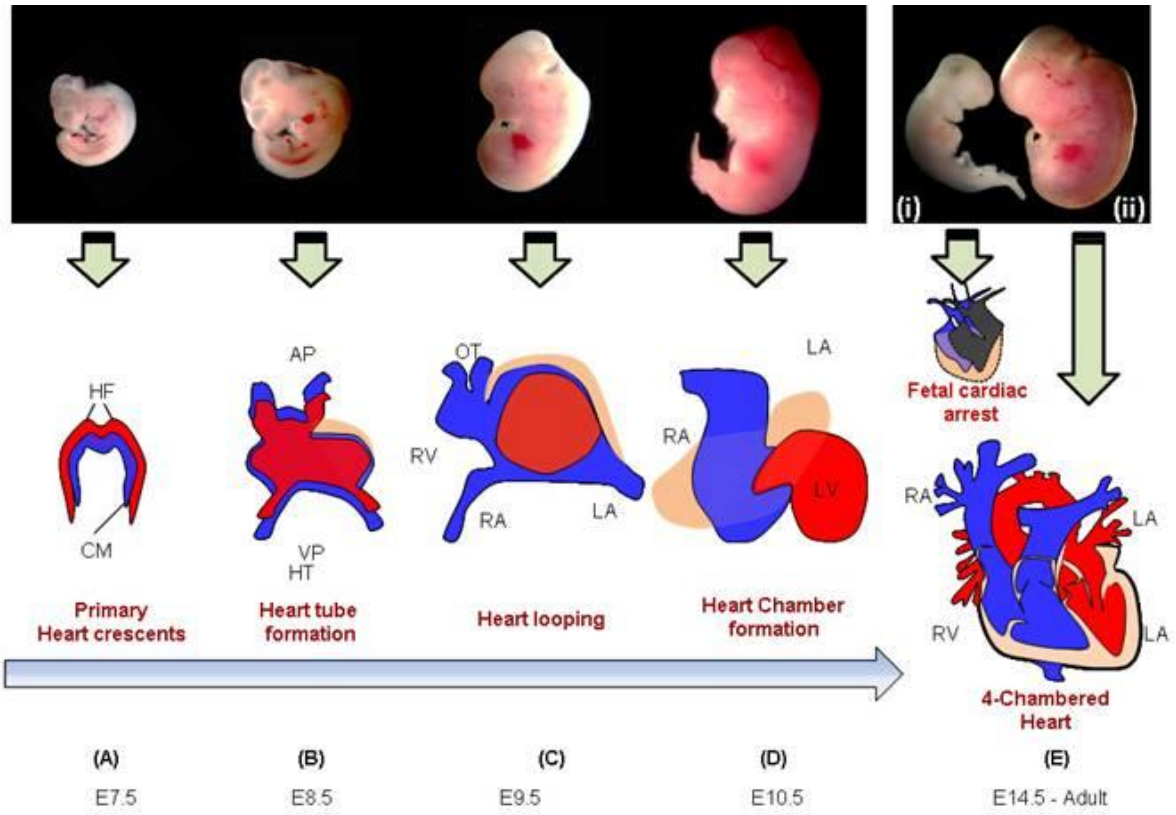

Figure 1. Schematic representation of embryonic cardiac developmental stages, growth and formation of four-chamber heart.

A. Formation of cardiac crescent at ~E7.5. B. Development of primary heart tube at ~E8.5 from the cardiac crescent cells. C. Formation of primitive atria and ventricles at ~E9.5 by looping of the heart tube. D. Heart chamber formation at ~E10.5 from primitive chambers. E (i) Defective cardiac development leads to embryonic heart failure and in-utero death by cardiac arrest at ~E14.5. (ii) Formation of the four-chamber heart at ~E14.5. The successive developmental stages during mouse embryogenesis are shown in top panel with representative pictures. Abbreviations: HF, Heart Fields; CM, Cardiogenic Mesoderm; AP, Arterial Pole; OT, Outflow Tract; HT, Heart Tube; VP, Venous Pole; RV, Right Ventricle; LV, Left Ventricle; RA, Right Atrium; LA, Left Atrium; PA, Pulmonary Artery; A; Aorta.

Source: (Nandi and Mishra, 2015)

1.2. Trabeculae development and function

Trabeculae are biological term of myocardial projections, and appear normally in the embryonic heart at the end of cardiac looping. Trabeculae can be found in both right and left ventricle at E10 in mouse and 1 month in human during heart development when blood vessels and arteries do not function yet (Zhang et al., 2013).

The development of an efficient myocardial ventricular wall necessitates several steps in cardiac maturity, including trabeculation and compaction. At late fetal stages, trabeculae pass through a compaction step to form a thick compacted layer with the establishment of the coronary vascular system. In the adult heart, the number of trabeculae is reduced with narrow recesses in the muscle wall (Captur et al., 2015). The purpose of the trabeculae is most likely to prevent suction that would occur with a flat surfaced membrane and thus impair the heart's ability to pump efficiently. It serves a function to prevent backflow of the blood from the ventricles into the atria during the contraction of the heart, and also could prevent inversion of the mitral (bicuspid) and tricuspid valves which would lead to subsequent leakage of the blood into the atria. Indeed, the early role of trabeculae is to be that of optimization of efficient nutrient and gas exchanges before the development of the coronary arteries which first appears at E12.5 in the mouse heart (Captur et al., 2015; Sedmera et al., 1997). Trabeculae in embryonic heart may have a role to increase surface to volume ratio, and may also serve to compartmentalize blood flow as separate ventricular streams prior to septation (Sedmera and McQuinn, 2008) .

Overall, trabecular development can be identified into 2 phases in the mouse: trabeculation and compaction. In trabeculation phase, trabecular cardiomyocytes invade to cardiac jelly layer and proliferate from E9.5 to E13.5 to form trabeculae (Figure 2). This phase is mediated through cardiomyocytes differentiation and terminal proliferation, and maintained by intact ligand/receptor interactions between endocardial cells and between endocardial and myocardial cells (Captur et al., 2015; Grego-Bessa et al., 2007). The compaction phase follows the trabeculation phase, and starts from E14 till after birth in the mouse heart (Figure 2). In this phase, trabecular zone is reduced and be occupied by a thick compacted layer. There is somehow a link between these two phases, but the link of trabecular remodeling and compact layer formation in the developing heart is still unclear and lack of compelling evidence (Captur et al., 2015). A schematic of trabeculae development has been given by Captur *et al* in the figure 3 (Captur et al., 2015).

Trabeculae are also a part of the compact myocardium, and participate in the formation of papillary muscles and ventricular conduction system. Defects in trabeculae development may affect ventricular conduction system function and therefore cause contraction defects.

Several growth factors and their intracellular signaling pathways have been demonstrated to be critical to ventricular growth and trabeculation, including *Bmp10*, *Notch1/2*, *RBPJk*, *FKBP12*, *Sgk1*, *Nrg1*, *Erbb2/4*, *Hesr1/2*, *Numb*, and *Mib1*. Mutations in these genes have been reviewed by Captur et al. as shown in the table 1 (Captur et al., 2015). Using several small animal models with genetic disruptions that affect the developing heart, we could see the consequences as either decreased or increased trabeculation, which can result in cardiac malformations or disease circumstances (Table 1).

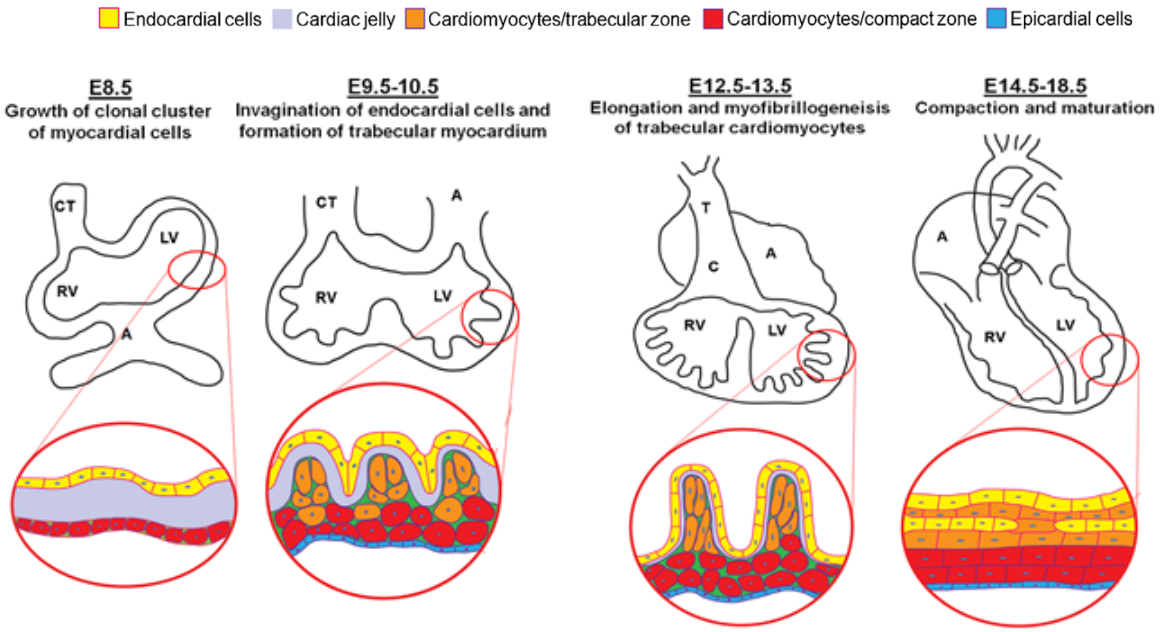

Figure 2. Schema of trabeculae development.

Source: adopted from (Zhang et al., 2013)

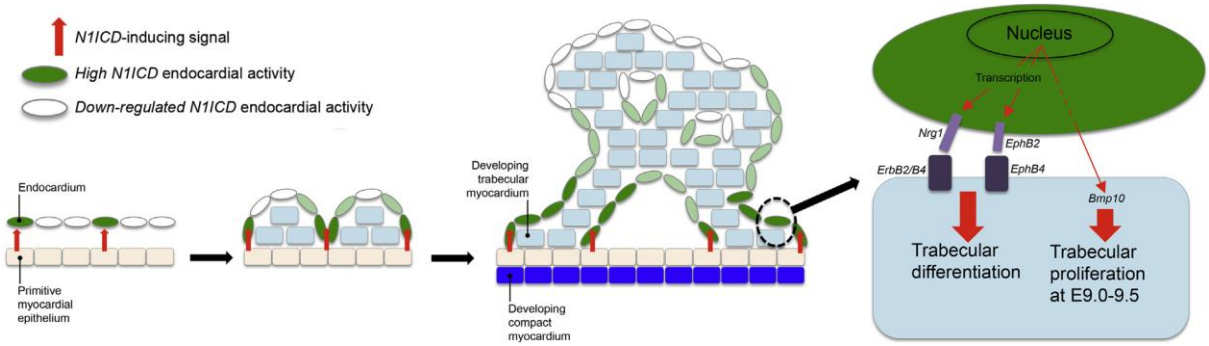

Figure 3. Morphological changes in the ventricular wall and development of trabeculae in the mouse.

During trabecular development there is spatial heterogeneity of expression of Notch components, for example, *Notch1*, *Notch4*, *Delta4*, *neuregulin-1*, *ephrin-B2* ligand and hairy and enhancer of split (hes) hes-related (hesr)1 activity is mainly restricted to the endocardium, and Notch2, Jagged1, bone morphogenetic protein-10, ephrin-B (*EphB*)4 receptor, erythroblastic leukemia viral oncogene homologues 2 and 4 receptors, mindbomb homolog 1 (*Mib1*) and *hesr2* activity predominates in the myocardium. A cue (red arrow) from the myocardium promotes *N1ICD* expression (dark green) in endocardial cells. Between embryonic day 9.0 and 9.5, bone morphogenetic protein-10 mediates trabecular muscle proliferation and neuregulin-1 through erythroblastic leukemia viral oncogene homologues 2 and 4, and *EphB2* through *EphB4*, mediate differentiation of primitive myocardial epithelium to trabecular and compact myocardium. As trabecular projections mature, the endocardium delaminates from the myocardium distancing itself from the *N1ICD*-inducing cue, resulting in *N1ICD* downregulation on the luminal aspect of trabeculae (dark green to white endocardial cells) compared with the base. By embryonic day E 10.5 a compact (dark blue) and trabecular layer (pale blue) can be distinguished. *Bmp*, bone morphogenetic protein; *N1ICD*, Notch 1 intracellular domain.

Source: (Captur et al., 2015)

Table 1. Mouse models showing defects in trabecular morphology

Source: (Captur et al., 2015)

Mutant	Function	Mutation effect	Reference
Bmp10	*Bmp10* is a signalling molecule transiently expressed in the trabeculated myocardium (between E9.0 and E13.5) and required for cardiomyocyte proliferation	*Bmp10*-deficient mutants show marked reduction in proliferation of cardiomyocytes leading to the formation of a hypoplastic ventricular wall and failure of trabeculation	(Chen et al., 2004)
Notch1	One of 4 heterodimeric transmembrane Notch receptor proteins	*Notch1* mutants are deficient of trabeculae	(Grego-Bessa et al., 2007)
RBPJk	Transcription factor	*RBPJk* mutants exhibit defective myocardial differentiation and severe hypotrabeculation compared with wild-type.	(Grego-Bessa et al., 2007)
FKBP12	This protein is a member of the immunophilin protein family, which plays a role in immunoregulation and basic cellular processes involving protein folding and trafficking. *FKBP12* interacts with several intracellular signal transduction proteins	Mutant embryos deficient in *FKBP12* exhibit an upregulation of *Bmp10* activity resulting in enormous overproduction of ventricular trabeculae. The mutation is embryonic lethal with hearts exhibiting impaired cardiac function	(Chen et al., 2004)
Nrg1 and *ErbB2/E*	Endocardial-derived *Nrg1* appears to be crucial for cardiac trabeculation by signalling to	Targeted deletion of *Nrg1* or cognate receptors *ErbB2/B4* results in the absence of	(Gassmann et al., 1995; Hertig et al.,

rbB4	cardiomyocytes through its receptor complex *ErbB2/B4* to drive trabecular initiation. Nrg1 is expressed in the endocardium and modulates trabecular differentiation by activating through *ErbB2/B4* receptors in the subjacent myocardium	trabecular formation in mice	1999)
EphB2/EphB4	The *EphB2/EphB4*-signalling system required for trabecular development, operates in myocardium and endocardium	Notch mutants with hypotrabecular phenotypes express reduced activity of *EphB2* ligand in the endocardium and *EphB4* receptor in the myocardium	(Wang et al., 1998)
Sgk1	A serine/threonine kinase lying downstream of the PI3 kinase pathway involved in cardiovascular development and in maintaining normal expression of Notch genes	Disruption of *Sgk1* in the mouse is embryonic lethal by E10.5-11.5 with severe heart failure and hypotrabeculation	(Catela et al., 2010)
hesr1; hesr2	Notch target genes	Double knockout hesr1;hesr2 mutant mice were used to confirm the presence of hypotrabeculation at E10.5	(Kokubo et al., 2005)
Numb/Numbl	*Numb* found in Drosophila and vertebrates, and its mammalian homologue, *Numbl*, found in vertebrates, regulate trabeculation and compaction by acting as endocytic adaptor proteins, suppressing *Notch2* and *Bmp10*	Double knockout *Numb* and *Numbl* mutant phenocopies *Notch2* overexpression (increased trabeculation) through increased *Bmp10* expression	(Yang et al., 2012)

	signalling during normal trabecular development		
Notch2	*Notch2* activity is specifically downregulated in the compact layer during normal cardiac development (by E13.5).	Hypomorphic *Notch2* mutants exhibit a defective trabecular phenotype and myocardial hypoplasia and expression of constitutively active *Notch2* in the myocardium of mutants results in increased trabeculation and reduced compaction of the ventricular wall	(McCright et al., 2002)
Mib1	*Mib1* is an E3 ubiquitin ligase which mediates ubiquitination of Jag1 in the myocardium resulting in endocardial *Notch1* activation at the base of trabeculae	*Mib1* deficient mutants are hypertrabeculated. The trabeculated myocardium remains abnormally proliferative, evidenced by the expansion of compact myocardial markers (like *hesr2*) to the trabeculae, late into embryonic development	(Luxán et al., 2013)

1.3. Cardiac conduction system development and function

Since its first discovery over 100 years, the cardiac conduction system (CCS) has been the subject of extensive studies. The CCS is a group of specialized cardiomyocytes, which plays a role to send electrical impulses to the heart muscle causing it to contract (Dobrzynski et al., 2013). The role of the heart is like a pump to circulate blood throughout the whole body, and the cardiac conduction system is a key factor in the synchronization of heart beats. That is to say, CCS has a very important role in maintaining normal function of the heart. Any defect in this system can cause trouble in heart beating, circulation system, and heart diseases like arrhythmias, heart failure, or even death.

Early during embryogenesis, myocardial cells of the primitive heart tube are automatic with spontaneous depolarization and a slow conduction of the electrical impulse with poor contraction properties. After the subsequent looping of the heart tube, ventricular chambers are formed. The chamber myocardial gene program, which is essential for conduction, is activated including the high conductance gap junctions *Cx40* and *Cx43*, and the cardiac sodium channel Scn5a. In contrast, the working myocardial gene program, which is essential for contraction properties, is repressed in myocytes of the developing sinus venosus, and atrioventricular canal. Thus, the specification pattern of the heart is already established at an early embryonic stage E9.5 in mice, although the components of the mature CCS are not morphologically recognizable (Weerd and Christoffels, 2016).

There are five main components of the cardiac conduction system, including sino-atrial (SA) node, atrio-ventricular (AV) node, His bundle, left and right bundle branches, and Purkinje fiber network (Figure 4). Three components, including His bundle, bundle branches, and Purkinje fibers are referred to as the ventricular conduction system (VCS). The cardiac conduction system components initiate and conduct the action potential and electrical signal required for the coordinated contraction of the cardiac chambers. They have special anatomical, molecular and functional properties that permit them to work collectively as the electrical system of the heart, which initiates and coordinates the contraction of the atria and ventricles to unique direction (Dobrzynski et al., 2013).

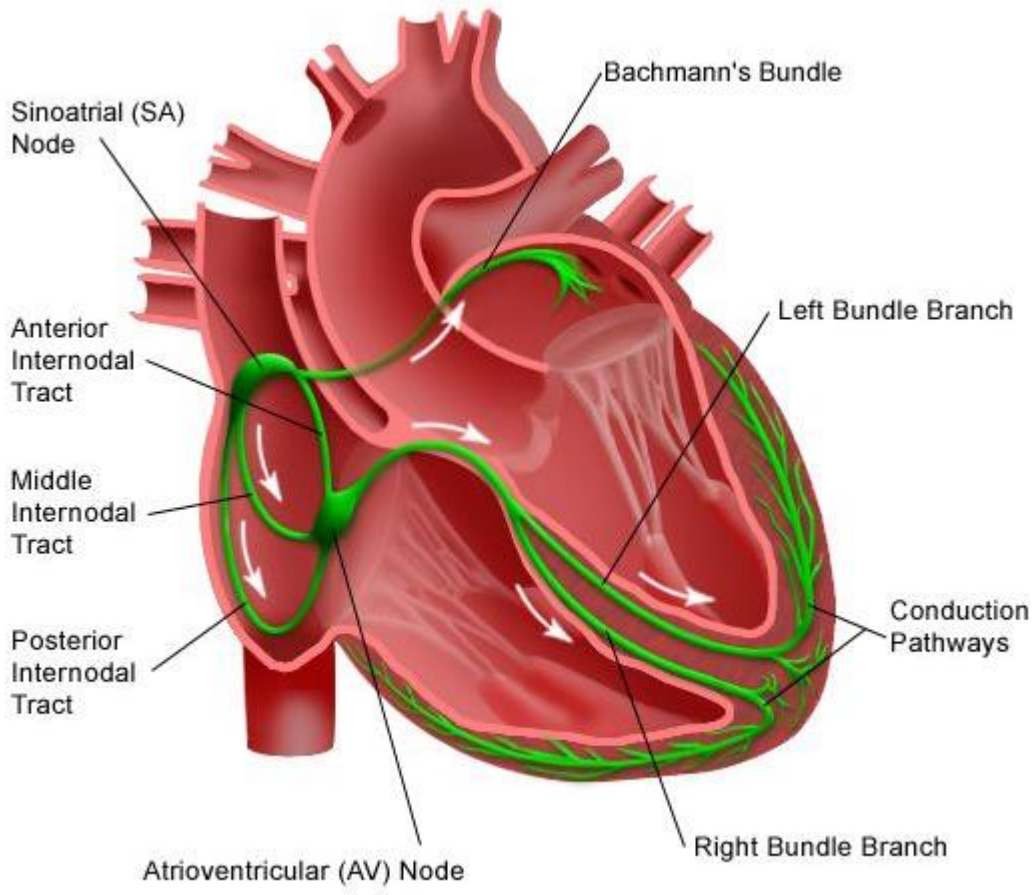

Figure 4. The components of the cardiac conduction system.

The various components of the CCS (green) are composed of a distinct set of cardiomyocytes that generate and propagate the electrical impulse required for contraction of the cardiac chambers. The sinoatrial node, which is located at the junction of the superior caval vein and right atrium, generates the impulse that then travels through the atria to the atrioventricular node, which delays the signal. The atrioventricular bundle forms the only myocardial connection between atria and ventricles through the non-myocardial atrioventricular junction. Propagation through the left and right bundle branches and the peripheral ventricular conduction system leads to activation of contraction of the ventricles. LA, left atrium; LV, left ventricle; RA, right atrium; RV, right ventricle.

Source :(Weerd and Christoffels, 2016)

There was a debate on the origin of conductive cells, which may come from cardiomyocytes, neural crest cells, and epicardially derived cells (Miquerol et al., 2011; Vincent and Buckingham, 2010). However, the hypothesis that the VCS cells are contributed by neural crest cells or/and epicardially derived cells have been refuted by recent clonal analysis (Miquerol and Kelly, 2013; Miquerol et al., 2010). Thus, the cardiac conduction system is essentially made of specialized cardiomyocytes. There are two kinds of cardiomyocytes: working myocytes and conductive myocytes. All components of the CCS are made up only of conductive myocytes which have specific properties, including the presence of a poor contractile apparatus with few sarcomeres, enriched glycogen content and reduced numbers of T tubules (James, 2003; Jongbloed et al., 2012; Miquerol et al., 2011; Virágh and Challice, 1980). Those properties distinguish conductive myocytes from working myocytes in both human and animal species in order to adapt to the role of generation as well as fast initiation and propagation of electrical impulses. Interestingly, clonal analysis of the VCS shows that conductive myocardium and working myocardium share a common progenitor (Figure 5). It means that development of the mammalian VCS is “biphasic” (Miquerol et al., 2011). However, the mechanisms responsible for how and when cardiomyocyte precursors differentiate into working and conductive myocytes are still unknown.

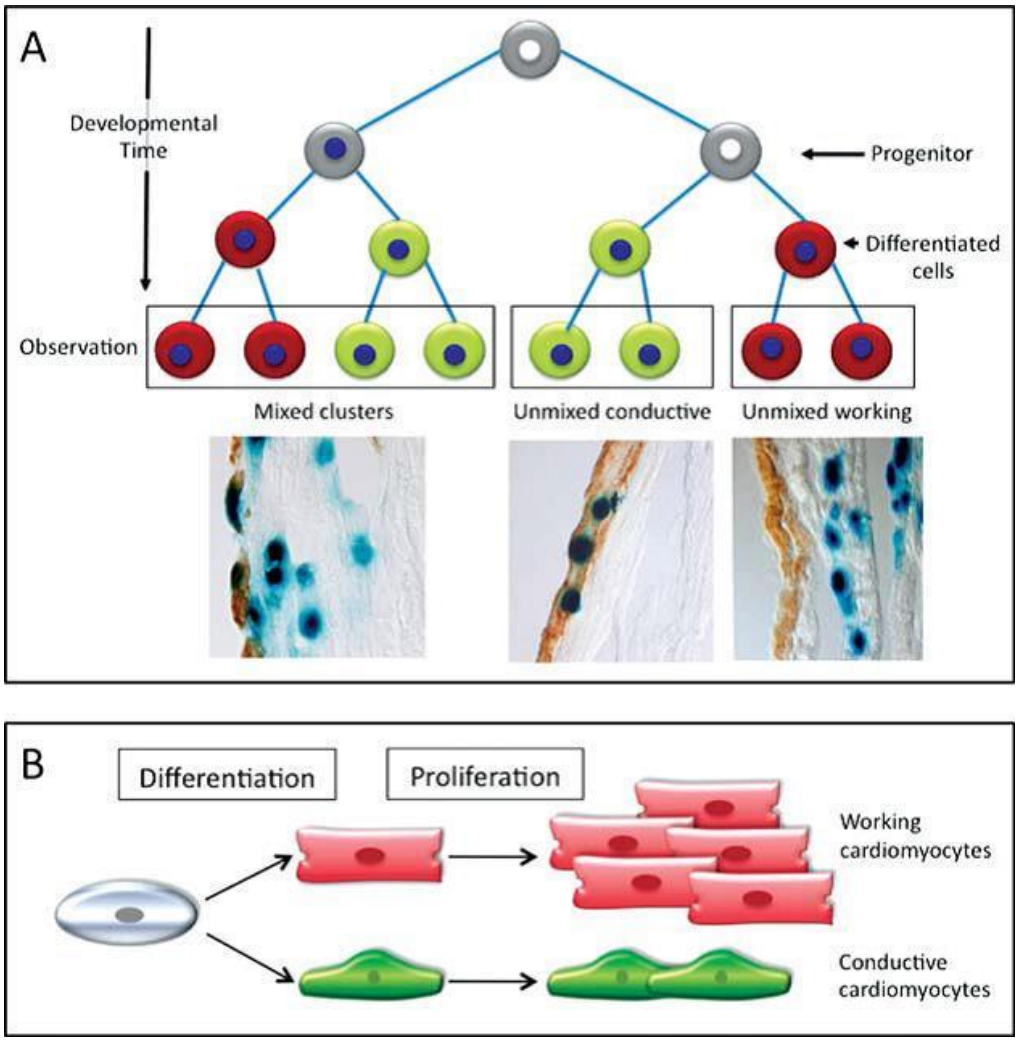

Figure 5. Biphasic development of the ventricular conduction system.

(A) Retrospective nlaacZ clonal analysis of the ventricular conduction system demonstrating two types of clusters: mixed clusters composed of conductive and working myocytes, and unmixed clusters composed of either conductive or working myocytes.

(B) Biphasic model showing differentiation from a common myogenic progenitor followed by limited proliferation of conductive myocytes.

Source: (Miquerol et al., 2011)

1.3.1. Sinoatrial node

The SA node, or sinus node, is located at the junction of the right atrium and the superior caval vein, and made up of specialized myocytes. The SA node is also known as the natural pacemaker of the heart, which controls the heart rate by generating electrical impulses and sending electrical signals through the heart muscle. It releases electrical stimuli at a regular rate, which is dictated by the need of the body. The myocardial cells of the atria create a wave of contraction when each stimulus passed through. The rapidity of atrial contraction is such that around 100 million myocardial cells contract in less than one third of a second. Even more than 100 years after the SA node first description, the molecular mechanisms underlying its pacemaker potential are hotly disputed suggesting an important role of SA node in heart function and cardiomyopathy (Dobrzynski et al., 2013; Monfredi et al., 2010).

The SA node develops within the sinus venosus myocardium, and can be recognized morphologically from E11.5 in mouse. There are several transcription factors which play pivotal roles in the SA node development and function. Combination of transcription factors *Nkx2.5*, *Tbx3*, and *Pitx2c* has been described as molecular determinants of the SA node (Mommersteeg et al., 2007). Other genes can also affect SA node development and function, including *Tbx5*, *Tbx18*, and *Shox2* (Weerd and Christoffels, 2016). Moreover, it is possible to distinguish the boundary between the SA node and the atrium by the expression of *Nkx2.5* gene. The *Nkx2.5* transcription factor is expressed in the heart tube, added to the venous pole, and expressed in cardiomyocystes of the atria (Weerd and Christoffels, 2016). This transcription factor, which suppressed the expression of pacemaker channel gene *Hcn4* and T-box transcription factor *Tbx3*, is not expressed at SA node (Sedmera and McQuinn, 2008). Thus it could induce a gene expression boundary between the atrium and SA node.

As a pacemaker, the SA node is responsible for the quick initiating and transmitting the electrical signal to other myocardial cells. Surrounding nodal myocytes, there is a network of connective tissue. The myocytes in the center of the SA node where the action potential originates are small compared to working atrial myocytes, and possess poorly organized myofilaments (Dobrzynski et al., 2013). Additionally, the gap juntions, *Cx40* and *Cx43*, are absent in the sinus node (Dobrzynski et al., 2013; Gros et al., 2004; Miquerol et al., 2010, 2011). The characteristics of these myocytes are suitable for quickly generating electrical impulses.

The rhythmic regularity of the heartbeat is controlled by the spontaneous diastolic depolarization governed by pacemaker automaticity. Although the diastolic depolarization events are not fully understood, scientists currently believe that they are the result of the synergistic interaction between two oscillators: the 'membrane voltage clock' and the 'Ca^{2+} clock' (Dobrzynski et al., 2013; Joung et al., 2009; Lakatta and DiFrancesco, 2009). Because the intact SA node is a heterogeneous structure including multiple different cell types interacting with each other, the relative importance of the voltage and Ca^{2+} clocks for pacemaking may be variable in different regions of the SA node (Joung et al., 2009).

1.3.2. Atrio-ventricular node

The AV node is an area of specialized tissue between the atria and the ventricles, specifically in the posteroinferior region of the interatrial septum near the opening of the coronary sinus, which conducts the normal electrical impulse from the atria to the ventricles (Aanhaanen et al., 2010; Bakker et al., 2010; Temple et al., 2013). It is a part of the cardiac conduction system which connects atrial and ventricular chambers. As Kurian described, the AV node is located within the triangle of Koch which is a region located at the base of the right atrium defined by the following landmarks: the coronary sinus ostium, the tendon of Todaro, and the septal leaflet of the tricuspid valve (Kurian et al., 2010).

The AV node plays an important role in coordinating and maintaining appropriate AV conduction from atria to the ventricles (Dobrzynski et al., 2013; Kurian et al., 2010). When the signal reaches the AV node, it is briefly delayed. This delay in the cardiac pulse is extremely important: it allows the atria to contract and contribute to fulfill the ventricles before the activation and contraction of the ventricles themselves (Weerd and Christoffels, 2016). The atrioventricular node delays impulses by approximately 0.12s. The valves between the atria and ventricles close when the atria are empty of blood.

Several studies have indicated a wealth of data on gene expression in the AV node, including *Hcn4*, *Tbx3*, *Cx45* (Aanhaanen et al., 2010; Bakker et al., 2010; Greener et al., 2009; Marionneau et al., 2005; Schram et al., 2002). In contrast, genes responsible for the fast conducting gap juction *Cx40*, *Cx43*, and the sodium channel *Scn5a* required for the rapid upstroke of the action potential are absent (Bakker et al., 2010). Moreover, the AV node development is highly dependent on the transcription factor *Nkx2.5*, which plays a role in the maintenance of the AV node in the postnatal heart (Miquerol et al., 2011). Mutations in the

gene encoded for *Nkx2.5* cause a variety of cardiac anomalies frequently associated with AV blocks both in human and mouse (Bakker et al., 2010; Bruneau, 2008; Miquerol et al., 2011). Taking all together, gene expression program in AV node controls the formation and function of the AV node to delay the electrical impulse from the atria to the ventricles.

1.3.3. Ventricular conduction system

The electrical impulses are transmitted to the ventricle by the fast-conducting atrio-ventricular bundle (AVB), or His bundle, which is connected to the AV node and runs through the crest of the ventricular septum. It conducts the impulse to the left and right bundle branches and the Purkinje fiber network to activate the ventricular myocardium contraction in order to pump out blood from the ventricles (Weerd and Christoffels, 2016).

Although the ventricular conduction system (VCS) just makes up of only 1% of the total muscle mass of the ventricles, it can enable rapid conduction of the impulses from the AV node to the ventricular working myocytes (Miquerol et al., 2010). VCS derive from subendocardial myocytes of the trabecules of the septum and trabecular myocardium. Depolarization of the ventricles occurs almost simultaneously, via the bundle branches and Purkinje fibers.

The VCS is made from myocardial derived cells, and shares a gene profile and some aspects of the nodal phenotype with SA node and AV node, including poor contractile apparatus, fewer sarcomeres, more glycogen, latent automaticity (Cheng et al., 1999; Gourdie et al., 1995; Weerd and Christoffels, 2016). However, *Cx40* and *Scn5a* which are absent in the AV node are, in contrast, highly expressed in the VCS (Bakker et al., 2010; Weerd and Christoffels, 2016). Additionally, *Cx40*, which is not expressed in the AV node or the ventricular working myocardium, is the best characterized and most specific known marker for VCS and essential for the fast impulse propagation through the AV bundle and bundle branches (Christoffels and Moorman, 2009; Kreuzberg et al., 2006; Miquerol et al., 2011; Weerd and Christoffels, 2016). High expression of *Cx40* and *Scn5a* in the VCS could explain the fast conduction of the impulse through VCS to the ventricular working myocytes, enabling the ventricles to contract quickly from apex to base after the atria contraction.

1.3.4. Electrical function of the heart *via* ECG recording

The depolarization and repolarization of the cardiac tissue can be recorded by electrocardiography (ECG) (Figure 6). ECG is a diagnostic tool and a simple test to perform in order to assess the rhythm of the heartbeat as well as electrical and muscular functions of the heart. This technique can provide precise idea concerning the cardiac electrical activity and informative supplement for pathological diagnoses.

Firstly, electrical impulses are generated by the SA node, and propagate into both atria. The conduction of the electrical impulses throughout the atria is distinguished by the P wave on ECG recording, and is measured by the PR interval, which represents atria activation and relaxation time. After passing through the atria, the electrical signal reaches the atrio-ventricular node where the impulses are delayed before continuing to propagate into the ventricles.

The electrical signal then passes through the ventricles via the ventricular conduction system. Activation of the ventricles is seen on ECG pattern as a QRS complex, which represents the rapid depolarization of the left and right ventricles. Because ventricles possess a muscular mass superior to the atria, the QRS complex is considerably larger than the P wave. T wave on ECG corresponds to the repolarization of the ventricles. The total time for ventricular activation and relaxation is represented by the time of QT interval. One cycle of ECG is equal to one heartbeat.

In the case where the electrical signal between the atria and ventricles is impaired, it leads to AV block or heart block. In AV block, the impulse from atria does not reach the ventricles or is impaired along the way. First-degree and second-degree blocks are partial meanwhile third degree blocks are complete. Those blocks can be recognized by ECG recording. In case of first-degree block, the conduction is slowed down without skipped beats. It means that all P waves are followed by a QRS complexe, but the PR interval is longer than normal. In second-degree block some P waves are followed by QRS complexes, but some are not. In third-degree block, there is no relationship between P waves and QRS complexes, and the P wave rate is greater than the QRS rate.

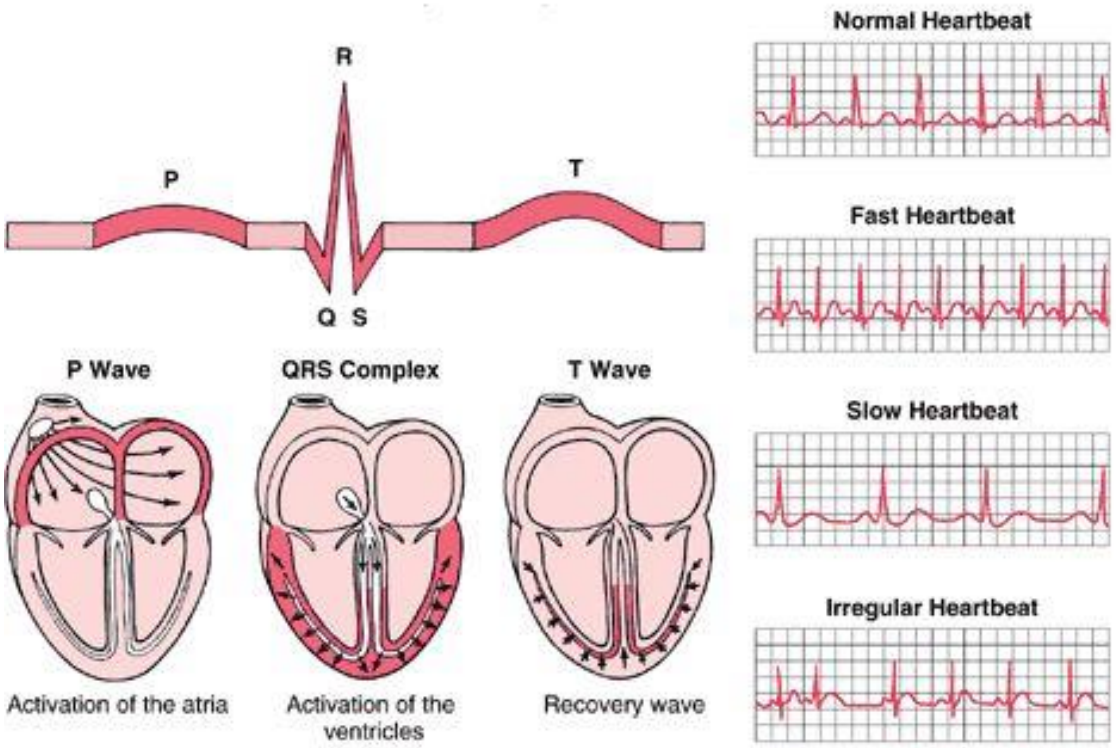

Figure 6. ECG recording pattern in human

Source: http://hubpages.com/education/Special-Investigations-In-Cardiology-Radiology-And-Electrocardiography-ECG

CHAPTER 2. LEFT VENTRICULAR NONCOMPACTION (LVNC)

2.1. LVNC definition and classification

Left ventricular noncompaction (LVNC) is a disease of the heart muscle characterized by prominent myocardial trabeculations and deep recesses in the muscle wall of the left ventricle (Figure 7). LVNC was first described in 1926 as a ‘spongy myocardium (Hussein et al., 2015), and the 2008 European Society of Cardiology Working Group on Myocardial and Pericardial Diseases categorized LVNC as an “unclassified” cardiomyopathy (Elliott et al., 2008). LVNC was also known as spongy myocardium or hypertrabeculation syndrome. This heart disease can be isolated or in association with other cardiomyopathies with a prevalence estimated of 0.014% to 0.17% (Gati et al., 2014). Although LVNC can occur as a primary disorder in the absence of other structural heart diseases, it is normally seen in association with other congenital cardiac abnormalities, for instance dilated cardiomyopathy, hypertrophic cardiomyopathy, and ventricular/atrial septal defect (Hussein et al., 2015). Besides, LVNC could lead to heart failure, thromboembolic events, arrhythmias and/or sudden cardiac death.

A novel classification system for cardiomyopathies termed MOGE(S) has been proposed by Arbustini et al. and reviewed by Gati and co-workers (Arbustini et al., 2014a; Gati et al., 2014). According to this system, which provides a pragmatic method to correlate the cause of disease with clinical phenotype by means of a single notation, cardiomyopathies could be classified based on the five characteristics, including Morphofunctional characteristics (M), Organ involvement (O), Genetic or familial inheritance pattern (G), Etiology (E), and functional Status (S) (Gati et al., 2014). Although this system is applicable to all cardiomypathies, LVNC provides a number of specific challenges that potentially limits the use of MOGE(S), including the heterogeneity in terms of genetic, clinical, functional capacity, and morphological change, and it remains a degree of uncertainty as to the precise etiological factors responsible for the development of LVNC (Gati et al., 2014). Thus, LVNC is still an unclassified cardiomyopathy, and more investigations are needed to clearly characterize the origin and pathology of this disease.

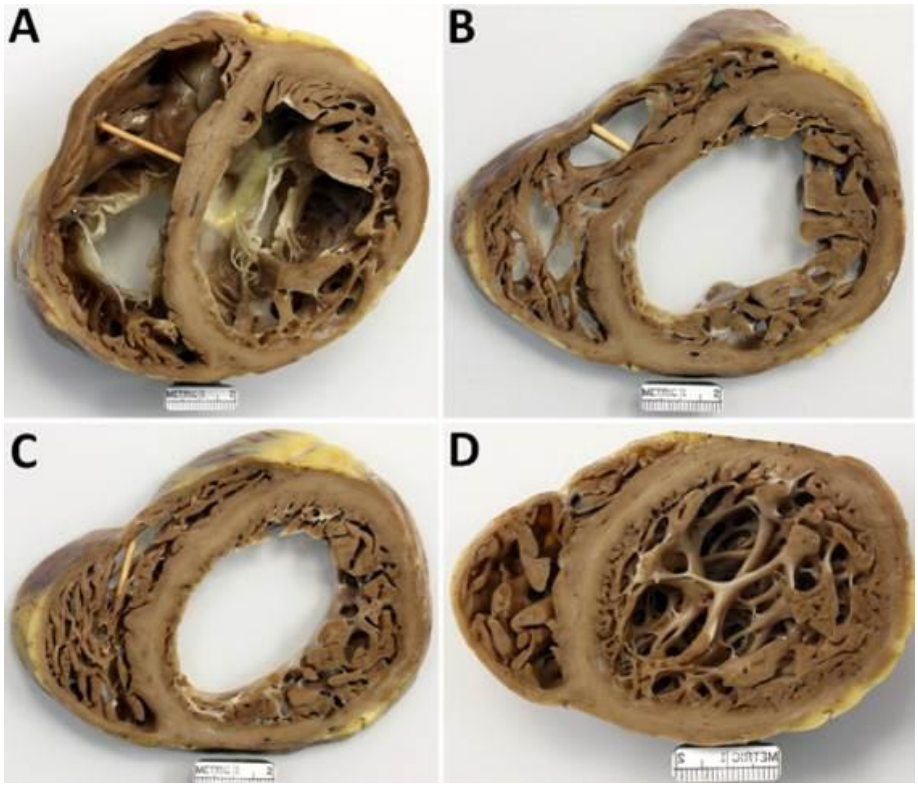

Figure 7. Views of the right and left ventricles of a patient.

(A) near to the base exposing the tricuspid and mitral valves, (B, C) intermediate levels, and (D) near to the apex. The noncompacted portion of the left ventricular free wall is thicker than the compacted portion, which is particularly thin in the basal portion *(A)*.

Source: (Roberts et al., 2011)

2.2. Anatomy and pathogenesis of LVNC

Anatomy of LVNC at autopsy is based on the presence of prominent trabeculae in the left ventricle and the calculation of the ratio between the compacted and noncompacted left ventricle wall (Arbustini et al., 2014b; Roberts et al., 2011). Prominent trabeculae and thin compacted myocardial layers can be quantified by sectioning of formalin-fixed hearts in order to measure the ratio of noncompacted/compacted. This ratio will give the idea of diagnostic of LVNC or increased trabeculation heart. According to Hussein and co-workers, the ratio of noncompacted/compacted layer ≥ 2 in adults at end systole is the cutoff value in the diagnosis of LVNC disease (Hussein et al., 2015).

The presence of numerous trabeculae is the principal anatomic characteristic of LVNC. Abnormal trabeculation is not only a key feature of LVNC but also common in congenital heart diseases and in cardiomyopathies such as dilated and hypertrophied. Furthermore, hypertrabeculated mutant mice exhibit severe heart failure and embryonic lethality suggesting an important role of trabeculae in cardiogenesis (Captur et al., 2015). Hypertrabeculation can also cause low ejection fraction value, which is an important measurement to determine how well the heart is pumping out blood and for the diagnostic and tracking heart failure. It means that in hypertrabeculated heart, a large volume of blood is kept within the ventricle at each contraction. An ejection fraction of 70 percent means that 70 percent of the total amount of blood in the left ventricle is pumped out with each heartbeat. In human, a normal heart's ejection fraction may be between 50% and 70%. A measurement under 40% may be evidence of heart failure or cardiomyopathy.

There is almost no difference in terms of anatomy between isolated LVNC and LVNC association with other cardiomyopathies (Ikeda et al., 2015; Udeoji et al., 2013). Besides, fibrosis including interstitial fibrosis and endocardial fibroelastosis has been described in many reports on endomyocardial biopsy (Burke et al., 2005; Finsterer et al., 2002; Ichida, 2009; Ikeda et al., 2015; Udeoji et al., 2013). Furthermore, at autopsy, a variety of LVNC patterns has been noted, including broad trabeculae, resembling multiple papillary muscles, and sponge-like interlacing smaller muscle bundles (Burke et al., 2005; Udeoji et al., 2013). Jenni and co-workers studied seven out of a series of 34 adult patients with isolated ventricular noncompaction indicating that interstitial fibrosis was found to be severe in one, mild to moderate in four, and absent in one patient (Jenni et al., 2001). Additionally, signs of chronic inflammation were present in one patient (Jenni et al., 2001). Thus, all together,

fibrosis and the absence of well-formed papillary muscles are perhaps associated with the diagnostic of LVNC (Burke et al., 2005).

Concerning the pathogenesis of LVNC disease, there is still a controversy about the origin of LVNC whether it is a congenital abnormality due to the arrest of the normal compaction process *in utero*, or acquired during life, or a consequence of other cardiomyopathies, we hypothesize that LVNC may be caused by the disturbance during compaction stage. Before the coronary vessels present during the early embryological development, the heart consists of a spongy meshwork of muscle fibers and trabeculations, which will be compacted and disappeared after the coronary vasculature develops (Ikeda et al., 2015). Normally, the myocardium becomes compacted between the fifth and eighth week in human (Gati et al., 2014), and after the fourteenth day in mouse (Zhang et al., 2013). The compaction starts from basal segments to the apex and from epicardium to endocardium (Gati et al., 2014; Udeoji et al., 2013). For unknown reasons in LVNC patients, the trabeculation and compaction transition does not completely occur, leading to a noncompacted endocardial layer with prominent trabeculations that are still present in left ventricle in adult heart (Ikeda et al., 2015). It means that somehow there is an arrest of myocardial morphogenesis during heart development causing the remaining of trabeculae with deep intertrabecular recesses (Figure 8). And normally, the topographic distribution of LVNC does not typically extend to the interventricular septum (Arbustini et al., 2014b). Thus the signs of hypertrabeculation or LVNC are usually observed clearly and most severe in apex or close to apex part.

It is important to understand the link between disturbances in trabeculae development and LVNC. Defects in the transition between trabeculation phase and compaction phase may cause overproliferation of trabeculae or somehow defects in the compaction step, both could lead to LVNC. Those defects would result in the persistence of numerous trabeculae in adult heart. One considerable hypothesis is that the severity of the myocardial noncompaction is dependent on the stage at which the arrest of the normal embryonic myocardial maturation takes place. Thus, defects occuring during trabeculation or compaction stages could lead to different phenotypes in LVNC pathology. This point could also explain the important phenotypical heterogeneity observed in LVNC patients. It means that in patients with different genetics and disturbances during heart development, the symptoms of LVNC may vary.

After all, looking at the pathogenesis of LVNC, there is a possibility of a direct relationship between trabeculae development disturbances and LVNC, but the origin and molecular mechanisms leading to this pathology are still unknown. Besides, there is no suitable explanation for the severity observed in LVNC patients who develop a large spectrum of symptoms with different outcomes, or even are asymptomatic. Thus, we hypothesize that the severity of LVNC may come from several reasons, one of them is that disturbances at different time points during trabecular development may affect the formation of trabeculation. To date, there is a lack of evidence to verify this hypothesis.

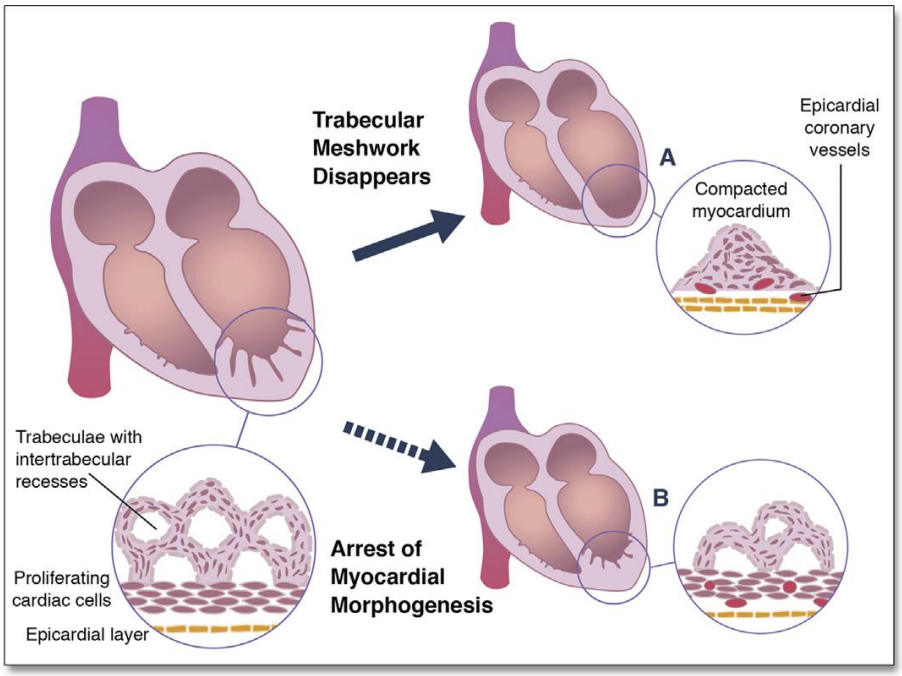

Figure 8. Embryonic development of LVNC.

The myocardium starts off as a meshwork of fibers that regress at weeks 5 to 8 to form compacted outer and inner smooth muscle layers (A). In left ventricular noncompaction (LVNC), there is retarded myocardial morphogenesis and persistence of the trabecular meshwork (B).

Source: (Gati et al., 2014)

2.3. Genetic aspects of LVNC

LVNC is a genetically heterogeneous disease, either familial or sporadic (Hussein et al., 2015; Udeoji et al., 2013). LVNC was classified as a primary genetic cardiomyopathy by the American Heart Association (Maron et al., 2006). According to Ichida's review, up to 44% of patients in clinical series have a family history of cardiomyopathy, and the studies in the etiology of LVNC are increasing rapidly (Ichida, 2009). Even if genetic testing does not change clinical management of LVNC disease, it may help for confirming diagnosis and determining potential development of the pathology in family members (Arbustini et al., 2014b). Besides, genetic studies in LVNC patients have revealed that familial recurrence in adults appear more commonly than in children, and may be associated with autosomal dominant, X-linked, or mitochondrial mutations (Hussein et al., 2015; Ichida et al., 2001; Sasse-Klaassen et al., 2003). However, gene mutations identified in LVNC patients are limited and infrequent, suggesting a genetic heterogeneity in this cardiomyopathy (Ichida et al., 2001). This heterogeneity highlights the difficulty in the diagnosis and management of LVNC patients. Nevertheless, studying this genetic heterogeneity and the major genetic cause for familial noncompaction may provide insight into the etiology of LVNC (Hussein et al., 2015).

LVNC disease is a genetic disorder, which has been associated with several mutations in the sarcomeric, cytoskeletal, Z-line, and mitochondrial proteins. Thus, genetic aspect is one of the major causes of LVNC. Unfortunately, the pathways leading to the LVNC phenotypes are still unknown (Gati, Rajani et al. 2014).

Hussein and co-workers reviewed several gene mutations, including *TAZ-G4.5*, *DTNA*, *Z-Band*, *FKBP12*, *LMNA*, *Nkx2.5*, *CSX*, *TBX5*, *ACTC*, *TNNT2*, *MYH7*, *SCN5A*, and *HCN4* in LVNC and other cardiac disorders shown in the table 2 (Hussein et al., 2015). This table shows that most of the major gene mutations associated with LVNC are also seen in other congenital cardiac abnormalities. For example, *MYH7* mutation is not only seen in LVNC but also in dilated cardiomyopathy, hypertrophic cardiomyopathy, and other conduction abnormalities like bundle blocks, AV nodal blocks, tachyarrhythmias, bradyarrhythmias. Notably, mutations in this gene, sarcomeric cardiac beta-myosin heavy chain gene (*MYH7*), linked restrictively with hypertrophic and dilated cardiomyopathy in previous studies, have also been identified in 2 families with isolated LVNC (Hussein et al., 2015; Klaassen et al., 2008). Another example, mutations in the *Nkx2.5* gene found in LVNC patients are also

associated with other heart disease, including ventricular/atrial septal defect, conduction abnormalities, Ebstein anomaly, X-linked endocardial fibroelastosis. Thus, gene mutations in cardiomyopathies may have a potential overlapping. It also could explain why in some patients, several types of cardiomyopathies co-exist.

As mentioned above there is a potential overlap between genes associated with LVNC and additional cardiac abnormalities, thus, the precise correlation between genotype and their phenotypical expression in cardiomyopathies is still unclear. Available data for certain mutations could suggest that noncompaction and hypertrophic, restrictive, and dilated cardiomyopathies are not clearly distinct entities (Sen-Chowdhry and McKenna, 2008; Xu et al., 2010). However, in the review of Arbustini and co-workers, evidences proving that LVNC is a cardiomyopathy were given (Arbustini et al., 2014b) and they contribute to unravel the controversy between the two viewpoints cited below: one aspect believes that LVNC is a distinct cardiomyopathy *versus* another aspect that considers LVNC as a trait shared by different cardiac diseases.

- Statement 1: "Specific mutations in genes in the Notch1 pathway in mice and humans leading to dysregulated signaling and hypertrabeculation and noncompaction."
- Statement 2: "Specific mutations in G4.5 in mice and humans disrupting the TAZ protein leading to dysregulated remodeling of cardiolipin and Barth syndrome, characterized by hypertrabeculation and noncompaction in utero and failure to thrive. In contrast, evidence that LVNC is a trait shared by multiple cardiac diseases has not been ruled out. The data presented on mechanical load from pregnancy and athletes is compelling."

Besides, Jenni and co-workers have also the same viewpoint as Arbustini *et al*., they suggested that the World Health Organization (WHO) classification of cardiomyopathies should consider LVNC as a distinct cardiomyopathy in order to be aware of this disease as well as to improve our knowledge of facilitating its diagnosis (Jenni et al., 2001). Thus, studies to understand the genetic aspects of LVNC could help to better characterize this disease and will contribute to apply treatment and healthcare.

Table 2. Major gene mutations associated with LVNC and their overlap with cardiac disorders

Disorder	Mutation								
	Taz-G4.5	*Dtna*	*Z-Band*	*Fkbp12*	*Lmna*	*Nkx2.5, Tbx5, Csx*	*Actc, Tnnt2, Myh7*	*Scn5a*	*Hcn4*
LVNC	x	x	x	x	x	x	x	x	x
Ventricular/atrial septal defect		x		x		x			
Arrhythmogenic right ventricular cardiomyopathy				x					
Dilated cardiomyopathy	x		x	x	x		x	x	
Hypertrophic cardiomyopathy							x		
Other cardiomyopathies*	x		x			x		x	
Other conduction abnormalities†					x	x	x	x	x
Tetralogy of Fallot						x			
Ebstein anomaly						x			
Brugada syndrome								x	
Romano-Ward syndrome								x	

*X-linked infantile cardiomyopathy, X-linked endocardial fibroelastosis, hypoplastic left heart syndrome.

†Bundle blocks, atrioventricular nodal blocks, tachyarrhythmias, bradyarrhythmias.

ACTC, alpha-cardiac actin (Hoedemaekers et al., 2007); *CSX*, cardiac specific gene located on 5q (Elliott et al., 2003; Hershberger and Morales, 1993); *DTNA*, alpha-dystrobrevin gene, transition C to T mutation, located on 18q12 (Ichida et al., 2001); *FKBP12*, responsible for release of calcium from sarcoplasmic reticulum via ryanodine receptor (Shou et al., 1998); *HCN4*, hyperpolarization-activated cyclic nucleotide channel 4 (Milano et al., 2014); *LMNA*, lamin A/C related sequence located on 1q22 (Ikeda et al., 2002); *MYH7*, B-myosin heavy chain (Hoedemaekers et al., 2007; Klaassen et al., 2008; Monserrat et al., 2007); *NKX2.5*, homeobox protein located on chromosome 5 (Elliott et al., 2003; Shou et al., 1998); *SCN5A*, human cardiac sodium channel alpha-subunit gene (Shan et al., 2008); *TAZ-G4.5*, encodes tafazzin located on Xq28, (Bleyl et al., 1997; Ichida et al., 2001; Klaassen et al., 2008); *TBX5*, T-box transcription factor located on chromosome 12 (Elliott et al., 2003; Hershberger and Morales, 1993); *TNNT2* = cardiac troponin T (Hoedemaekers et al., 2007); *ZASP* = Z-band alternatively spliced PDZ motif-containing protein on 10q22.2-q23.3 (Vatta et al., 2003).

Source: (Hussein et al., 2015)

2.4. Diagnosis of LVNC and treatment

LVNC presents a strong heterogeneity with a large spectrum of symptoms from asymptomatic to severe symptoms like arrhythmias or heart failure. It means that some people with LVNC do not present any obvious symptoms or are asymptomatic, they can live normally during their life, while other patients can develop severe symptoms. This heterogeneity causes difficulties in the diagnostic and the selection of appropriate treatment. Because LVNC possesses a large variability of symptoms, it is commonly discovered through the screening of family members of affected patients during early, nonsymptomatic stages, or detected in patient with other cardiomyopathies (Hussein et al., 2015; Lofiego et al., 2007). Due to heterogeneity in genetics and morphological changes, prominent left ventricular trabeculation can be found in healthy hearts or in association with other heart diseases, for instance, hypertrophic cardiomyopathy, left ventricular hypertrophy secondary to dilated, valvar or hypertensive cardiomyopathy (Jenni et al., 2001). Most isolated LVNC cases are diagnosed in patients with unexplained heart failure and with clinical symptoms usually related to systolic or diastolic dysfunction or arrhythmias (Hussein et al., 2015).

The diagnosis of LVNC is usually attained by echocardiography and magnetic resonance imaging (MRI) (Ichida, 2009; Ikeda et al., 2015; Udeoji et al., 2013) although its diagnosis is often delayed due to failure of recognition and the absence of a consensus of absolute diagnostic criteria (Hussein et al., 2015). A summary of diagnostic criteria of LVNC as well as their advantages and disadvantages have been given by Gati *et al.* in the table 3 (Gati et al., 2014). Other methods can be used in the diagnosis of LVNC, including computed tomography (CT) scan, and contrast left ventriculography (LVG) (Udeoji et al., 2013).

Echocardiography is the most commonly used technique for the diagnosis of LVNC according to Udeoji (Udeoji et al., 2013). The criteria for diagnosing LVNC have been proposed by three groups: Chin et al. (Chin et al., 1990), Jenni et al. (Jenni et al., 2001), and Stollberger et al. (Stöllberger et al., 2002), and reviewed quite clearly by several groups, including Ichida (Ichida, 2009), Udeoji et al. (Udeoji et al., 2013), Gati et al. (Gati et al., 2014), Arbustini et al. (Arbustini et al., 2014b), Ikeda et al. (Ikeda et al., 2015), and Hussein et al. (Hussein et al., 2015). Briefly, the criteria used in echocardiography with/without color Doppler to follow up LVNC diagnosis include several points detailed below:

- Absence of coexisting cardiac abnormalities in case of isolated LVNC

- Presence of prominent trabeculations and deep recesses in the left ventricle
- The ratio of noncompaction/compaction ≥ 2 in adults or > 1.4 in children at end systole.

Although these criteria are the most widely used for the diagnosis of LVNC, they have still several limitations which have been shown by Gati et al (Gati et al., 2014). One of the limitations is that these criteria were based from a small number of patients and have not been validated in large cohorts from different ethnic origins. This could lead to overestimate or underestimate LVNC. In addition, the two common difficulties in establishing a diagnosis of LVNC during echocardiographic assessment are the identification of abnormal trabeculations and their accurate assessment (Gati et al., 2014). It is also difficult to correctly identify the ratio of noncompacted/compacted. Thus, a better understanding of this pathology will bring to the design of a gold standard for LVNC diagnosis.

Besides echocardiography, cardiac magnetic resonance imaging (MRI) is increasingly used in the diagnosis of LVNC (Gati et al., 2014; Hussein et al., 2015; Ichida, 2009). In MRI measurement, a ratio of noncompaction/compaction ≥ 2.3 in diastole is considered the cutoff for LVNC diagnosis (Petersen et al., 2005). Additionally, a study by Grothoff *et al* (Grothoff et al., 2012) and a recent review by Hussein *et al.* (Hussein et al., 2015) have given the 4 basic criteria with good reproducibility in establishing quantitative MRI, which could differentiate noncompaction from other cardiomyopathies. These criteria include:

- "Noncompacted LV myocardial mass > 25%
- Total noncompacted LV myocardial mass index 15 g/m^2
- Noncompacted/compacted myocardium ratio ≥ 3:1 in at least 1 segment, excluding the apical segment
- Trabeculation in segments 4 to 6 ≥ 2:1 (noncompacted/compacted)."

Furthermore, in the study of Thuny et al. (Thuny *et al*., 2010), patients with suspected LVNC were evaluated by both techniques, and cardiac MRI provides a more accurate and reliable evaluation of the extent of non-compacted myocardium than echocardiography, and MRI revealed a good agreement to echocardiography at end-diastole (Ikeda et al., 2015). However, according to Dawson et al. (Dawson *et al.*, 2014), "a gold standard for the diagnosis of LVNC continues to be lacking as no imaging or pathology signature has yet been agreed".

There are still no specific guidelines for management of LVNC, and also no specific therapeutic treatments for isolated LVNC patients (Arbustini et al., 2014b). In general,

patients with LVNC have quite similar management than to other cardiomyopathies, including appropriate evidence-based heart failure treatments for left ventricular systolic dysfunction, appropriate management of arrhythmias, and consideration of oral anticoagulation to prevent mural thrombus formation (Hussein et al., 2015). The treatment management will depend on the phenotype in patients according to their clinical needs and corresponding guidelines (Arbustini *et al*., 2014b).

Table 3. Summary of LVNC Criteria and Their Advantages and Disadvantages

Source: (Gati et al., 2014)

	Chin *et al.*	Jenni *et al.*	Stollberger *et al.*	Petersen *et al.*	Jacquier *et al.*	Captur *et al.*
Patients (n)	8	34	62	7	16	30
Selection criteria	Patients referred for echocardiography	Patients referred for echocardiography fulfilling LVNC criteria presented below	Patients referred for echocardiography demonstrating >3 trabeculations distal to papillary muscle on 4CV	Clinical diagnosis of LVNC based on echo or MRI appearance of a 2-layered trabeculated and compacted myocardium Plus 1 of the following: a. 1st degree relative with similar appearance b. associated neuromuscular disorder c. thromboembolism or RMMA	Diagnosis of LVNC was established on Jenni et al. echocardiographic criteria were enrolled	Fulfillment of Jenni et al. echocardiographic criteria for LVNC and the additional presence of at least 1 of the following: positive family history, associated neuromuscular disorder, RWMA, LVNC-related complications (arrhythmia, heart

						failure, or thromboembolism
Age range	11 months to 22.5 yrs	16 ro 75 yrs	18 to 75 yrs	11 to 46 yrs	48 ± 17 yrs	41 ± 13 yrs
Asymptomatic patients (n)	2		7	4	Not reported	
Available pathological correlation (n)	3	7	Not reported	Not reported	Not reported	Technique validated in 24 embryonic murine hearts
Description of criteria	2-layered structure with an epicardial compacted and endocardial noncompacted layer	2-layered structure with a compacted epicardial and noncompacted ebdocardial layer Color Doppler evidence of intertrabecular recesses supplied by	>3 trabeculations protruding from LV wall apically to papillary muscle in 1 imaging plane (Later revised to include ratio and a 2-layered myocardium)	2-layered structure with a compacted epicardial and noncompacted ebdocardial layer Images from horizontal and long-axis views at points of prominent trabeculations	Calculated total LV trabeculated mass from SSFP short axis; papillary muscles excluded from trabeculated mass Myocardial	Global LV trabecular complexity as a continuous variable termed fractal dimension 2D space is divided into a grid of boxes and skeletonized data within are calculated for 4 different-sized

		intraventricular blood Absence of coexisting cardiac structural abnormalities			mass	grids The exponent of line of best fit across the points on log-log plot of box counts represent fractal dimension
Cardiac phase	End diastole	End systole	End diastole	End diastole	End diastole	
Ratio*	X/Y ≤ 0.5	NC/C ≥ 2	NC/C ≥ 2	NC/C ≥ 2.3	LV trabecular mass >20%	
Advantages	Echocardiography widely available Portable investigation Cost-effective test			Superior contrast-to-noise ratio Unlimited imaging planes Ability to use tissue characterization in the diagnosis High sensitivity and specificity Interobserver reproducibility of trabecular mass measurement in Jacquier criteria reported to be high		

		Interobserver and intraobserver variability of Captur criteria high
Disadvantages	Based on small cohorts for Chin and Jenni criteria Not validated properly Measurements in different phases of the cardiac cycle Image quality dependent on body habitus Oversensitive in certain populations Nonspecific in low-risk populations	Based on small cohorts Not prospectively derived Petersen criteria require high pre-test probability Reproducibility of the trabecular mass percentage not reported in Jacquier criteria Not widely available Expensive Requires expertise in the field Captur criteria not available for replication and assessment yet

*C = compacted; FD = fractal dimension; N = noncompacted.; 2D = 2-dimensional; 4CV = 4-chamber view; MRI = magnetic resonance image; LV = left ventricle/ventricular; LVNC = left ventricular noncompaction; RWMA = regional wall motion abnormality;

CHAPTER 3. *NKX2.5* AND MOUSE MODELS FOR STUDYING LVNC

3.1. Expression and role of *Nkx2.5* in cardiac function

Nkx2.5 is one of the transcription factors critical to normal cardiac development across vertebrate species, and belongs to the NK2 family of homeobox genes which is a homolog of the Tinman gene found in *Drosophila melanogaster*. The official name of *Nkx2.5* is NK-2 transcription factor related, locus 5, in which NK is the abbreviation of Nirenberg and Kim (Kim and Nirenberg, 1989), who carried out a search for *Drosophila* genes containing homeodomain-encoding genes, and "x" in Nkx refers to designate vertebrate members of the family (Bartlett *et al*., 2010). There are many aspects of cardiogenesis in which the homeodomain protein *Nkx2.5* is implicated. They include regulating the proliferation of cardiac precursors, terminal differentiation of the myocardium, establishment of the ventricular conduction system and postnatal conduction function (Bartlett et al., 2010).

Among the NK-2 genes expressed in the cardiac system of vertebrates, including *Nkx2.3*, *Nkx2.5*, *Nkx2.6*, *Nkx2.7*, *Nkx.8*, and *Nkx2.10*, *Nkx2.5* is involved directly in early cardiac formation and is a key factor for normal morphologic and physiologic development (Bartlett *et al.*, 2010). Although *Nkx2.5* is expressed in the several developing organs, including foregut, thyroid, spleen, stomach and tongue, it is widely known to be the early marker of cardiac progenitor cells (Reecy *et al*., 1999). This transcription factor is expressed in both the first and second heart fields, and plays not only a pivotal role in the early steps of mammalian cardiogenesis but also an important role in later stages of cardiac morphogenesis during the development of discrete atrial, ventricular, and conduction cell lineages (Pashmforoush et al., 2004). *Nkx2.5* continues to be expressed throughout cardiac development and into adult life (Postma *et al.,* 2011). In adult, *Nkx2.5* expression is restricted to the heart, therefore, its functions is critical not only for embryonic heart development but also for both conduction and contraction in the adult heart (Briggs *et al*., 2008).

There are approximately 50 identified mutations of this gene in human, but only a few have been functionally characterized (Chung and Rajakumar, 2016). Besides, mutations in the *Tinman* gene in Drosophila embryos result in the loss of heart formation, while *Nkx2.5* knockout mice showed early embryonic lethality, and heterozygotes exhibited an array of cardiac abnormalities such as scattering of AV bundle, reduced His and AV node cellular

density and abnormal levels of gap junction proteins (Chung and Rajakumar, 2016). In human, a variety of cardiac anomalies as well as atrioventricular abnormalities are caused by dominant mutations in *NKX2.5* (Postma *et al*., 2011). Besides, in *Nkx2.5*-deficient embryos, the expression of several cardiac genes was dysregulated, including atrial natriuretic peptide (*ANP*), brain natriuretic peptide (*BNP*), *Bmp10, Hcn1*, ion channel (*mink, Scn5a*), calcium handling (*Myh7*, *Serca2a*, *Ryr2*), *N-myc*, iroquois homeobox gene 4 (*Irx4*), and homeodomain-only protein (*HOP*) (Biben and Harvey, 1997; Bruneau *et al.*, 2000; Lyons *et al*., 1995; Shin *et al*., 2002; Tanaka *et al.*, 1999; Terada *et al*., 2011; Zou *et al*., 1997) (Table 4). *Nkx2.5* also regulates several downstream target genes, which are transcription factor, calcium-binding, ion exchanger, and some other important genes (Table 5). Thus, the altered gene expression in *Nkx2.5*-deficient hearts indicates that this transcription factor plays a crucial role in the transcriptional regulation of several sets of cardiac-specific genes (Akazawa and Komuro, 2005). This could explain why mutations in *Nkx2.5* gene in both human and mouse result in a variety of cardiac dysfunctions and disease.

Table 4. Misregulated gene expression in *Nkx2.5*-deficient hearts

	Genes	Gene product
Down-regulated genes	*MEF-2C*	Transcription factor
	eHAND/HAND1	Transcription factor
	Irx 4	Transcription factor
	N-myc	Transcription factor
	Myocardin	Transcriptional coactivator
	CARP	Transcriptional corepressor, titin-binding protein
	HOP	Homeoprotein
	MLC2v	Contractile protein
	ANP	Natriuretic peptide
	BNP	Natriuretic peptide
	Connexin 40	Structural protein in gap junction
	minK	Ion channel
	MLCK	Serine/Theorine specific protein kinase
	SCN5a	Ion channel
	Serca2a	Ca^{2+} handling
	RYR2	Ca^{2+} handling
Up-regulated genes	*BMP10*	Morphogenic protein
	Sarcolipin	Inhibitor for sarcoplasmic reticulum calcium-ATPase
	HCN1	Ion channel

	Myh7	cardiac myosin protein

ANP, atrial natriuretic peptide; *BNP*, brain natriuretic peptide; *CARP*, cardiac ankyrin repeat protein; *HOP*, homeodomain-only protein; *Irx4*, Iroquois homeobox gene 4; *MLC2v*, myosin light chain 2v; *MEF-2C*, myocyte enhancer factor 2-C

Source: adopted from (Akazawa and Komuro, 2005)

Table 5. Direct downstream target genes for *Nkx2.5*

Genes	Gene product	References
ANP	Natriuretic peptide	Durocher et al., 1996; Lee et al., 1998; Shiojima et al., 1999
Cardiac α-actin	Contractile protein	Chen and Schwartz, 1996
MEF-2C	Transcription factor	von Both et al., 2004
A1 adenosine receptor	Adenosine receptor	Rivkees et al., 1999
Calreticulin	Calcium-binding protein	Guo et al., 2001
Sodium-calcium exchanger 1	Ion exchanger	Müller et al., 2002
Connexin 40	Structural protein in gap junction	Bruneau et al., 2001
Endothelin-converting enzyme-1 (*ECE-1*)	Endothelin-converting enzyme	Funke-Kaiser et al., 2003
HOP	Homeoprotein	Chen et al., 2002; Shin et al., 2002
Myocardin	Transcriptional coactivator	Ueyama et al., 2003a
CARP	Transcriptional corepressor, titin-binding protein	Zou et al., 1997
Csm	RNA helicase	Ueyama et al., 2003b

ANP, atrial natriuretic peptide; *CARP*, cardiac ankyrin repeat protein; *HOP*, homeodomain-only protein; *MEF-2C*, myocyte enhancer factor 2-C.

Source: (Akazawa and Komuro, 2005)

3.2. Recent studies about *Nkx2.5* mutant mice in relation to trabeculation, conduction defects and heart diseases

In 2004, Pashmforoush and co-workers demonstrated that the loss of ventricular myocyte lineage specification leads to progressive cardiomyopathy and complete heart block (Pashmforoush *et al.*, 2004). They mentioned that human mutations in *Nkx2.5* gene cause a diverse set of congenital heart malformations, including septal defects, cardiomyopathy, outflow tract defects, hypoplastic left heart, and associated arrhythmias (Benson *et al*., 1999; Elliott *et al*., 2003; Goldmuntz *et al.*, 2001; Gutierrez-Roelens *et al.*, 2002; Schott *et al*., 1998). The central challenge was to understand the link between *Nkx2.5* gene loss of function with the observed cardiac phenotypes. For that, they generated ventricular restricted *Nkx2.5* deficient mice by crossing mouse containing *Nkx2.5* floxed allele to MLC2v-Cre mouse and injected tamoxifen at around E8 to E8.5 in order to delete *Nkx2.5* gene in the cardiomyocytes of the ventricular myocardium. They observed phenotypes of congenital heart disease as well as conduction system disease. In addition, a progressive AV block and hypertrabeculation in association with cardiomyocytes dropout and fibrosis in the central conduction system were observed. To identify the molecular pathways involved in conduction defects and hypertrabeculation in adult *Nkx2.5* deficient mice, gene expression profile by microarray experiments was carried out. This profile exhibited a dysregulation of downstream target genes and altered gene expression in the conduction system in *Nkx2.5* mutant hearts. Moreover, high expression of *Bmp10*, *HCN1,* and Sarcolipin, which are normally suppressed in adult ventricular myocytes, indicates a defect in lineage specification and maturation that could lead to the hypertrabeculation phenotype.

Later research was carried out by Meysen *et al.* demonstrating that *Nkx2.5* gene is also required for postnatal formation of the peripheral ventricular conduction system (Meysen *et al.*, 2007). Using $Nkx2.5^{+/-}/Cx40^{eGFP/+}$ mice, they analyzed the anatomy and functional disturbances of hypoplasia and disorganization of the Purkinje fiber network in the ventricular apex. The results reveal that the transcription factor *Nkx2.5* controls the formation of the peripheral conduction system.

One year after the finding of Meysen and co-workers (Meysen *et al*., 2007), Briggs *et al.* published research on phenotypical characteristics of mouse models with perinatal loss of *Nkx2.5* in the ventricular myocardium and demonstrate the role of *Nkx2.5* in cardiac

conduction and contraction in neonates (Briggs *et al.*, 2008). They applied Flox/loxP system by crossing Nkx2.5^{flox} mouse with *CMV*$^{Cre\text{-}ER}$ mouse to delete *Nkx2.5* gene after the injection of tamoxifen at different time points. Tamoxifen was injected into pregnant mouse at E19 (just before birth) and researchs were carried out at P2, 4, 7, and 12 days after birth. In contrast to Pashmforoush *et al.* (Pashmforoush *et al.*, 2004) in which the deletion of *Nkx2.5* occurred only in cardiomyocytes of the ventricle at very early embryonic stages around E8-E8.5, Briggs and co-workers deleted *Nkx2.5* in all cardiomyoctyes of the entire heart at perinatal stage E19. The main results observed in neonatal mutant mice are conduction and contraction defects phenotype. From ECG recordings, a progressive AV block, and prolongation of PR and QRS duration were shown. Furthermore, they confirmed a reduction in ion channels expression in *Nkx2.5* knockout hearts, for example, *T-type Ca* channel both *α-1H* and *α-1G*, *RyR2*, *Na$_v$1.5-α* subunit, *KcneI/mink*. It means that *Nkx2.5* plays not only an important role in embryonic stages but also in postnatal stages by regulating a critical set of genes to maintain proper cardiac function. They mentioned that their finding may provide potential explanations for progressive conduction and contraction defects, which have been seen in patients with congenital heart disease associated with *NKX2.5* mutations.

Later on, Takeda *et al.* continued to characterize the phenotypes of *Nkx2.5^{flox}/CMV$^{Cre\text{-}ER}$* mutant mice after cardiomyocytes terminal differentiation by injecting tamoxifen in 2-week-old mice (Takeda *et al.*, 2009). The characterisation of the phenotypes of these mutant mice was carried out at 3, 6, 9, 24 weeks. Finally, they observed conduction and contraction defects similar to the perinatal loss of *Nkx2.5*, but with a slow progression.

Continuing using *Nkx2.5^{flox}/CMV$^{Cre\text{-}ER}$* mutant mice, but with different strategy, Terada and co-workers have shown that *Nkx2.5* is necessary for the survival as well as for the cardiac function and formation after the mid-embryonic stage (Terada *et al.*, 2011). Tamoxifen was injected into pregnant female at E12.5 to delete *Nkx2.5* gene throughout the whole embryonic heart. The analyses were carried out at E16.5 to study cardiac functions and expression of specific genes and proteins. The results indicate that inducible *Nkx2.5* deletion at early embryonic stage leads to the death of these fetuses by E17.5 that was not demonstrated in ventricular myocyte-specific *Nkx2.5* gene targeting in the study performed by Pashmforoush *et al.* (Pashmforoush *et al.*, 2004). The main defects in cardiac function were arrhythmias, contraction defects, cardiac malformations, including atrial septal defects. Genes and proteins expression showed dysregulation of transcripts critical for conduction and contraction, including *Na$_v$1.5-α* subunit, *Cx40*, *KcneI/mink*, and sarcolipin. The authors concluded that the

different spectrum of cardiac abnormalities leading to embryonic death was resulting from global deletion of *Nkx2.5* at the mid-embryonic stage.

Another *Nkx2.5* mutant mouse model using *Sln-Cre* line from Nakashima *et al.* was a subject for studying roles of *Nkx2.5* in heart development and cardiac disease (Nakashima *et al.*, 2014). The mutant mice were generated by crossing $Sln^{Cre/+}$ mice and $Nkx2.5^{flox/flox}$ mice. By using atrial specific *Nkx2.5* mutant mice under the control of *Sln* promoter, the authors observed massive enlargement of working and conduction myocardium, leading to a lethal cardiac abnormality with atrial septal defect, hyperplastic atrial myocardium, AV conduction block, bradycardia, and transient pulmonary hypertension in the absence of major ventricular dysfunction. Moreover, Notch activity in the atria was suppressed by *Nkx2.5* in genome-wide transcriptome analysis. They summarized that *Nkx2.5* regulates the proliferation of both working and conduction myocytes in the atria in coordination with Notch activity.

Several *Nkx2.5* specific knockout mouse models were studied by several groups to evaluate the role of *Nkx2.5* transcription factor in early embryonic and postnatal cardiac development. Some of them observed left ventricular noncompaction phenotypes in those *Nkx2.5* mutant mice. In particular, a novel mouse model having a heterozygous *Nkx2.5* missense mutation in the homeodomain was studied by Ashraf *et al.* (Ashraf *et al.*, 2014). The heterozygous mice presented ventricular noncompaction phenotypes along with diverse cardiac anomalies, including atrioventricular defects. This finding supports the existence of a direct link between *NKX2.5* mutations and LVNC disease. Thus, all together these data suggest a link between *Nkx2.5* gene and cardiac conduction defects in LVNC disease.

3.3. Our LVNC mouse models by conditional deletion of *Nkx2.5*

3.3.1. A novel mouse model for studying heart disease

There are several mouse models for studying heart diseases as reviewed above. *Nkx2.5* was deleted whether restrictively in the ventricle, or atria, or in the global heart by several groups of authors. In our study, we will focus on novel *Nkx2.5* mutant mouse models by the conditional deletions of *Nkx2.5* in the cardiomyocytes of the atria, trabecular zone, and ventricular conduction system.

We apply the Flox/loxP system to generate conditional mutant mouse models inducible by tamoxifen. This system is a site-specific recombinase technology in order to carry out deletions, insertions, translocations and inversions at specific sites in the DNA of target cells. The principle of this technique is that the activated Cre enzyme will recognize the loxP site to initiate the recombination as shown in figure 9. The recombination will be triggered by a specific external stimulus, for example, a chemical signal or a heat shock so that the activity of the Cre enzyme can be controlled. The combination of both conditional and inducible gene targeting approaches have led to tissue-specific genetic alterations under temporal control (Doetschman and Azhar, 2012). The widely used chemicals include tamoxifen (Tam) -inducible, tetracyclin (Tet), or its analog doxycycline (Dox) -inducible Cre recombinase. By using this technique, we could activate the deletion of a target gene in a specific tissue at desired time points.

To generate our mutant mice, *Nkx2.5* floxed mice were crossed with *Cx40-Cre* mice and the induction of tamoxifen to delete *Nkx2.5* gene is occuring only in tissues where the *Cx40* gene is expressed (Figure 10). *Cx40* gene encodes for a gap-junction protein which is expressed in cardiomyocytes of both right and left atria, in trabecular zone of the ventricles, and in the conduction system except the sinoatrial node and the central AV node. After tamoxifen injection, Cre protein was activated under the control of *Cx40* promoter to trigger the deletion of *Nkx2.5* exons 1 and 2 floxed by two loxP sites. Without tamoxifen stimulus, the recombination or deletion does not occur. Thus, we delete *Nkx2.5* gene in cardiomyocytes of atria, trabecular zone of the ventricle and conduction system including AV bundle, bundle branch, and purkinje fibers.

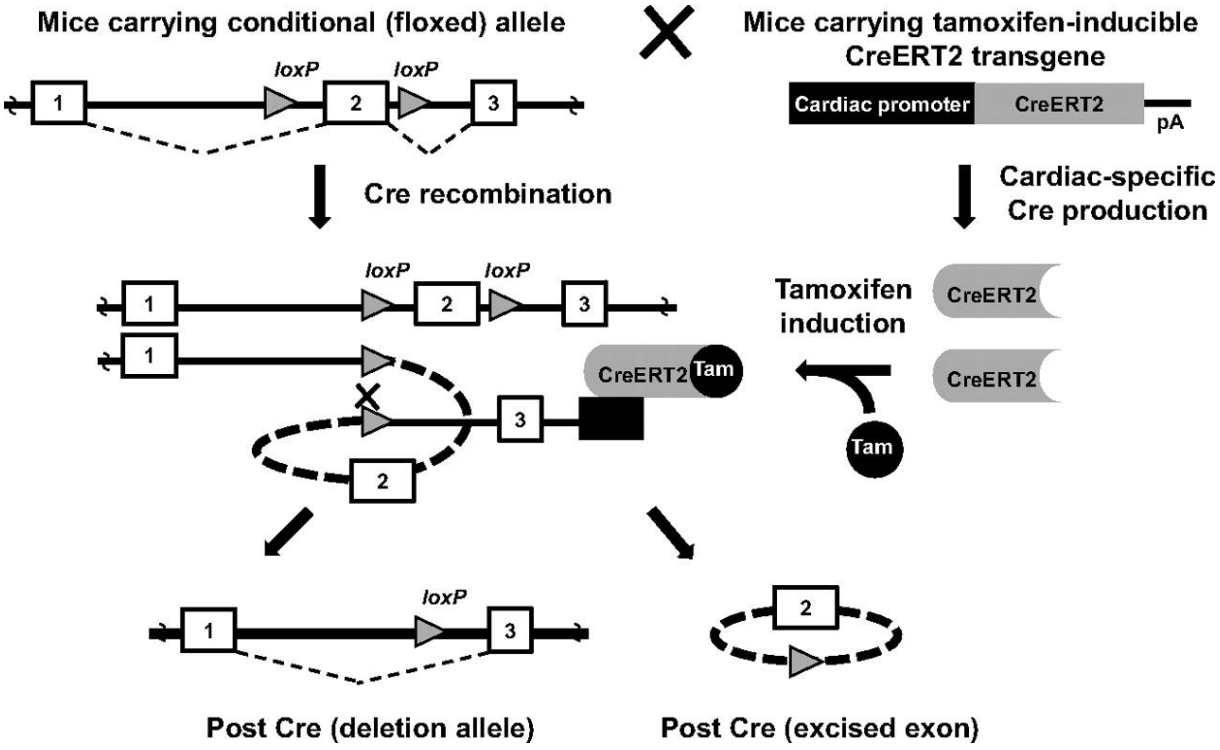

Figure 9. Schematic of inducible conditional gene targeting

A schematic representation of cardiac-specific conditional and Tam-inducible genetic deletion in mice.

Spatiotemporally controlled cardiac-specific mutagenesis can be achieved by cardiac-specific expression of *CreER*^{T2} in transgenic or knock-in mice. When cardiac-specific-CreER^{T2} transgenic or knock-in mice are crossed to a mouse line carrying a conditional or floxed allele, the floxed gene is rapidly removed in response to Tam induction. In the absence of Tam, *CreER*^{T2} is retained in the cytoplasm. Binding of Tam to the mutant ligand-binding domain of *CreER*^{T2} results in translocation of the Cre recombinase into the nucleus where it can recombine and delete floxed DNA in a conditional and Tam-inducible fashion. pA indicates poly A.

Source: (Doetschman and Azhar, 2012)

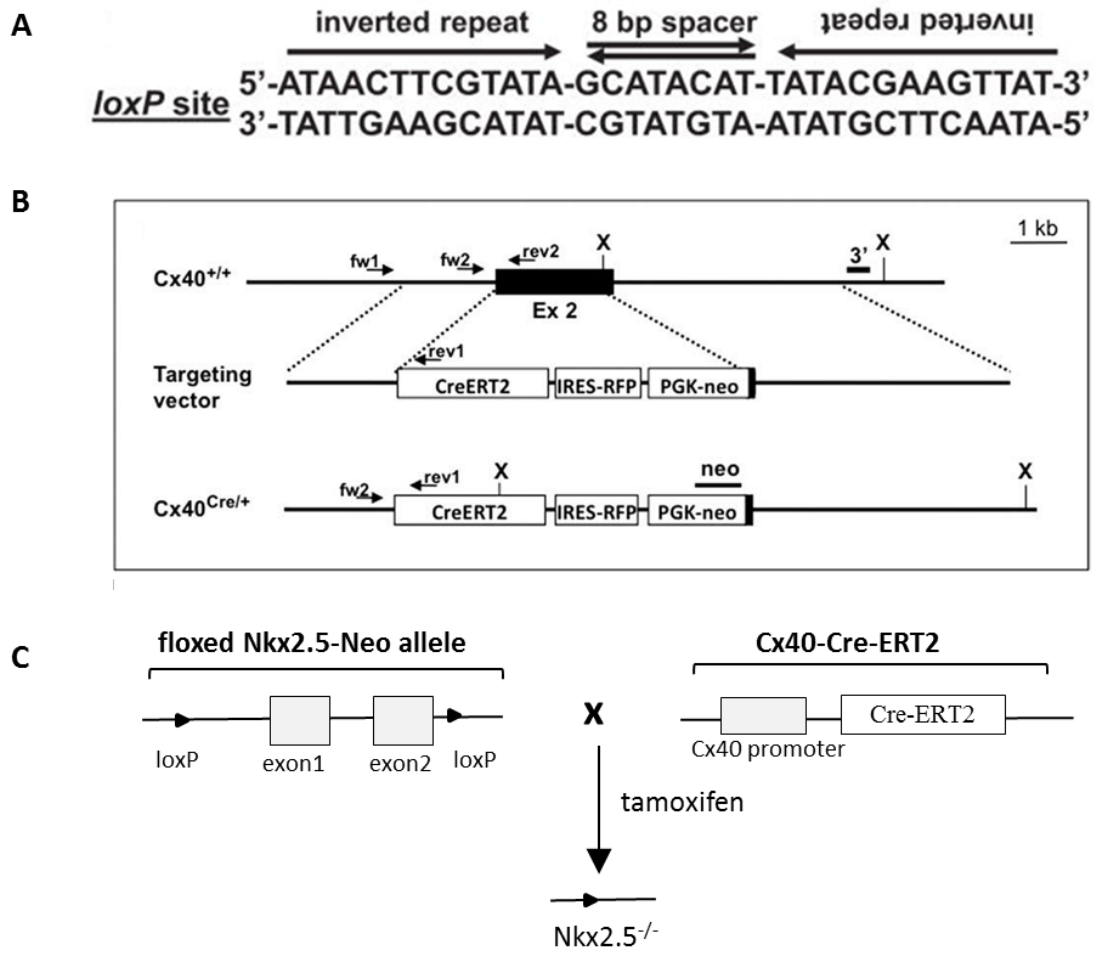

Figure 10. Generation of a mutant mouse model by conditional deletion of *Nkx2.5* gene

. (A) Sequence of loxP. These 34-bp sequences contain 13-bp inverted repeats flanking 8 bp unique sequence motifs that have directionality. When 2 loxP sites line up a recombination occurs at the 8 bp motif. Depending on whether the 8-bp motifs are in the same or opposite orientation a deletion or insertion, inversion or translocation can occur. (B) Strategy for generating the Cre targeting vector and $Cx40^{Cre}$ allele. A *CreERT2-IRESmRFP1* cassette is introduced into *Cx40* exon2 (black box). (C) Schema illustration for generation of *Nkx2.5* mutant mice under control of *Cx40* promoter in the inducible of tamoxifen injection.

Sources: (Beyer et al., 2011; Doetschman and Azhar, 2012)

3.3.2. Strategy of generating *Nkx2.5* mutant mice

As mentioned in the chapter 1 during heart development, trabeculae appear around E9.5 when there is no cardiac vascular network found at this time, and later on trabeculae go through a compaction step starting at around E13.5 to form a compacted layer with functional coronary arteries and cardiac vessels (Captur et al., 2015). Thus, we injected tamoxifen at 3 different time points: at E10-11 when trabeculae are forming, at E13-14 when trabeculae start to compact, and at P1 when the compaction step is almost finished. The consecutive injection was carried out to maximize the deletion of *Nkx2.5* at each time point. The study of the consequences on the cardiac function in these different mice should tell us if disturbances during trabeculae development might influence the severity of LVNC and explain a part of the heterogeneity observed in LVNC patients. The three different time points of tamoxifen injection were used to test the hypothesis whether LVNC disease is caused by disturbances during compaction step, or trabeculation step. We also would like to know the origin of LVNC and compare the severity of cardiac symptoms between these time-points. It means that if the disturbances during cardiac development occur at embryonic stages, or after birth, the consequences in the pathology will be different.

With tamoxifen injection at different times, we hope to disturb different processes during heart development. The mice in which tamoxifen was injected at E10-11 are called $Nkx2.5^{\Delta trab}$ mice. In those mice, we target trabecular development and trabecular differentiation process. The $Nkx2.5^{\Delta comp}$ and $Nkx2.5^{\Delta VCS}$ mice present mutant mice after tamoxifen injections at E13-14 and P1, respectively. In $Nkx2.5^{\Delta comp}$ mice, we will disturb compaction process, while in $Nkx2.5^{\Delta VCS}$ mice the ventricular conduction system will be only affected.

After tamoxifen injection, we expect to have different percentage of *Nkx2.5* deletion and diverse consequences. The percentage of *Nkx2.5* deletion in $Nkx2.5^{\Delta trab}$ mice may be highest or quite similar to $Nkx2.5^{\Delta comp}$ mice because at early embryonic heart, *Cx40* is highly expressed in cardiomyocytes in the trabecular zone of the ventricles. In contrast, after tamoxifen injection at P1 mice, we expect to delete a smaller percentage of *Nkx2.5* expression level in the ventricles because the heart nearly finishes the compaction step and *Cx40* expression is now restricted to the VCS. Thus, with different percentage and region of *Nkx2.5* deletion, we would like to know if it has any effect on adult ventricular trabeculation and cardiac functions.

For those three groups of mice, we will follow up cardiac functions by MRI and ECG techniques every 2 months from 2 month-old to 12-month-old mice as well as study the cardiac phenotypes at 3-month-old mice and molecular mechanisms by microarray experiments in 6-month-old mice. Immunofluorescence experiments were carried out to study cardiac phenotypes in the 3 groups of mutant and control mice using specific antibodies. We disturb trabecular development process, including trabeculation and compaction steps, so that later on we will quantify the level of trabeculation for each group. This will be one of the criteria as indicator of LVNC disease.

By using this strategy, we generate the conditional deletion of *Nkx2.5* gene in specific regions of mouse hearts under the control of *Cx40* promoter. As shown above in the chapter 3 part 1, *Nkx2.5* is expressed in the several organs, including foregut, thyroid, spleen, stomach, tongue, and heart. *Cx40* is only expressed in lung and heart (Hertzberg, 2000), but not in other organs expressing *Nkx2.5* except the heart. Thus, the deletion via stimulation of tamoxifen injection occurs only in cardiac tissue. Moreover, in the heart, *Cx40* is expressed in cardiomyocyes and endothelial cells as shown in the Table 6. Besides, the expression of *Cx40* is different in each tissue or each stage during the development processes, the *Nkx2.5* deletion will be different in each mutant group in term of level and specificity of tissue. For example, at embryonic stage E10-11, *Cx40* is highly expressed in cardiomyocytes of ventricular trabeculae, atria, and conductive cells (Purkinje fibers), but not in cells that will give rise to the His bundle and bundle branches or endothelial cells of coronary vessels. Thus, in $Nkx2.5^{\Delta trab}$ mice, we do not delete *Nkx2.5* in myocytes of the His and bundle branches and endothelial cells of the coronary vessels. In $Nkx2.5^{\Delta comp}$ mice, the deletion is quite similar to that in $Nkx2.5^{\Delta trab}$ mice, excepted in the His bundle and bundle branches where *Cx40* expression starts from E14.5. In contrast to early embryonic mutant mice $Nkx2.5^{\Delta trab}$ and $Nkx2.5^{\Delta comp}$, in $Nkx2.5^{\Delta VCS}$ mice, *Nkx2.5* will be deleted in endothelial cells of coronary vessels and in conductive cells of the VCS because the expression pattern of *Cx40* after birth is restricted to the VCS (Miquerol *et al.*, 2004).

To sum up, we have generated 3 groups of *Nkx2.5* conditional mutant mice in specific cardiac tissues with different level and stage of gene deletion. The functional defects and molecular analysis have been studied to figure out the severity of LVNC as well as the role of the *Nkx2.5* transcription factor in the ventricular conduction system development and function at both embryonic and perinatal stages. We have also studied whether the deletion of *Nkx2.5*

at different stages during trabeculae development leads to hypertrabeculation and cardiac functional defects.

Table 6. Spatio-temporal inducible Cx40-Cre activity

Source: (Beyer et al., 2011)

Tamoxifen injection		-	E9.5	E10.5	E12.5	E14.5	E16.5	E18.5
Cardiomyocytes	Atria	-	+	++	++	++	+++	+++
	His and bundle branches	-	-	-	-	+	++	+++
	Purkinje fibers	-	+	++	++	++	+++	+++
	Working myocardium	-	+	+++	+++	++	+/-	-
Endothelial cells	Dorsal aorta	-	+++	+++	+++	+++	+++	+++
	Intersomitic vessels	-	-	+	+	+	++	++
	Coronary vessels	-	-	-	-	+/-	++	+++
	Lung vasculature	-	-	-	-	-	++	+++
Other	Thymus	-	++	-	-	-	-	-
	Skeletal muscle	-	-	-	-	-	-	-

PART II. MATERIALS AND METHODS

1. Generation of *Nkx2.5* conditional knockout mice

To produce cardiac-specific inducible and conditional gene targeting mice, Flox/LoxP system was applied (Robert Kelly's team, Developmental biology institute of Marseille (IBDM), CNRS, France). Floxed *Nkx2.5* mice were bred with transgenic mice carrying the Cre-ERT2 gene under the Cx40 promoter. Tamoxifen (1mg/g body weight) was used as an inducible chemical to induce Cre recombination to delete *Nkx2.5* gene between two LoxP sites. It means that after tamoxifen injection, *Nkx2.5* will be deleted in the mouse heart where *Cx40* gene expresses. We injected tamoxifen consecutively at E10 and E11, or E13 and E14, or at P1 to generate three mouse models. All animal care protocols are fully conformed to the Animal Facility (IBDM – CNRS, France).

In order to distinguish mutant and control mice, genotyping was performed by PCR from finger tissues from neonatal mice using specific primers against Cre, *Cx40*, floxed *Nkx2.5*, and *Nkx2.5* gene. The finger tissues were homogenized and lysed by incubation in proteinase K buffere for 2h at 55^{o}C and 15min at 95^{o}C to stop the reaction. PCR experiments were carried out with required reagents, including 5 µl buffer (5X Green GoTaQ), 2.5 µl MgCl2, 0.1 µl each primer, 0.25 µl dNTP, 0.2 µl TaQ polymerase, 16 µl RNA- DNA-free water, and 1 µl DNA lysate. After that, the PCR products were loaded into 2% agarose gel and migrated by electrophoresis.

2. Histological analyses

To perform histological experiments, transverse or frontal cryosections were used. Firstly, harvested mouse hearts were fixed in PFA 4% for 2 hours under agitation in a cold room (4 ^{o}C), and then incubated in sucrose 15% in at least 2 hours at 4 ^{o}C and sucrose 30% overnight. The samples were embedded in OCT freezing media and snap frozen using dry ice before storage at -80 ^{o}C until sectionning. Eighteen micron sections were cut on a cryostat machine (CM-1900; Leica Microsystems, Germany), and were collected onto Superfrost Plus glass slides (Fisher Scientific).

Immunofluorescence on cryosection slices was carried out. In brief, the slices were permeabilized in a buffer solution composed of 0.2% Triton X-100 diluted in PBS 1X for 20 minute, and incubated in the saturation buffer, including 0.2% BSA and 0.05% saponine diluted also in PBS 1X for 1 hour. Specific primary antibodies were incubated overnight before washing 3 times for 5 minute each with PBS 1X, and incubated with secondary antibodies for 2h at room temperature. After washing secondary antibodies in PBS 1X 3 times for 5 minute each, nuclei staining was obtained by incubation with Hoechst solution for 20 minutes at room temperature. Finally, slides were mounted in fluomount G (SouthernBiotech, USA) and dried in air overnight. The images were digitized and analyzed under a microscope (Leica Apotome Z1, Leica Microsystems, Germany) using Zen software (ZEN-ZEISS Efficient Navigation, Carl Zeiss, France) and ImageJ (Fiji is just ImageJ) software.

3. Electrocardiogram (ECG)

ECG recording was applied to figure out the electrical activity though the mouse heart by using a digital acquisition and analysis system (AD Instruments). Recording of standard lead configurations from 3 lead wires were used to measure ECG lead II and lead III by connecting a "Dual Bio amplifier" to an "ECG Lead Switch Box". To start, mice were gently removed from their cage and positioned into the 5% isoflurane anesthesia chamber before putting on the ECG recording platform. Mouse was anaesthetized during whole recording time with 1-2% isoflurane in 700 ml O_2/min *via* facemask pipe. The body temperature was maintained by using a heat pad. To record lead II ECG, 3 needle electrodes are inserted subcutaneously in the left forelimb and into the right and left hindlimb, and secured with tape. Lead III was recorded by inserting needle electrodes in the right forelimb and each hindlimb, and also secured with tape. The surface ECG traces are filtered using a high pass setting of 0.03s, low pass setting of 120 kHz and recorded during 1 min after few minutes stabilization of the signal. After the recording, the anesthesia instruments were turned off, the limb electrodes were removed. The mouse wakes up very fast and then was returned to its cage. Each recording takes around 10 min in total including anesthetic induction and recovery time.

The recorded ECG is analyzed offline using Chart 5 for Window software (v 5.5.6 for Macintosh, AD Instruments) for examining unusually shape P, QRS, T or J waves and for time-

varying phenomenon. High pass filtering with cut-off frequency of 50 Hz, or no calculation was used for analyzing traces. Several values were measured including PR, QRS, QT, and RR. Among those values, only QRS was calculated by lead III, meanwhile others were calculated by lead II. The characteristic and meaning of the important values in ECG recording were presented in the table 1 below.

There is an important note regarding the mouse J wave. The principle and most of the marker wave in ECG recording are the same between human and mouse, except J wave which is just only present in mouse ECG (Boukens et al., 2014; Liu et al., 2004). The J wave corresponds to early ventricular repolarization in the mouse and follows by the S wave (Figure 11). It means that the ventricular repolarization phase of ECG is different in mice compare to human, and results in major consequence differences for the morphology of the ECG.

Table 1. The ECG measurement marker for calculating interval time

Name of interval measurement	Characteristic	Meaning in cardiac function
PR (milliseconds, ms)	Time interval between starting of P wave marker and the beginning of QRS marker	Atria activation and relaxation time
QRS (ms)	Time interval between starting of Q wave marker and ending of S when it crosses with baseline	Ventricle activation time
QT (ms)	Time interval between the first Q marker and the time when the T wave crosses the baseline	Ventricle activation and relaxation time
RR (ms)	Time interval between two R peaks	Time between two cycle of beating
Heart beat (beat per minute, bpm)	The reciprocal of the average RR interval between valid beats	Rhythm of the heart

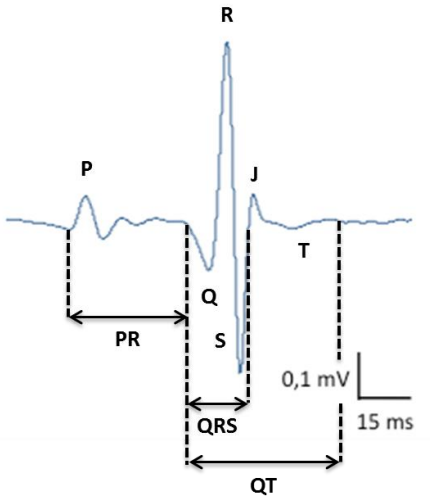

Figure 11. Mouse ECG recording in lead II and measurement

4. RNA isolation, cDNA synthesis, and quantification of gene expression

The mouse hearts were dissected and cutted into 6 different parts including the left and right atria (LA, RA), left ventricle (LV), right ventricle (RV), apex, and interventricular septum (IVS). Each dissecting part was put into 1.5 ml eppendorf tube, and frozen immediately in liquid nitrogen. The samples were stored at -80^{o}C until use.

Total RNA was isolated by using TRIzol Reagent (Invitrogen, Life technologies). The RNA extraction procedure follows manufacturer's protocol by Invitrogen (Life technology). In detail, each tissue sample was crashed mechanically and homogenized in 1ml of Trizol reagent, before adding 200 microliters chloroform. After centrifugation, the sample mixture was separated into 3 phases: a lower red phenol – chloroform phase, an interphase, and a colorless aqueous upper phase. The upper aqueous phase was moved into a phase-locked-gel tube and centrifuged in order to absorb remaining organic reagents (phenol, chloroform, salt, etc). The RNA exclusively in the aqueous phase was precipitated by adding 0.5 ml isopropanol. After centrifugation, RNA is often visible and forms a gel-like pellet in the bottom of the eppendorf tube. The RNA pellet was washed by centrifugation with 1 ml of 75% ethanol, and air dried. RNase-free water was used for the resuspension of the RNA pellet before incubating in a 55^{o}C water bath for 10 min. RNA samples were stored at -80 ^{o}C until process.

RNA concentration was then quantified by using the NanoDrop machine (NanoDrop ND-1000, ThermoScientific). The absorbance reading results are converted into concentration (ng/µl), and absorbance ratios of 260/280 and 260/230 are verified. A 260/280 ratio from 1.9 to 2.0 indicates that we had successfully extracted RNA of good purity.

In order to verify RNA integrity, Aligent RNA 6000 Nano kit (Agilent Technologies, Germany) was utilized on Agilent 2100 Bioanalyzer (Agilent technologies, Germany). RNA Integrity was validated based on traditional gel electrophoresis principles. The input RNA concentration was 25 – 500 ng/µL. There are 5 steps including preparing the gel, preparing the gel-dye mix, loading the gel-dye mix, loading the Agilent RNA 6000 nano marker, and loading the ladder and samples according to the manufacturer‟s protocol (Agilent RNA 6000 Nano Kit Quick Start Guide). RNA integrity number (RIN) from 1.8 to 2.0 indicates that we had successfully extracted total RNA without degradation.

5. cDNA synthesis and quantitative RT-qPCR

In order to synthesize cDNA, we used superscript VILO MasterMix (Invitrogen, Thermo Fisher Scientific, Netherlands). The composition for each reverse transcriptase reaction was1 µg of total RNA, 4 µL of master mix VILO, and Nuclease-free water for a final volume of 20 µl. The reaction was carried out according to the manufacturer‟s guidance including 10 min at 25 °C, 60 min at 42 °C, 5 min at 85 °C, and left at 4°C before storing at -20°C. cDNAs were diluted 5 times before using as template in real-time q-PCR.

To evaluate expression variation of candidate genes (Table 2), we carried out relative quantitation of gene expression using real-time quantitative PCR, by using SYBR Green PCR master mix (Applied Biosystem, Life technologies, UK). Stratagene‟s Mx3000P machine (Agilent technologies) was utilized for real-time detection of fluorescent signal emitted by amplicons. Two methodologies for relative quantitation of gene expression, relative standard curve method and comparative C_T method (ΔΔCt), were used. The relative quantity between test and control samples were calculated by normalizing with the *RPL32* housekeeping gene.

Table 2. List of genes and the primer sequences

	Primer F	Primer R	Product Length
Six1	TTAAGAACCGGAGGCAAAGA	GGGGGTGAGAACTCCTCTTC	154
Timp1	CGCATCAAGGAGCTCACC	CCTGCAGCCGCATTAAGT	61
Vav1	TAACAACCTGCTTCCCCAGG	CAGGGTGTAGATGACCTTTCCA	196
V-maf	AGACCACCTCAAGCAGGAGA	GGAGTCCCTTGGGTACATGA	154
Mcpt4	GTGGGCAGTCCCAGAAAGAA	GCATCTCCGCGTCCATAAGA	107
Bmp10	AACAAATTCGCCACAGACCG	TCAGCCATGACGACCTCTTC	164
Gbp1	GCAGAAGGGTGACAACCAGA	CCTGCTGGTTGATGGTTCCT	101
Myh7	CAACCTGTCCAAGTTCCGCA	TACTCCTCATTCAGGCCCTTG	135
Vsig4	CTCACCTATGGCCACCCCAC	CACCAAAACTTGCCTGTAGCC	117
Cd207	GTCCTCAGAATCGGAACAAAAGT	GCTCATTGTTCCCTGCGTTG	182
Rorb	TAGCTCCCGGGATAACAATG	GCCAGCTGATGGAGTTCTTC	180
Gcgr	AATGCCACCACAACCTAAGC	GCCCACACCTCTTGAACACT	180
Vgll2	CCCTACCACCAGAAACTAGCC	GCCCTCCTCTTCCTTGACAC	132
Prkcz	TGATTACCAGCGTGGATGCC	ACAAGGGTCACCTTCACTGT	125
RPL32	GCTGCTGATGTGCAACAAA	GGGATTGGTGACTCTGATGG	115
Nkx2.5	CAAGTGCTCTCCTGCTTTCC	CTTTGTCCAGCTCCACTGC	134

6. Microarray analysis

Total RNA extraction from LV in 3 groups of mice and 4 mice per group, including tamoxifen injected mice at E10 and E11 ($Nkx2.5^{\Delta trab}$), at E13 and E14 ($Nkx2.5^{\Delta comp}$), and noninjected control mice were used in the microarray experiment. Microarray hybridization was

performed by TGML platform (TAGC, Inserm, France) using the SurePrint G3 Mouse GE8x60K Microarray Kit which provides comprehensive coverage of genes and transcripts using the latest annotation databases, and following guidance of manufacturer and established protocols. Gene expression signal values were generated and normalized by the quantile method before applying filter to keep only probes overexpressed compare to the background in all the four replicates in each group. This filtered list was used as input file in TM4 Microarray Software Suite (www.tm4.org) with 1000 permutations number. Significance analysis of microarray (SAM) method and false discovery rate (FDR) 5% were applied for statistical test of significally expressed probes. The statistically significant list of genes was then used for biological themes in David database (https://david.ncifcrf.gov).

PART III. RESULTS

1. Introduction

As I mentioned in the chapter 2 of the introduction, the etiology of LVNC is still unknown. So far, there is no mouse model for studying specifically LVNC disease and the entire molecular pathways leading to this disease are not understood. Moreover, the origin, heterogeneity, and severity of LVNC ask important questions without answers or explanations up to now. For all these reasons, our main objective was to generate mouse models, which could be suitable models for studying the etiology of LVNC disease. The goal of my thesis project was to study functional defects and molecular pathways of these hypertrabeculated mouse models.

To generate mutant mice, we crossed *Nkx2.5*$^{flox/flox}$ with *Cx40*$^{Cre\text{-}ERT2}$ mice and induced the Cre activity by injecting tamoxifen at different time points during trabecular development. Our working hypothesis is that disturbances at different critical steps during trabecular development will result in different consequences, which could explain the pathological severity of LVNC. Thus, disturbing trabecular development at several steps, including when trabeculae are formed (*Nkx2.5*$^{\Delta trab}$), when trabeculae start to compact (*Nkx2.5*$^{\Delta comp}$), and when the compaction step is almost finished (*Nkx2.5*$^{\Delta VCS}$), could reveal the possible correlation between trabecular proliferation or compaction and severity in the LVNC disease. The level of *Nkx2.5* mRNA in mutant mice was quantified by qPCR proving that we were successful in deleting the gene in mutant mouse models depending on the timing of tamoxifen injection. Phenotypical characteristics of *Nkx2.5* mutant mice were studied by immunofluorescence experiments in 3-month-old mice and a follow-up of cardiac function was carried out in the same mice from 2-month to 12-month old. The results show that our mouse models, by the conditional deletion of *Nkx2.5* in the trabecular zone and the ventricular conduction system, are suitable for studying LVNC disease because they present functional and phenotypical characteristics of LVNC patients, including LV hypertrabeculation, fibrosis, and defects in cardiac conduction. Furthermore, the most severe phenotypes were seen after early embryonic deletion at E10-11. *Nkx2.5* deletion at E13-14 (Nkx2.5$^{\Delta comp}$) presented intermediate phenotypes, while mice deleted later at P1 (*Nkx2.5*$^{\Delta VCS}$) were quite normal in term of trabeculation, fibrosis area, and Purkinje fiber network. Additionally, in the follow-up of the cardiac function from 2-month to 12-month old mice, we could observe a progression and an adaptation of the phenotypes over time. These results are presented in the article 1, in which we characterized the cardiac function and the

molecular pathways in LVNC mouse models after the conditional deletion of *Nkx2.5* gene at critical steps during ventricular trabeculae development.

In this first article, we showed that different percentages of *Nkx2.5* deletion result in different levels of hypertrabeculation and severity in the pathological outcomes of LVNC. However, there is a remaining question on which levels of *Nkx2.5* expression cause hypertrabeculation. It means that we still do not know if a low expression level of *Nkx2.5* could lead to hypertrabeculation and cardiac functional defects. To answer this question, we characterized trabeculation and cardiac function in mice with different doses of *Nkx2.5* expression as described in the part 2 of the results. In these mice, *Nkx2.5* gene was not deleted, but the global level of *Nkx2.5* expression in the hearts was different due to alleles where the *Nkx2.5* locus was genetically modified. Immunofluorescence experiments were also carried out to quantify the level of trabeculation and number of Purkinje fibers. The results showed no significant hypertrabeculation in all groups, with a slight difference in the group of mice with the lowest level of *Nkx2.5* expression. Thus, hypertrabeculation can be obtained after the condictional deletion of *Nkx2.5* at the different steps of ventricular trabeculae development, but not when we reduce the level of *Nkx2.5* expression in the heart. Quantification of the number of Purkinje fibers showed a decrease in mice with a low expression of *Nkx2.5* gene. Thus, normal expression of *Nkx2.5* gene (100%) is required for maintaining the normal anatomical structures of the heart and the ventricular conduction system.

2. Results 1: Temporal deletions of *Nkx2.5* induce hypertrabeculation and progressive conduction defects and heart failure.

Minh T.H Nguyen[1,2*] , Caroline Choquet[1*], Pierre Sicard[3], Frank Kober[4], Isabelle Varlet[4], Pascal Rihet[2], Sylvain Richard[3], Catherine Nguyen[2], Monique Bernard[4], Robert G. Kelly[1], Nathalie Lalevée[2#], Lucile Miquerol[1#]

1- Aix-Marseille Univ, CNRS, IBDM, Marseille, France

2- Aix-Marseille Univ, INSERM, TAGC, Marseille, France

3- PHYMEDEXP, INSERM, CNRS, Université de Montpellier, CHU Arnaud de Villeneuve, Montpellier, France.

4- Aix-Marseille Univ, CNRS, CRMBM, Marseille, France

* These authors contribute equally to this work

 # Corresponding authors:

Lucile MIQUEROL, PhD

Aix Marseille Université, CNRS, IBDM UMR 7288, Campus de Luminy - Case 907, 13288 Marseille Cedex 9, France.

Fax: +33 4 91 26 93 16

Tel: +33 4 91 26 97 34

email: lucile.miquerol@univ-amu.fr

Nathalie Lalevée, PhD

Technological Advances for Genomics and Clinics (TAGC)- UMR/INSERM 1090- Campus de Luminy Case 928- 13288 Marseille Cedex 9, France

Tel. +33 491 82 87 25

Fax. +33 491 82 87 01

email: nathalie.LALEVEE@univ-amu.fr

Abstract

LVNC is a rare cardiomyopathy, characterized by hypertrabeculation and deep trabecular recesses in the left ventricle. It is still unclear whether LVNC results from a defect occurring during cardiac development and if the severity of this pathology depends on the embryonic stage at which arrest of myocardial compaction occurs. Here, we describe the pathological consequences of ventricular hypertrabeculation on the cardiac function of adult mouse models.

To establish a LVNC mouse model, we generated specific *Nkx2.5* conditional knockout leading to the deletion of *Nkx2.5* allele in atria and trabecular derived cardiomyocytes at embryonic stages, when trabeculae arise, during fetal stage, when they start to compact, or at neonatal stages, when the heart has almost finished to compact.

The loss of *Nkx2.5* at embryonic stages provokes a hypertrabeculated phenotype associated with an important subendocardial fibrosis and Purkinje fibers hypoplasia. These phenotypes are milder when the deletion of *Nkx2.5* occurred at fetal stages and deletion only in the ventricular conduction system, at neonatal stage, leads to a progressive disappearance of this tissue without signs of hypertrabeculation nor fibrosis. However, all these mice develop progressively conduction defects and heart failure. The analysis of molecular pathways, associated to these cardiac phenotypes, demonstrated that *Nkx2.5* plays pleiotropic roles during ventricular trabeculae development.

This study demonstrates that deletion of *Nkx2.5* during trabecular development represents a good mouse model for studying the cellular and molecular mechanisms associated with LVNC. Furthermore, our results show a differential phenotype associated with the timing of deletion of *Nkx2.5* with a more pronounced disorder when induced at earlier stages.

Introduction

Left ventricular non-compaction (LVNC) is a rare cardiomyopathy characterized by an extremely thick sub-endocardial layer with prominent trabeculation and deep recesses that communicate with the left ventricular (LV) cavity (Jenni et al. 2007). LVNC may appear in adult life where it has been described as an acquired phenotype isolated or in association with cardiomyopathy (Towbin 2010). LVNC is also described as a genetic disorder caused by mutations in genes encoding sarcomere, cytoskeletal, nuclear membrane, ionic channels and chaperon proteins (Klaassen et al. 2008, Towbin 2014). LVNC can lead to heart failure, thromboembolism and malignant arrhythmia (Stollberger et al. 2002). Moreover, the presence of LVNC is significantly associated with a rapid deterioration of LV function and higher mortality when associated with abnormal ECG measurements (Kimura et al. 2013). This high mortality rate is also found in cases of isolated LVNC in association with arrhythmias in children (Brescia et al. 2013) or in adult patients (Bhatia et al. 2011). All these data show the strong heterogeneity of the pathological outcomes among LVNC patients and suggest that LVNC has a higher incidence of cardiac death when associated with cardiac dysfunction and arrhythmias.

The presence of ventricular trabeculae is a normal component of ventricular myocardium during embryonic development (Sedmera et al. 1996). In contrast to fish and reptiles, ventricular trabeculae in mammals are transient structures, disappearing to give rise to an efficient and smooth muscular wall by a process of compaction that initiates during fetal stages and ends after birth. During this step, endocardial cells are progressively incorporated into the myocardium to form numerous coronary vessels (Tian et al. 2014). Studies of comparative anatomy between human cases of LVNC and embryonic or lower vertebrate hearts strongly suggest that this anomaly may result from an arrest of myocardial compaction during embryogenesis (Freedom et al. 2005). However, this hypothesis has never been demonstrated. Moreover, trabecular development is directly coupled with development of the ventricular conduction system. Indeed, trabeculae acquire fast-conducting electrical properties through the expression of Connexin40 (Cx40) and so become the preferential conduction pathway in embryonic heart (Miquerol et al. 2011). The function of the conduction system is to generate and orchestrate the propagation of the electrical activity through the heart in order to coordinate the sequential contraction of atria and ventricles. Indeed, the cellular and molecular mechanisms involved in the compaction of

ventricular trabeculae and the acquisition of the electrical function of the ventricular myocardium are still unknown.

The transcription factor *Nkx2.5* is an important regulator of ventricular trabeculae and conduction system development. In transgenic mice the expression of a mutant version of *NKX2.5* that is unable to bind DNA, similar to that found in patients, results in profound cardiac conduction defects and heart failure (Kasahara et al. 2001). Homozygous *Nkx2.5* null mutant mice die around embryonic day (E) 10. In contrast *Nkx2.5*$^{+/-}$ embryos and mice appear normal and reproduce the phenotype observed in patients, including atrial septal defects and conduction disturbances (Tanaka et al. 2002, Jay et al. 2003). Electrocardiogram analysis reveals that *Nkx2.5* haploinsuficient mice present a prolonged QRS and a progressive elongation of the PR. These mice display ventricular conduction defects that can be correlated with hypoplastic development of the His-Purkinje system. More recently, mutations of *NKX2.5* have been identified in LVNC patients indicating a role of this transcription factor in non-compaction (Costa et al. 2013, Ashraf et al. 2014). Indeed, the conditional knock-out of *Nkx2.5* throughout the ventricular myocardium showed that this deficiency provokes a hypertrabeculated phenotype resulting from proliferation defects of myocardial cells (Pashmforoush et al. 2004).

One hypothesis to consider is that the severity of LVNC depends on which embryonic stage the arrest of myocardial compaction occurs. Our aim was to study the pathological evolution of LVNC by characterizing functional defects and identifying molecular mechanisms in mouse models with abnormal ventricular trabeculae development. To understand what critical step of cardiac development is the most sensitive to provoke ventricular non-compaction, we inactivate the expression of *Nkx2.5* gene, in a temporal and spatial manner. This study demonstrates that deletion of *Nkx2.5* during trabecular development represents a good mouse model for studying the cellular and molecular mechanisms associated with LVNC. Furthermore, our results show a differential phenotype associated with the timing of deletion of *Nkx2.5* with a more pronounced disorder when induced at earlier stages.

Material and Methods

Generation of mouse models

Animal procedures were approved by the ethic committee for animal experimentation from French ministry (n° 01055.02). *Cx40-cre,* and *Rosa26-YFP* mouse lines were genotyped as previously reported (Srinivas et al. 2001, Beyer et al. 2011). A conditional null allele of *Nkx2.5* was generated as described recently (*Nkx2.5flox)* (Furtado et al. 2016). To remove the Frt-flanked neomycin cassette present in this allele, *Nkx2.5flox* mice were bred with a ubiquitous flipase mouse line (ACTB:FLPe) (Rodriguez et al. 2000). The *Floxed-Nkx2.5-Neo* allele was used in the subsequent breedings with the *Cx40-cre* mouse line. To delete the *Floxed-Nkx2.5-Neo* gene, tamoxifen was injected intraperitoneally to pregnant females (200µl) for two consecutive days or to newborn (10µl) in a single injection. Tamoxifen (T-5648, Sigma) was dissolved at the concentration of 20mg/ml in ethanol/sunflower oil (10/90). After tamoxifen treatment to pregnant females, newborn mice were recovered after caesarian and gave for adoption to CD1 females. Fifty mice were assigned to four groups: $Nkx2.5^{\Delta trab}$ who received tamoxifen injections at embryonic stages (E10.5 and E11.5), $Nkx2.5^{\Delta comp}$ who received tamoxifen injections at fetal stages (E13.5 and E14.5), $Nkx2.5^{\Delta trab}$ who received tamoxifen injection at postnatal day 1, and control mice without tamoxifen injection.

Macroscopic and histological analyses

Macroscopic examination of the internal surface of the ventricles was previously described (Miquerol et al. 2004). For histological studies, adult hearts were dissected, fixed for four hours in 4% paraformaldehyde (vol/vol) in PBS, washed in sucrose gradient, then embedded in OCT and cryosectioned. To quantify interstitial fibrosis, transverse sections were counterstained with wheat germ agglutinin-TRITC (WGA-TRITC from Sigma-Aldrich) as described previously (Emde et al. 2014). For immunofluorescence, sections were permeabilized in PBS 1X / 0.2% Triton X100 for 20min and incubated for 1 hour in saturation buffer (PBS 1X / 3% BSA / 0.1% Triton X100). The primary antibodies were incubated in saturation buffer for overnight at 4°C.

Secondary antibodies coupled to fluorescent molecules were incubated in saturation buffer and after washes, hearts were observed under a Zeiss Apotome microscope.

For whole-mount immunofluorescence, adult hearts were pinned on petri dish to expose the left ventricle and fixed in 4% paraformaldehyde for 2 hours at 4°C, washed in PBS, permeabilized in PBS 1X / 0.5% Triton X100 for 1h and incubated for 3 hours in saturation buffer (PBS 1X / 3% BSA / 0.1% Triton X100). The primary antibodies were incubated in saturation buffer for 24 hours at 4°C. Secondary antibodies coupled to fluorescent molecules were incubated in saturation buffer and after washes, hearts were observed under a Zeiss LSM780 confocal microscope.

Antibodies used in this study are specific to Nkx2.5 (Sc8697 Santa-Cruz), GFP (AbD Serotec), RFP (Rockland), Contactin-2 (AF1714 R&D system), Pecam-1 (MEC13.3-BD Pharmingen), endoglin CD105 (MJ7/18-DSHB), VEGFR2 (AF644-R&D SYSTEMS), □-Smooth Muscle Actin (F3777-SIGMA).

Cardiac magnetic resonance imaging (MRI)

MRI was carried out every two months on the same animal groups from 2 to 12 months-old mice. The experiments were performed on a Bruker Biospec Avance 4.7 T/30 imager (Bruker Biospin GmbH, Ettlingen, Germany), as previously described (Kober et al. 2005). Anesthesia was maintained during MRI with 1.5-2% Isoflurane in a constant flow of room air (270 ml/min) through a nose cone using a dedicated vaporizer (univentor anaesthesia unit, univentor high precision instrument Zejtun, Malta). Temperature was maintained at 39°C. Breath and cardiac rhythm were monitored and signals were used to trigger MRI acquisition using a monitoring and gating system (SA Instruments, Inc. Stony Brook, NY, USA). Cine MR imaging (ECG gating, repetition time 5 ms, echo time 1.51 ms, flip angle 20°, slice thickness 1 mm, pixel size 1×1 mm^2) were performed in short axis view. Ten phases per heartbeat were acquired from base to apex to cover the whole left ventricle. High resolution cine imaging (ECG gating, repetition time 15 ms, echo time 1.68 ms, flip angle 30°, slice thickness 1.1 mm, pixel size 0.086×0.086 mm^2) in short axis view, at the mid base-apex location was performed to evaluate trabeculation in each mouse.

Surface Electrocardiography

Surface ECGs were performed on anesthetized mice. An induction with 5% isoflurane was followed by maintenance at 1 to 2% in a constant flow of oxygen at 700 ml/min. ECGs were recorded every two months from 2 to 12 months using a bipolar system in which the electrodes were placed subcutaneously at the right (negative) and left forelimb (reference) and the left hindlimb (positive) for lead II and at the right (reference) and left forelimb (negative) for lead III. Electrodes were connected to a Bioamp amplifier (AD Instruments) and were digitalized through an A/D converter ML 825 PowerLab 2/25 (AD Instruments). Digital recordings were analyzed with Chart software for windows version 5.0.2 (AD Instruments). Events were registered to 100 K/s and were filtered to 50 Hz. ECG recordings were obtained for 1 min after stabilization of the signal. Post-analysis was performed for heart rate, PR, QRS, QT intervals, P duration, QRS and P amplitudes.

Echocardiography

Echocardiography was performed using a Vevo 2100 ultrasound system (VisualSonics, Toronto, Canada) equipped with a real-time micro-visualization scan head probe (MS-550D) operating at a frame rate ranging from 740 frames per sec (fps). Mice were anesthetized with isoflurane (IsofloH, ABBOTT S.A, Madrid, Spain) at a concentration of 3.5% for induction and between 1 to 1.5% for maintenance during the analysis with 100% Oxygen. Each animal was placed on a heated table in supine position with extremities tied to the table through four electrocardiographic leads. The chest was shaved using a chemical hair remover (Veet, Reckitt Benckise, Granollers, Spain). Ultrasound gel (Quick Eco-Gel, Lessa, Barcelona, Spain) was applied to the thorax surface to optimize the visibility of the cardiac chambers. The heart rate (HR) and respiratory rate of mice were recorded during the echocardiographic study. Two mice were excluded from the study due to very low HR. Echocardiograms were acquired at baseline. Left ventricular (LV) characteristics were quantified according to the standards of the American Society of Echocardiology and the Vevo 2100 Protocol-Based Measurements and Calculations guide, as described in the following paragraphs. LV diameters were measured on a two-dimensional (B-

mode) parasternal long axis and short axis view. The functional parameters of the heart were evaluated based on LV diameter measurements.

Microarrays

Total RNA was isolated from LVs of 6 month-old control, *Nkx2.5*$^{\Delta trab}$ and *Nkx2.5*$^{\Delta comp}$ mice (n=4 for each group) using TRIzol Reagent according to the manufacturer's procedure (Invitrogen, Life Technologies). The quality of RNA was confirmed on the Agilent 2100 Bioanalyzer (Agilent technologies, Germany) with the Agilent RNA 6000 Nano chips and the concentration of RNA was determined by reading absorbance at 260/280 nm on NanoDrop (ND-1000, ThermoScientific). RIN (RNA Integrity Number) was ranged from 1.8 to 2.0 indicating the good integrity of RNA without degradation. cDNA synthesis was carried out with superscript VILO MasterMix (Invitrogen, Thermo Fisher Scientific, Netherlands) on 1 µg of total RNA in 20 µl of final volume. Microarray hybridization, washing and scanning were performed by TGML platform (TAGC, UMR 1090-Inserm, France) using the SurePrint G3 Mouse GE8x60K Microarray Kit (Agilent Technologies, Santa Clara, CA) and Agilent DNA Microarray Scanner using the Agilent Feature Extraction Software (Agilent technologies). Quantile normalization was applied to sample data to correct for global intensity and dispersion. Significant Analysis of Microarray (SAM) procedure was applied with a False Discovery Rate (FDR) at 5% to look for mutant specific variation in gene expression in the dataset. Hierarchical clustering of the samples was obtained with TM4 Microarray Software Suite V4.9 (https://www.tm4.org) using average linkage clustering metrics and Pearson correlation for the distance. We identified functional annotations for the clusters using DAVID Bioinformatics Resources 6.7 (https://david.ncifcrf.gov) and gene network design was performed with Cytoscape (http://www.cytoscape.org).

qPCR

On the same cDNA samples used for microarray experiments, we performed quantitative real-time PCR (qPCR) analyses of genes and housekeeping genes using SYBR Green PCR master

mix (Applied Bio-systems, Life technologies, UK) on the Stratagene Mx3000P (Agilent Technologies). Supplementary Table S1 summarizes primer sequences.

Results

Temporal deletions of Nkx2.5 in ventricular trabeculae target different cardiac regions

Our strategy to create series of LVNC adult mouse models is summarized in Figure 1A. We crossed *Floxed-Nkx2.5-neo* alleles with *Cx40-creERT2* mice to generate the conditional knockout of this gene specifically at critical step of ventricular trabeculae development or in the ventricular conduction system. To remove *Nkx2.5* during the formation of ventricular trabeculae, tamoxifen was injected into pregnant females at E10.5 and E11.5 and homozygous mutants were subsequently designed as $Nkx2.5^{\Delta trab}$. To remove *Nkx2.5* during the step of ventricular compaction, tamoxifen was injected at E13.5 and E14.5, and these mice were designed as $Nkx2.5^{\Delta comp}$. Finally, *Nkx2.5* was specifically deleted from the entire ventricular conduction system after one tamoxifen injection to newborn pups at P1 and these mice are named $Nkx2.5^{\Delta VCS}$. Control mice correspond to mice of the same genotype $Nkx2.5^{fl/fl}::Cx40^{cre/+}$ that did not receive tamoxifen injections. All these mice were viable and kept for 12 months during which a follow up of cardiac function were realized every two months. During this period, only 2 out of 68 died prematurely at adult stage.

The efficiency of Nkx2.5 deletion was verified by qPCR analysis to quantify the level of Nkx2.5 expression from mRNA extracted from atria where *Cx40* is ongoing expressed. A strong reduction of *Nkx2.5* transcripts is observed in $Nkx2.5^{\Delta trab}$ and $Nkx2.5^{\Delta comp}$ mutants after two consecutive tamoxifen injections at embryonic or fetal stages, while this reduction is less important in $Nkx2.5^{\Delta VCS}$ mutants after a single injection at postnatal stage (Figure 1B). Then we performed a genetic tracing analysis of *Cx40-cre* derived cells to check the extension of cardiac tissue affected by *Nkx2.5* deletion. To define the progeny of ventricular trabeculae during development, we crossed *Cx40-cre* mice with *Rosa26-YFP* reporter mice and observed the

localization of YFP-positive cells in adult hearts by immunofluorescence on sections after tamoxifen induction at E10, E14 or P1. Numerous YFP-positive cardiomyocytes were observed in the apex, the papillary muscles and left ventricular free wall when the tamoxifen is injected at embryonic or fetal stages while these cells are restricted to the ventricular conduction system as shown with the co-expression of RFP present in the *Cx40-cre* allele (Figure 1C). These data show that ventricular trabeculae at embryonic and fetal stages largely participate to the morphogenesis of the papillary muscles and ventricular free wall but not to the interventricular septum. So, conform to *Cx40* expression pattern, this strategy is well appropriate to target the conditional knockout of *Nkx2.5* in the ventricular trabeculae or in the conduction system depending on the time of tamoxifen injection. As summarized in figure 1D, these results show that a tamoxifen injection at embryonic stage touches a broader population of cardiomyocytes derived from ventricular trabeculae in the apex and middle part of the heart than after injection at fetal stage. Nevertheless, a postnatal injection will only target cardiomyocytes of the ventricular conduction system.

The level of hypertrabeculation is dependent on the time of tamoxifen injections

To evaluate the morphological consequences of the loss of *Nkx2.5* in ventricular trabeculae or in the VCS, we looked at the anatomy of the left ventricle in adult mice. Hearts were opened to expose the left ventricle cavity with the left ventricular free wall on the left and the interventricular septum (IVS) on the right (Figure 2A). In control mice, the papillary muscles (stars) form two straight columns on the free wall and the endocardial surface of the IVS is particularly smooth. In *Nkx2.5* mutants, papillary muscles are enlarged and not well formed (separated in few strands), also numerous trabeculations are present in the apex of both sides of left ventricle, and these anatomical features are more pronounced in $Nkx2.5^{\Delta trab}$ than in $Nkx2.5^{\Delta comp}$ mutants. No anatomical defect in papillary muscles or trabeculations was observed in $Nkx2.5^{\Delta VCS}$ mutants. We confirmed these results by histological analysis on transverse sections of adult hearts (Figure 2B). To visualize ventricular trabeculae, we performed a co-immunofluorescence using two antibodies against endothelial cells, *i.e.* Endoglin (Eng) and

VEGFR2, to distinguish the $Eng^{+}/VEGFR2^{-}$ endocardium from $VEGFR2^{+}/Eng^{low}$ subendocardial endothelial cells. This staining shows the presence of numerous invaginations of the endocardium and several isolated trabeculations in the ventricular lumen (arrows in figure 2B) in the apex of both *Nkx2.5*$^{\Delta trab}$ and *Nkx2.5*$^{\Delta comp}$ mutants in comparison to control or *Nkx2.5*$^{\Delta VCS}$ hearts. To quantify this hypertrabeculated phenotype, we used two different criteria, the length of the endocardium and the number of isolated trabeculae, both measurements were realized at two levels of the heart, in the apex or at the mid level. In figure 2C, the graph shows that the lengths of the endocardium measured in the apex and at the mid level, are superior in *Nkx2.5*$^{\Delta trab}$ and *Nkx2.5*$^{\Delta comp}$ mutants in comparison to control or *Nkx2.5*$^{\Delta VCS}$ hearts. The number of isolated trabeculae is also larger in *Nkx2.5*$^{\Delta trab}$ and *Nkx2.5*$^{\Delta comp}$ mutants in comparison to control and *Nkx2.5*$^{\Delta VCS}$ hearts and this increase is more important in the apex than at the mid level for both mutants (Figure 1D). This result confirms the observation of numerous trabeculations in the apical part of the ventricle by anatomical studies. In summary, both criteria demonstrate that a more severe hypertrabeculation is obtained in mutants when *Nkx2.5* is deleted at embryonic stage rather than at fetal stage and that the postnatal loss of *Nkx2.5* in the VCS does not provoke the apparition of this phenotype.

Nkx2.5-induced hypertrabeculation is accompanied by subendocardial fibrosis and vascular defects

To study this cardiac phenotype in more details, we performed immunofluorescence on transverse sections using specific markers such as WGA (Wheat germ agglutinin), a lectin used to quantify cardiac fibrosis (Emde et al. 2014), Pecam-1, VEGFR2 or Endoglin to detect endothelial cells and SMA (Smooth Muscle Actin) to stain smooth muscle cells serving for the identification of coronary arteries. Important subendocardial fibrosis is detected in *Nkx2.5*$^{\Delta trab}$ and *Nkx2.5*$^{\Delta comp}$ mutants while no evident sign of fibrosis was observed in *Nkx2.5*$^{\Delta VCS}$ or control mice (Figure 3A). This interstitial fibrosis was quantified by measuring the percentage of fibrotic area in the left ventricle and shows a more extended fibrosis in *Nkx2.5*$^{\Delta trab}$ than in *Nkx2.5*$^{\Delta comp}$ mutant hearts (Figure 3D). Knowing that the formation of coronary vasculature accompanied the

postnatal ventricular compaction (Tian et al. 2014), we looked at the development of coronary arteries by counting the number of arteries identified by SMA staining (Figure 3B). We then compared the density of coronary arteries in the left ventricular free wall to the density in the interventricular septum as an individual reference (Figure 3E). We did not observed significant difference in the density of coronary arteries in these mice. However, we observed a vascular phenotype in these mutants using Endoglin and VEGFR2 markers. As previously described, Endoglin expression in endothelial cells is strong in veins and endocardium and low in capillaries or arteries while VEGFR2 is strongly expressed in capillaries and not in arteries or endocardium (Miquerol et al. 2015). In Figure 3C, large vessels with strong expression of Endoglin (arrows) are detected in the subendocardial myocardium. These vessels are negative for VEGFR2 and not supported by SMCs suggesting that they may correspond to veins or to deep invaginations of endocardial cells forming endocardial islets. Quantification of these endocardial islets indicates that their number is larger in *Nkx2.5*$^{\Delta trab}$ and *Nkx2.5*$^{\Delta comp}$ mutants than in control or *Nkx2.5*$^{\Delta VCS}$ hearts (Figure 3F). In contrast to isolated trabeculations, the presence of these endocardial islets is more prominent in the mid ventricle than in the apex. However, this phenotype is still more pronounced in *Nkx2.5*$^{\Delta trab}$ than in *Nkx2.5*$^{\Delta comp}$ mutants suggesting that this phenotype is also related to hypertrabeculation.

Nkx2.5-induced hypertrabeculation is accompanied by hypoplasia of the ventricular conduction system

To visualize if the Purkinje fiber network is affected in *Nkx2.5*-induced hypertrabeculation mouse models, we carried out whole-mount immunofluorescence using contactin-2 (Cntn-2) marker on opened left ventricle. In control hearts, Cntn-2 is detected in the entire VCS including the atrioventricular bundle (AVB), left bundle branch (LBB) and Purkinje fibers (PF) (figure 4A). In mutants with *Nkx2.5* deletion induced at embryonic or fetal stages, the PF network is strongly reduced while the LBB and AVB develop normally. In contrast, the PF network is less affected in *Nkx2.5*$^{\Delta VCS}$ mutants neither the AVB nor LBB. These data suggest that the loss of Nkx2.5 at postnatal stage does not disturb the formation of the PF network. To analyze the morphological

evolution of the VCS at later stages, we performed immunofluorescence on sections from 12-month old mice and stained for Cntn-2 and SMA. This staining on sections shows a strong reduction of PF network in all Nkx2.5 mutants including those induced at postnatal stage (Figure 4C). Also, we detect a reduced AVB in *Nkx2.5*$^{\Delta Comp}$ and *Nkx2.5*$^{\Delta VCS}$ mutants induced at fetal or postnatal stages but not in control or *Nkx2.5*$^{\Delta trab}$ hearts. These results demonstrate a progressive loss of the conduction system in compartments where *Nkx2.5* is deleted suggesting a major role for this transcription factor in the maintenance of the entire VCS in old mice.

Nkx2.5-induced hypertrabeculation is associated with conduction defects and progressive heart failure

To study the possible impact of *Nkx2.5* deficiency on the pathological evolution of hypertrabeculation, we realized a follow up of the cardiac morphology and function in the same mice over a year using cine-MRI. We used this non-invasive imaging technique to compare the trabecular morphology between the different *Nkx2.5* mutant groups. High-resolution cine-s images reveal the presence of distinct trabeculations in the LV of *Nkx2.5*$^{\Delta trab}$ and *Nkx2.5*$^{\Delta comp}$ mutants in comparison to the smooth endocardium observed in *Nkx2.5*$^{\Delta VCS}$ and control hearts (Figure 5A). The follow-up of these trabeculations from 2 to 12 month-old does not show morphologic evolution in term of number or size. Moreover, these images pointed out the enlarged and divided papillary muscles in *Nkx2.5*$^{\Delta trab}$ and *Nkx2.5*$^{\Delta comp}$ mutants as we described previously by anatomical analyses (Figure 2). These results show that the level of hypertrabeculation induced by the conditional inactivation of *Nkx2.5* in ventricular trabeculae at embryonic or fetal stages is stable over a year suggesting no morphological evolution with aging. Several cardiac function parameters were measured from these CMR images and the data measured at two and ten months are summarized in Table 1. The graph in figure 5B represents the follow-up of the ejection fraction (EF) calculated from MRI analyses performed on the same groups of animals every two months. The EF of *Nkx2.5*$^{\Delta trab}$ mutants is reduced in comparison to the other groups and is constant over time with a mean of 53% in 12-month-old mice. The EF is similar in *Nkx2.5*$^{\Delta comp}$, *Nkx2.5*$^{\Delta VCS}$ and control mice until 6 months, after we observed a slight

decreased to 60% in control and a more important decrease in both mutants reaching the same level of EF than in *Nkx2.5*$^{\Delta trab}$ mutants. These results show a progressive decrease in EF from 8 months for *Nkx2.5*$^{\Delta comp}$ and *Nkx2.5*$^{\Delta VCS}$ mutants.

We next investigated the consequences of *Nkx2.5* deficiency on cardiac electrical activity by measuring surface electrocardiograms. A follow up of surface ECGs was performed in the same group of mice over one year in which EF was determined by echocardiography at 12 months.

The heart rate is similar in mutants and control mice suggesting that basal pacemaker activity is not impacted by *Nkx2.5* gene deletion in *Cx40* expressing cells (Table 2). In contrast, electrical conduction in *Nkx2.5*$^{\Delta trab}$ and *Nkx2.5*$^{\Delta comp}$ mutant hearts is disturbed as shown by 1st degree atrioventricular blocks (*i.e.* an increase in the PR interval) (Figure 6E and Table 2). The PR interval in *Nkx2.5*$^{\Delta VCS}$ is the same than in control mice (Figure 6E). To complete the atrial conduction characterization, we also measured the P wave amplitude and duration that present no difference with the control mice (Table 2). The QRS complexes, measured in lead III, are broaden since 2 months in *Nkx2.5*$^{\Delta trab}$, since 4 months in *Nkx2.5*$^{\Delta comp}$ and since 12 months *in Nkx2.5*$^{\Delta VCS}$ when compared to control mice (Figure 6F). This evolution of QRS intervals is comparable when measured in lead II (Table 2) and illustrates bundle branch blocks in mutants when compared to control mice. The QRS amplitudes are similar in mutants and control mice but intrinsic variability is present in 80% of *Nkx2.5*$^{\Delta trab}$, in 75% of *Nkx2.5*$^{\Delta comp}$ and 50% of *Nkx2.5*$^{\Delta VCS}$ mutant mice as illustrated for *Nkx2.5*$^{\Delta trab}$ in Figure 5B. Regarding the morphology of QRS complexes, only 2 control mice present defects since 10 months with negative and inseparable J and T waves but PR and QRS intervals are normal. One of them shows also a QT elongation at 12 months and both have also a moderated lowered ejection fraction (EF at 50 and 60%). ECGs in all *Nkx2.5*$^{\Delta trab}$ mutants exhibit high defects in QRS morphology with negative and inseparable J and T waves, no or very small S wave, very large R wave in lead II (Figure 6B) or Q wave in lead III. The PR and QRS intervals are broaden since 2 months and for 60% of them, QT interval is also higher than in control mice. A large decrease of EF, ranging from 60 to 31 %, is associated with these electrical defects (Table 2). In *Nkx2.5*$^{\Delta comp}$, the phenotype observed is less pronounced than in *Nkx2.5*$^{\Delta trab}$, with negative and inseparable J and T waves observed in only 50% of mice and after 4 months for one animal (Figure 6C). QRS duration is prolonged in all *Nkx2.5*$^{\Delta comp}$ mutant mice but only 50% of them present an elongated PR and QT intervals.

Enlarged R and Q waves in lead III are observed in 75% of mice and EF varies from 70 to 40%. In *Nkx2.5*$^{\Delta VCS}$ negative and inseparable J and T waves are observed in 75% of mice, accompanied by an elongation of PR and QT intervals but only 50% of mice show an increased QRS (Figure 6D). The EFs range from 37 to 60% (Figure 6H).

These results demonstrate important disorders in ECG resulting from many defects of conduction in *Nkx2.5* deficient mice. In particular, the prolonged QRS interval associated with enlarged Q and R waves and normal or absent S wave support the hypothesis of a left bundle branch block. *Nkx2.5*$^{\Delta trab}$ is the most affected mutant mice with the earlier disturbance of electrical activity and the lowest EF suggesting that conditional inactivation of *Nkx2.5* in ventricular trabeculae at embryonic stage leads to the highest prevalence of heart failure. The phenotypes in *Nkx2.5*$^{\Delta comp}$ and in *Nkx2.5*$^{\Delta VCS}$ are almost similar although delayed and less strong.

Molecular signaling associated with Nkx2.5-induced hypertrabeculation

In order to identify transcriptional changes associated with the non-compaction cardiomyopathy, we performed a microarray analysis on LVs from *Nkx2.5*$^{\Delta trab}$ and *Nkx2.5*$^{\Delta comp}$ adult hearts. We searched for genes differentially expressed in these mutants compared to control and associated with the different observed phenotypes. To this purpose, we used the SAM (Significant Analysis of Microarrays) procedure with a FDR (False Discovery Rate) at 5% showing 679 significant probes. A hierarchical clustering in both dimension (samples and genes) showed a clear differentiation between the 3 groups without any degree of overlap (Figure 7A). An unsupervised hierarchical clustering based on the similarities of expression was also performed and gene ontology analysis, made with David Database, indicated a clear difference of functional pathways represented in these 4 clusters (Figure 7A, 7B). As presented in Figure 7B, Cluster I shows genes down-regulated in both mutants linked essentially to ion binding and transport, calcium binding and transmembrane transport; Cluster II represents genes up regulated in *Nkx2.5*$^{\Delta comp}$ and linked essentially to intracellular signaling cascades; Cluster IV corresponds to genes up-regulated in both mutants and associated to cardiovascular development, inflammatory processes and extracellular matrix remodeling. In Figure 8A, Venn diagrams show the number of genes (corresponding to the 679 significant probes) significantly up- and down-regulated in *Nkx2.5*$^{\Delta trab}$

vs control (207 and 105 genes respectively), in *Nkx2.5*$^{\Delta comp}$ *vs* control (174 and 68 genes respectively) and in *Nkx2.5*$^{\Delta trab}$ *vs Nkx2.5*$^{\Delta comp}$ (26 and 19 genes respectively). It appears that only 3 out of the 22 326 screened genes were jointly up-regulated in the three conditions, no common down-regulated gene was found.

To confirm microarray data, we selected 14 genes most up- or down-regulated and on the basis of their cardiovascular-related function. qPCR experiments were performed with the same RNA samples as those used for microarray experiments. Among the genes up-regulated in *Nkx2.5*$^{\Delta trab}$ *vs* control, *Vav-1*, *Timp1* and *Six1* transcripts were quantified. Regarding the up- and down-regulated genes in *Nkx2.5*$^{\Delta comp}$ *vs* control, *Gbp1*, *Bmp10* and *Mcpt4* transcripts were investigated. We selected also lists of genes in the common parts of the Venn diagram like *Prkcz*, *Cd207*, *Vsig4*, and *Myh7* that are deregulated in both mutants *vs* control. V-maf is specifically deregulated in *Nkx2.5*$^{\Delta trab}$. And finally, we looked for the expression of the 3 transcripts corresponding to the 3 genes jointly up-regulated in the three conditions, *Vgll2*, *Gcgr* and *Rorb*.

Results obtained with real-time RT-PCR analysis are reported Figure 7C and confirm the microarray results with regard to fold change and significance.

To get a comprehensive overview of functional patterns associated with the non-compaction cardiomyopathy, we used Cytoscape in combination with functional annotations given by David Database from the lists obtained with Venn diagrams. The integrating network presented Figure 8B shows the deregulated genes related to significant functional pathways for the 3 conditions tested in Venn diagrams. In particular, we clearly see that in *Nkx2.5*$^{\Delta trab}$ numerous deregulated genes are implicated in cardiovascular differentiation and development, in cell death and immune response compared with control mice. Altogether, our results show that the early deletion of *Nkx2.5* at the embryonic stage disturbed the normal development and differentiation of the cardiovascular system and the pathways implicated in these processes remain disrupted at the adult stage. In parallel, this deletion leads also to the activation of immune response and cell death pathway that probably participate to the remodeling of the cardiac tissue. In *Nkx2.5*$^{\Delta comp}$ *vs* control, we found many deregulated genes with a role in vascular development and in response to hypoxia. Additionally, pathways concern extracellular matrix organization and calcium binding that are essential for development of cardiovascular tissues and cardiac function. These data support the idea that *Nkx2.5* deletion performed later in the development, at the fetal stage,

affects the vascular development that usually occurs at this stage and remodeling of vasculature persists at the adult stage. The genes that are significantly different in both mutant mice are implicated in immune response, extracellular matrix organization, calcium binding and regulation of growth. We observed defects in *Nkx2.5*$^{\Delta trab}$ and in *Nkx2.5*$^{\Delta comp}$ that are different like for hypoplasia, or more severe phenotypes in *Nkx2.5*$^{\Delta trab}$, in particular for fibrosis development or for conduction defects in which these pathways could participate.

Discussion

The relatively recent interest of clinicians in LVNC comes from the increasing number of patients presenting signs of hypertrabeculation in the last 25 years, due to significant improvements in cardiac imaging using echocardiography or cardiac magnetic resonance imaging (CMR). However, the numerous variants of this anomaly raise major problems for clinicians concerning its pathological nature. This wide spectrum of clinical signs makes prognosis of LVNC difficult. To understand the etiology of this anomaly, the mouse presents several advantages through the different genetic manipulations and developmental studies that can be performed in order to establish and characterize mouse models of LVNC. In this study, we have analyzed the pathological consequences on the cardiac function of adult mouse models with ventricular hypertrabeculation generated by the spatio-temporal deletion of *Nkx2.5* gene during ventricular trabeculae development. The loss of *Nkx2.5* at embryonic stages, during the formation of ventricular trabeculae, provokes a hypertrabeculated phenotype associated with an important subendocardial fibrosis and Purkinje fibers hypoplasia, while these phenotypes are milder when the deletion of *Nkx2.5* occurred at fetal stages during the compaction of ventricular trabeculae. In contrast, the deletion of this gene in the ventricular conduction system leads to a progressive disappearance of this tissue without signs of hypertrabeculation nor fibrosis. However, all these mice develop progressively cardiac function defects including conduction defects and heart failure. The characterization of these cardiac phenotypes and associated molecular pathways demonstrates that this transcription factor plays pleiotropic roles during ventricular trabeculae development.

The first challenge of this study was to obtain adult mouse models with ventricular hypertrabeculation as this phenotype leads in mice very often to premature lethality (Chen et al. 2009). To overcome this problem, we have used the strategy to delete *Nkx2.5*, a good candidate gene for LVNC, only in the ventricular trabeculae. After *Mib-1* mutants (Luxan et al. 2013), this is only the second model describing ventricular hypertrabeculation in adult mice. In Human, the "hypertrabeculed" phenotype is difficult to define because residual trabeculae are normal constituents of the LV chamber and the distinction between normal trabeculation and hypertrabeculation is still debated in the literature. Even in absence of gold standard, the most common criteria to evaluate LVNC is to measure by echocardiography the ratio between the Non-Compacted and Compacted area, which should be NC/C >2.2 (Jenni et al. 2001). More recently, CMR appears to be a more sensitive and accurate technique to detect hypertrabeculation in patients (Jacquier et al. 2010). For technical reason, echocardiography was not appropriate for our mouse model, but we could detect the presence of trabeculations in left ventricle of *Nkx2.5* mutants using MRI technique. However, the size and extend of ventricular trabeculae detected in HR cineS images appear strongly different than from those recorded in patients, so we could not use the same diagnostic criteria to evaluate the extend of the phenotype. Instead, we quantify the extension of hypertrabeculation by measuring the length of the endocardium which reflects the Non-Compacted area and the number of free trabeculations in the ventricular lumen. A new criteria based on a fractal index was recently established to calculate the meshwork complexity of ventricular trabeculae from HREM (High-Resolution Episcopic Microscopy). This technique has been used in *Mib1* mutants to show the different pattern of trabeculae in embryonic heart (Captur et al. 2016). This criterion is based on the complexity of trabecular architecture, which also includes endocardial invaginations but was only used to quantify the embryonic development of trabeculae. In our analysis, we show that the level of hypertrabeculation is much more important when *Nkx2.5* deletion occurred at embryonic stages than at fetal stages. However, no aggravation for this hypertrabeculated phenotype was observed after aging. These data suggest that the degree of hypertrabeculation may be more important when disturbances occurred during the growth than during the compaction of the ventricular trabeculae. So altogether, these results demonstrate that the severity of hypertrabeculated phenotype may come from defects during developmental stages

and not from aging defects. One restriction of these models is that they do not reproduce or phenocopy the level of hypertrabeculation seen in patients.

Another feature linked to hypertrabeculation is the important subendocardial fibrosis observed in our *Nkx2.5*-induced hypertrabeculated heart. To comfort our results, it was recently described that subendocardial fibrosis is actually very often associated with LVNC in human patients (Gerger et al. 2013). However, this subendocardial fibrosis is more pronounced in $Nkx2.5^{\Delta trab}$ mutants compared to other mutants induced at fetal stages. These results are consistent with previous studies showing the absence of fibrosis in heart after conditional knockout of Nkx2.5 at mid-gestation, perinatal or postnatal stages (Briggs et al. 2008, Terada et al. 2011). Regarding our molecular analyses, numerous genes associated with fibrosis are specifically overexpressed in left ventricle after embryonic deletion of *Nkx2.5* and not at fetal stages. Altogether, these data strongly suggest that subendocardial fibrosis originates from an early event due to a dysfunction of ventricular trabeculae development rather than a direct consequence of aging as it was suggest for human (Gerger et al. 2013).

Because mutations in *NKX2.5* are associated with a myriad of congenital heart diseases (CHD) in humans, this transcription factor has received much attention for its role in cardiac dysmorphogenesis (Costa et al. 2013). The numerous genetically modified mouse models in which this transcription factor is conditionally knocked-out or in which mutated forms have been overexpressed, testify its major role during cardiac development (Kasahara et al. 2001, Briggs et al. 2008, Terada et al. 2011, Ashraf et al. 2014). These analyses have also pointed out the importance of *Nkx2.5* in the cardiac conduction and contraction at postnatal stages. We have previously shown that *Nkx2.5* haploinsufficient mice display ventricular conduction defects recorded by a large QRS associated with the disruption of the Purkinje fibers network (Meysen et al. 2007). In these mice, the development of ventricular trabeculae occurred normally and the hypoplasia of PF appeared after birth. In our *Nkx2.5*-induced hypertrabeculated hearts, a total or quasi-absence of PF are observed in mutant mice in which *Nkx2.5* has been deleted during embryonic or fetal development. These mice display early conduction defects, in particular

LBBB in agreement with this hypoplasia phenotype. In contrast, the same anatomic and conduction anomalies appear only in 10-months old mice when *Nkx2.5* is deleted in the postnatal VCS. These results are conformed to previous analyses showing a progressive loss with age of AVN and AVB in the conditional deletion of *Nkx2.5* at perinatal or postnatal stages (Briggs et al. 2008, Takeda et al. 2009). Altogether, these data highlight the importance of *Nkx2.5* in the development and maintenance of a functioning conduction system and the importance of the presence of the VCS in sustaining a normal cardiac function.

Besides the important role of this transcription factor in the cardiac conduction system, *Nkx2.5* is known to act directly on cardiac contractility. Indeed, reduced and irregular ventricular contractions are recorded by echocardiography in newborn mice after the conditional deletion of *Nkx2.5* at E13.5 (Terada et al. 2011). In these mouse models, *Nkx2.5* disturbed calcium handling and sarcomere organization, which are known trigger to reduce contractility (Jay et al. 2003, Pashmforoush et al. 2004, Briggs et al. 2008, Takeda et al. 2009). In our *Nkx2.5*-induced hypertrabeculated hearts, we found numerous deregulated genes, from microarray analysis or qPCR experiments (data not shown), involved in calcium signaling (*Ryr2*, *Sln* or *SERCA2)*, in the contractile apparatus (*Myh7*, *Tnnt2)*, in transmembrane ionic transport (*HCN1*, *HCN4*, *Scn5a*, *Cacna1g*, *Cacna1h*, *Kcne1)*, in cardiovascular regulation (*Nppa* and *Nppb)*, and in cardiac development (*BMP10)*. All of them were previously described deregulated in different mutant mouse models of *Nkx2.5* and for some of them, *Myh7*, *HCN4* (Terada et al. 2011), *Tnnt2* (Luedde et al. 2010), *Scn5a* (Shan et al. 2008), *Ryr2* (Ohno et al. 2014), associated to LVNC.

It has been recently shown that cardiac contractility may also depend directly from endothelial signaling through the NRG-1/Erbb2 pathways (McCormick et al. 2015). Indeed, Pecam-1 null mice display a slight decreased EF without morphological defects in cardiomyocytes or capillary densities but resulting from a disturbed communication between endothelial and cardiomyocytes. In our study, *Nkx2.5*-induced hypertrabeculated hearts present vascular defects such as endocardial islets and a vast list of genes involved in vascular or coronary arteries development are found deregulated. Interestingly, we observed an upregulation of endoglin correlated with the hypertrabeculated phenotype. These data suggest that hypertrabeculation is directly linked with the apparition of vascular defects. Indeed, LVNC patients are known to present defects in cardiac

perfusion and embolic thrombosis is one the pathological feature associated with this cardiomyopathy (Jenni et al. 2002, Towbin 2010). However, in our *Nkx2.5* mutants, the vascular phenotype varies in function of the timing of deletion suggesting that the formation of coronary vasculature is directly linked to trabecular development. This assumption is coherent with the microarray data in which different lists of genes involving endothelial cells signaling or vasculature are found deregulated between the two mutants.

Conclusion

In conclusion, our extensive analysis of hypertrabeculated mouse models highlights the fact that the severity of the pathological outcomes in these mice is dependent on the timing of *Nkx2.5* deletion during ventricular trabeculae development. Perturbations in the formation of ventricular trabeculae seems directly link to the malformation of the conduction system and the development of fibrosis. In contrast, the compaction of the ventricular trabeculae appears specifically involved in the development of coronary vasculature. Interestingly, the loss of *Nkx2.5* in the VCS is sufficient to induce conduction defects that progressively turn to heart failure without hypertrabeculation or fibrosis, demonstrating the strong importance of these specialized cardiomyocytes in the maintenance of cardiac function.

References

Ashraf, H., L. Pradhan, E. I. Chang, R. Terada, N. J. Ryan, L. E. Briggs, R. Chowdhury, M. A. Zarate, Y. Sugi, H. J. Nam, D. W. Benson, R. H. Anderson and H. Kasahara (2014). "A mouse model of human congenital heart disease: high incidence of diverse cardiac anomalies and ventricular noncompaction produced by heterozygous Nkx2.5 homeodomain missense mutation." Circ Cardiovasc Genet 7(4): 423-433.

Beyer, S., R. G. Kelly and L. Miquerol (2011). "Inducible Cx40-Cre expression in the cardiac conduction system and arterial endothelial cells." Genesis 49(2): 83-91.

Bhatia, N. L., A. J. Tajik, S. Wilansky, D. E. Steidley and F. Mookadam (2011). "Isolated noncompaction of the left ventricular myocardium in adults: a systematic overview." J Card Fail 17(9): 771-778.

Brescia, S. T., J. W. Rossano, R. Pignatelli, J. L. Jefferies, J. F. Price, J. A. Decker, S. W. Denfield, W. J. Dreyer, O. Smith, J. A. Towbin and J. J. Kim (2013). "Mortality and sudden death in pediatric left ventricular noncompaction in a tertiary referral center." Circulation 127(22): 2202-2208.

Briggs, L. E., M. Takeda, A. E. Cuadra, H. Wakimoto, M. H. Marks, A. J. Walker, T. Seki, S. P. Oh, J. T. Lu, C. Sumners, M. K. Raizada, N. Horikoshi, E. O. Weinberg, K. Yasui, Y. Ikeda, K. R. Chien and H. Kasahara (2008). "Perinatal loss of Nkx2.5 results in rapid conduction and contraction defects." Circ Res 103(6): 580-590.

Captur, G., R. Wilson, M. F. Bennett, G. Luxan, A. Nasis, J. L. de la Pompa, J. C. Moon and T. J. Mohun (2016). "Morphogenesis of myocardial trabeculae in the mouse embryo." J Anat 229(2): 314-325.

Chen, H., W. Zhang, D. Li, T. M. Cordes, R. Mark Payne and W. Shou (2009). "Analysis of ventricular hypertrabeculation and noncompaction using genetically engineered mouse models." Pediatr Cardiol 30(5): 626-634.

Costa, M. W., G. Guo, O. Wolstein, M. Vale, M. L. Castro, L. Wang, R. Otway, P. Riek, N. Cochrane, M. Furtado, C. Semsarian, R. G. Weintraub, T. Yeoh, C. Hayward, A. Keogh, P. Macdonald, M. Feneley, R. M. Graham, J. G. Seidman, C. E. Seidman, N. Rosenthal, D. Fatkin and R. P. Harvey (2013). "Functional characterization of a novel mutation in NKX2.5 associated with congenital heart disease and adult-onset cardiomyopathy." Circ Cardiovasc Genet 6(3): 238-247.

Emde, B., A. Heinen, A. Godecke and K. Bottermann (2014). "Wheat germ agglutinin staining as a suitable method for detection and quantification of fibrosis in cardiac tissue after myocardial infarction." Eur J Histochem 58(4): 2448.

Freedom, R. M., S. J. Yoo, D. Perrin, G. Taylor, S. Petersen and R. H. Anderson (2005). "The morphological spectrum of ventricular noncompaction." Cardiol Young 15(4): 345-364.

Furtado, M. B., J. C. Wilmanns, A. Chandran, M. Tonta, C. Biben, M. Eichenlaub, H. A. Coleman, S. Berger, R. Bouveret, R. Singh, R. P. Harvey, M. Ramialison, J. T. Pearson, H. C. Parkington, N. A. Rosenthal and M. W. Costa (2016). "A novel conditional mouse model for Nkx2.5 reveals transcriptional regulation of cardiac ion channels." Differentiation 91(1-3): 29-41.

Gerger, D., C. Stollberger, M. Grassberger, B. Gerecke, H. Andresen, R. Engberding and J. Finsterer (2013). "Pathomorphologic findings in left ventricular hypertrabeculation/noncompaction of adults in relation to neuromuscular disorders." Int J Cardiol 169(4): 249-253.

Jacquier, A., F. Thuny, B. Jop, R. Giorgi, F. Cohen, J. Y. Gaubert, V. Vidal, J. M. Bartoli, G. Habib and G. Moulin (2010). "Measurement of trabeculated left ventricular mass using cardiac magnetic resonance imaging in the diagnosis of left ventricular non-compaction." Eur Heart J 31(9): 1098-1104.

Jay, P. Y., C. I. Berul, M. Tanaka, M. Ishii, Y. Kurachi and S. Izumo (2003). "Cardiac conduction and arrhythmia: insights from Nkx2.5 mutations in mouse and humans." Novartis Found Symp 250: 227-238; discussion 238-241, 276-229.

Jenni, R., E. Oechslin, J. Schneider, C. Attenhofer Jost and P. A. Kaufmann (2001). "Echocardiographic and pathoanatomical characteristics of isolated left ventricular non-compaction: a step towards classification as a distinct cardiomyopathy." Heart 86(6): 666-671.

Jenni, R., E. N. Oechslin and B. van der Loo (2007). "Isolated ventricular non-compaction of the myocardium in adults." Heart 93(1): 11-15.

Jenni, R., C. A. Wyss, E. N. Oechslin and P. A. Kaufmann (2002). "Isolated ventricular noncompaction is associated with coronary microcirculatory dysfunction." J Am Coll Cardiol 39(3): 450-454.

Kasahara, H., H. Wakimoto, M. Liu, C. T. Maguire, K. L. Converso, T. Shioi, W. Y. Huang, W. J. Manning, D. Paul, J. Lawitts, C. I. Berul and S. Izumo (2001). "Progressive atrioventricular conduction defects and heart failure in mice expressing a mutant Csx/Nkx2.5 homeoprotein." J Clin Invest 108(2): 189-201.

Kimura, K., K. Takenaka, A. Ebihara, K. Uno, H. Morita, T. Nakajima, T. Ozawa, I. Aida, Y. Yonemochi, S. Higuchi, Y. Motoyoshi, T. Mikata, I. Uchida, T. Ishihara, T. Komori, R. Kitao, T. Nagata, S. Takeda, Y. Yatomi, R. Nagai and I. Komuro (2013). "Prognostic impact of left ventricular noncompaction in patients with Duchenne/Becker muscular dystrophy - Prospective multicenter cohort study." Int J Cardiol.

Klaassen, S., S. Probst, E. Oechslin, B. Gerull, G. Krings, P. Schuler, M. Greutmann, D. Hurlimann, M. Yegitbasi, L. Pons, M. Gramlich, J. D. Drenckhahn, A. Heuser, F. Berger, R. Jenni and L. Thierfelder (2008). "Mutations in sarcomere protein genes in left ventricular noncompaction." Circulation 117(22): 2893-2901.

Kober, F., I. Iltis, P. J. Cozzone and M. Bernard (2005). "Myocardial blood flow mapping in mice using high-resolution spin labeling magnetic resonance imaging: influence of ketamine/xylazine and isoflurane anesthesia." Magn Reson Med 53(3): 601-606.

Luedde, M., P. Ehlermann, D. Weichenhan, R. Will, R. Zeller, S. Rupp, A. Muller, H. Steen, B. T. Ivandic, H. E. Ulmer, M. Kern, H. A. Katus and N. Frey (2010). "Severe familial left ventricular non-compaction cardiomyopathy due to a novel troponin T (TNNT2) mutation." Cardiovasc Res 86(3): 452-460.

Luxan, G., J. C. Casanova, B. Martinez-Poveda, B. Prados, G. D'Amato, D. MacGrogan, A. Gonzalez-Rajal, D. Dobarro, C. Torroja, F. Martinez, J. L. Izquierdo-Garcia, L. Fernandez-Friera, M. Sabater-Molina, Y. Y. Kong, G. Pizarro, B. Ibanez, C. Medrano, P. Garcia-Pavia, J. R. Gimeno, L. Monserrat, L. J. Jimenez-Borreguero and J. L. de la Pompa (2013). "Mutations in the NOTCH pathway regulator MIB1 cause left ventricular noncompaction cardiomyopathy." Nat Med 19(2): 193-201.

McCormick, M. E., C. Collins, C. A. Makarewich, Z. Chen, M. Rojas, M. S. Willis, S. R. Houser and E. Tzima (2015). "Platelet endothelial cell adhesion molecule-1 mediates endothelial-cardiomyocyte communication and regulates cardiac function." J Am Heart Assoc 4(1): e001210.

Meysen, S., L. Marger, K. W. Hewett, T. Jarry-Guichard, I. Agarkova, J. P. Chauvin, J. C. Perriard, S. Izumo, R. G. Gourdie, M. E. Mangoni, J. Nargeot, D. Gros and L. Miquerol (2007). "Nkx2.5 cell-autonomous gene function is required for the postnatal formation of the peripheral ventricular conduction system." Dev Biol 303(2): 740-753.

Miquerol, L., S. Beyer and R. G. Kelly (2011). "Establishment of the mouse ventricular conduction system." Cardiovasc Res 91(2): 232-242.

Miquerol, L., S. Meysen, M. Mangoni, P. Bois, H. V. van Rijen, P. Abran, H. Jongsma, J. Nargeot and D. Gros (2004). "Architectural and functional asymmetry of the His-Purkinje system of the murine heart." Cardiovasc Res 63(1): 77-86.

Miquerol, L., J. Thireau, P. Bideaux, R. Sturny, S. Richard and R. G. Kelly (2015). "Endothelial plasticity drives arterial remodeling within the endocardium after myocardial infarction." Circ Res 116(11): 1765-1771.

Ohno, S., M. Omura, M. Kawamura, H. Kimura, H. Itoh, T. Makiyama, H. Ushinohama, N. Makita and M. Horie (2014). "Exon 3 deletion of RYR2 encoding cardiac ryanodine receptor is associated with left ventricular non-compaction." Europace 16(11): 1646-1654.

Pashmforoush, M., J. T. Lu, H. Chen, T. S. Amand, R. Kondo, S. Pradervand, S. M. Evans, B. Clark, J. R. Feramisco, W. Giles, S. Y. Ho, D. W. Benson, M. Silberbach, W. Shou and K. R. Chien (2004). "Nkx2.5 pathways and congenital heart disease; loss of ventricular myocyte lineage specification leads to progressive cardiomyopathy and complete heart block." Cell 117(3): 373-386.

Rodriguez, C. I., F. Buchholz, J. Galloway, R. Sequerra, J. Kasper, R. Ayala, A. F. Stewart and S. M. Dymecki (2000). "High-efficiency deleter mice show that FLPe is an alternative to Cre-loxP." Nat Genet 25(2): 139-140.

Sedmera, D. and P. S. Thomas (1996). "Trabeculation in the embryonic heart." Bioessays 18(7): 607.

Shan, L., N. Makita, Y. Xing, S. Watanabe, T. Futatani, F. Ye, K. Saito, K. Ibuki, K. Watanabe, K. Hirono, K. Uese, F. Ichida, T. Miyawaki, H. Origasa, N. E. Bowles and J. A. Towbin (2008). "SCN5A variants in Japanese patients with left ventricular noncompaction and arrhythmia." Mol Genet Metab 93(4): 468-474.

Srinivas, S., T. Watanabe, C. S. Lin, C. M. William, Y. Tanabe, T. M. Jessell and F. Costantini (2001). "Cre reporter strains produced by targeted insertion of EYFP and ECFP into the ROSA26 locus." BMC Dev Biol 1: 4.

Stollberger, C., J. Finsterer and G. Blazek (2002). "Left ventricular hypertrabeculation/noncompaction and association with additional cardiac abnormalities and neuromuscular disorders." Am J Cardiol 90(8): 899-902.

Takeda, M., L. E. Briggs, H. Wakimoto, M. H. Marks, S. A. Warren, J. T. Lu, E. O. Weinberg, K. D. Robertson, K. R. Chien and H. Kasahara (2009). "Slow progressive conduction and contraction defects in loss of Nkx2.5 mice after cardiomyocyte terminal differentiation." Lab Invest 89(9): 983-993.

Tanaka, M., C. I. Berul, M. Ishii, P. Y. Jay, H. Wakimoto, P. Douglas, N. Yamasaki, T. Kawamoto, J. Gehrmann, C. T. Maguire, M. Schinke, C. E. Seidman, J. G. Seidman, Y. Kurachi and S. Izumo (2002). "A mouse model of congenital heart disease: cardiac arrhythmias and atrial septal defect caused by haploinsufficiency of the cardiac transcription factor Csx/Nkx2.5." Cold Spring Harb Symp Quant Biol 67: 317-325.

Terada, R., S. Warren, J. T. Lu, K. R. Chien, A. Wessels and H. Kasahara (2011). "Ablation of Nkx2.5 at mid-embryonic stage results in premature lethality and cardiac malformation." Cardiovasc Res 91(2): 289-299.

Tian, X., T. Hu, H. Zhang, L. He, X. Huang, Q. Liu, W. Yu, Z. Yang, Y. Yan, X. Yang, T. P. Zhong, W. T. Pu and B. Zhou (2014). "Vessel formation. De novo formation of a distinct coronary vascular population in neonatal heart." Science 345(6192): 90-94.

Towbin, J. A. (2010). "Left ventricular noncompaction: a new form of heart failure." Heart Fail Clin 6(4): 453-469, viii.

Towbin, J. A. (2014). "Ion channel dysfunction associated with arrhythmia, ventricular noncompaction, and mitral valve prolapse: a new overlapping phenotype." J Am Coll Cardiol 64(8): 768-771.

Legend to Figures

Figure 1: Gene targeting strategy and validation of conditional deletion of *Nkx2.5* in ventricular trabeculae and conduction system.

(A) Schematic illustration of the gene targeting strategy. The conditional *Nkx2.5* inactivation (*Nkx2.5*$^{-/-}$) was obtained by crossing *Nkx2.5* floxed allele with tamoxifen-inducible *Cx40-cre-ERT2* mice. Time course of tamoxifen injections and cardiac phenotyping analyses are represented on a time scale and the corresponding *Nkx2.5* mutant groups, i.e. Δtrab, Δcomp, and ΔVCS are indicated below the scale. (B) Quantification of *Nkx2.5* expression levels in the left atria from different *Nkx2.5* mutant adult mice (3 months) by real time RT-PCR. (C) Genetic tracing of ventricular trabeculae in *Cx40-creRFP::R26-YFP* mice at P20 by immunofluorescence showing the distribution of YFP+ cells in the apex and mid ventricle after tamoxifen injection at E10 or E14 and postnatal day 1 and their co-localization in the VCS with RFP expression. (D) Schematic representation of the Cx40-derived cells distribution in the apex or in the mid ventricle after tamoxifen injection at embryonic stages (Δtrab), fetal stages (Δcomp), or in postnatal newborn (ΔVCS).

Figure 2: Morphology of adult hypertrabeculation induced by conditional deletion of *Nkx2.5* in cardiomyocytes during trabecular development.

(A) Anatomical structure of opened left ventricle of 12 months-old control and *Nkx2.5*$^{\Delta trab}$, *Nkx2.5*$^{\Delta comp}$ and *Nkx2.5*$^{\Delta VCS}$ mutant mice. The dotted lines delimit the free wall (FW) on the left and the interventricular septum (IVS) on the right. Stars indicate the papillary muscles. (B) Immunofluorescence with endoglin and VEGFR2 antibodies to delineate endocardium and capillary on transverse sections of ventricular apex from control, *Nkx2.5*$^{\Delta trab}$, *Nkx2.5*$^{\Delta comp}$ and *Nkx2.5*$^{\Delta VCS}$ adult mice (3-month-old mice). On the right panel, high magnifications of the left ventricular lumen show the numerous free trabeculae in *Nkx2.5*$^{\Delta trab}$ and *Nkx2.5*$^{\Delta comp}$ mutants (arrows). Scale bar = 1mm. (C-D) Quantification of hypertrabeculation levels by measuring the total length of the endocardium layer (C) and counting the number of free trabeculae per section

(D). These measures were performed for 3 sections at the level of the apex and at mid-ventricle from control (N=2), *Nkx2.5*$^{\Delta trab}$ (N=3), *Nkx2.5*$^{\Delta comp}$ (N=2), and *Nkx2.5*$^{\Delta VCS}$ (N=2) adult hearts.

Figure 3: Fibrosis and endocardial vascular defects associated with *Nkx2.5*-induced hypertrabeculation

(A) Immunofluorescence with WGA-lectin and Pecam-1 antibody to delineate the zone of institial fibrosis (arrows) on transverse sections at the mid-ventricular level from control, *Nkx2.5*$^{\Delta trab}$, *Nkx2.5*$^{\Delta comp}$ and *Nkx2.5*$^{\Delta VCS}$ adult mice (12 months). Stars indicate papillary muscles. (B) Immunofluorescence with Endoglin and SMA antibodies to delineate endocardium and coronary arteries on transverse sections at the mid-ventricular level from control, *Nkx2.5*$^{\Delta trab}$, *Nkx2.5*$^{\Delta comp}$ and *Nkx2.5*$^{\Delta VCS}$ adult mice (3 months). (C) High magnification of panel B mmunofluorescence with Endoglin, VEGFR2 and SMA antibodies to delineate endocardium islets (arrows) from capillaries at the mid-ventricular level from control, *Nkx2.5*$^{\Delta trab}$, *Nkx2.5*$^{\Delta comp}$ and *Nkx2.5*$^{\Delta VCS}$ adult mice (3 months). (D) Quantification of fibrosis by measuring the percentage of WGA positive area in the left ventricle. (D-E) Quantification of vascular defects by counting the arteries density in the IVS and FW (D) and the number of endocardium islets per section (E). These measures were performed for 3 sections at the level of the apex and at mid-ventricle from control (N=2), *Nkx2.5*$^{\Delta trab}$ (N=3), *Nkx2.5*$^{\Delta comp}$ (N=2), and *Nkx2.5*$^{\Delta VCS}$ (N=2) adult hearts. (A-B) scale bar = 1mm; (C) scale bar = 500µm.

Figure 4: Ventricular conduction system defects in *Nkx2.5*-induced hypertrabeculated hearts

(A-C) Whole-mount immunofluorescence with Contactin-2 antibody to visualize the entire VCS on opened left ventricle from control, *Nkx2.5*$^{\Delta trab}$, *Nkx2.5*$^{\Delta comp}$ and *Nkx2.5*$^{\Delta VCS}$ adult mice. (B-C) High magnifications at the level of the left bundle branch (B) or peripheral Purkinje fibers (C). (D) Immunofluorescence with Contactin-2 and SMA antibodies to delineate the atrioventricular bundle (AVB) on frontal sections of the IVS from control, *Nkx2.5*$^{\Delta trab}$, *Nkx2.5*$^{\Delta comp}$ and *Nkx2.5*$^{\Delta VCS}$ adult mice (12 months).

Figure 5: Follow up of the cardiac function by Magnetic Resonance Imaging *Nkx2.5* mutant mice

(A) Short-axis cine images recorded by MRI at the end-diastole (DIA) and the end-systole (SYS). Images represent the follow-up of the same heart per mutant groups at 2, 8 and 10 month-old, with the yellow line indicating the endocardial outline and the blue line indicating the epicardial outline. Signs of hypertrabeculation are highlighted by arrows, and papillary muscles by stars.

(B) The graph represents the evolution of the ejection fraction (EF) measured in the same mice every two months over a year. The EF corresponding to the left ventricle capacity of contraction, was estimated by manually volumetric measurements from cine long and short axis images.

Figure 6: Follow up of the cardiac conduction by surface electrocardiograms in *Nkx2.5* mutant mice

Representative electrocardiogram in lead II of control (A), *Nkx2.5Δtrab* (B), *Nkx2.5Δcomp* (C) and *Nkx2.5ΔVCS* (D) 12-month old mice. Upper traces show representative baseline tracings and bottom traces correspond to a magnification of the corresponding trace. Prolongation of PR and QRS intervals and intrinsic amplitude variations are indicated. (E) Bar graphs representating follow up of PR and (F) QRS durations from 2 to 12 months. (G) Scatter plot showing Ejection Fraction *vs* QRS duration for each animal tested. (H) The bar graph represents the Ejection Fraction measured in 12 month-old mice by Echography.

The color code is the same for all data: black for the Control, red for *Nkx2.5Δtrab*, orange for *Nkx2.5Δcomp* and green *Nkx2.5ΔVCS*. Data are expressed as mean of 6 Control, 5 *Nkx2.5Δtrab*, 4 *Nkx2.5Δcomp* and 4 *Nkx2.5ΔVCS*.

Figure 7: Transcriptomic analysis of *Nkx2.5*-induced hypertrabeculated hearts

(A) 2D Hierararchical clustering (p-value < 0,01 and FC > 1.5) shows clearly the 3 differentiate groups corresponding to Control, *Nkx2.5Δtrab* and *Nkx2.5Δcomp* mice. Experiment was performed on left ventricule of 6 month-old mice with 4 samples per group. Unsupervised hierarchical clustering based on the similarities of expression reveals 4 clusters.

(B) Gene ontology analysis realized for the 4 clusters show molecular, cellular and physiological functions. Note that these functions are specific of each cluster. Solid bars: numbers of significant genes involved.

(C) Quantitative real-time PCR performed on the same samples than for (A) for a list of selected genes. Housekeeping gene used was RPL32.

Figure 8: Functional analysis of molecular pathways associated to defects in *Nkx2.5*-induced hypertrabeculated hearts

(A) Venn diagram show the number of genes significantly up- and down-regulated in the three groups of comparison : *Nkx2.5Δtrab vs* Control, *Nkx2.5Δcomp vs* Control and *Nkx2.5Δtrab vs Nkx2.5Δcomp*.

(B) Gene network diagram made from the 601 genes identified in the Venn diagram. In red, Nkx2.5Δtrab *vs* Control, in orange, Nkx2.5Δcomp *vs* Control and in pink, *Nkx2.5Δtrab vs Nkx2.5Δcomp*. The network represents the main significant pathways (octagons) and the genes implicated in these pathways (circles).

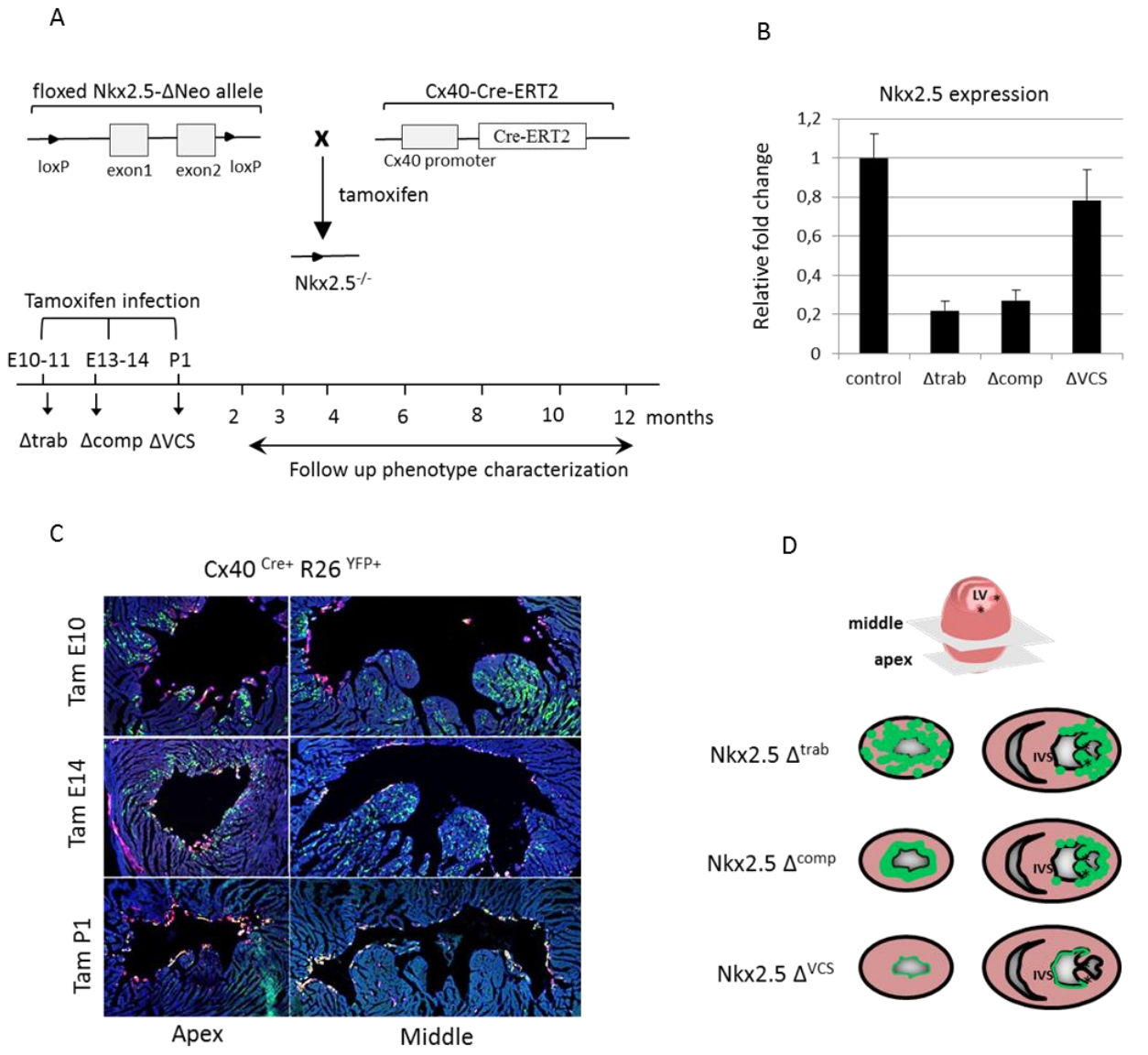
A
floxed Nkx2.5-ΔNeo allele
loxP
exon1
exon2
loxP
X
Cx40-Cre-ERT2
Cre-ERT2
Cx40 promoter
tamoxifen
Nkx2.5-/-
Tamoxifen infection
E10-11
E13-14
P1
Δtrab
Δcomp
ΔVCS
2
3
4
6
8
10
12
months
Follow up phenotype characterization
B
Nkx2.5 expression
Relative fold change
1,2
1
0,8
0,6
0,4
0,2
0
control
Δtrab
Δcomp
ΔVCS
C
Cx40 Cre+ R26 YFP+
Tam E10
Tam E14
Tam P1
Apex
Middle
D
middle
apex
LV
Nkx2.5 Δtrab
Nkx2.5 Δcomp
Nkx2.5 ΔVCS
IVS

Figure 1.

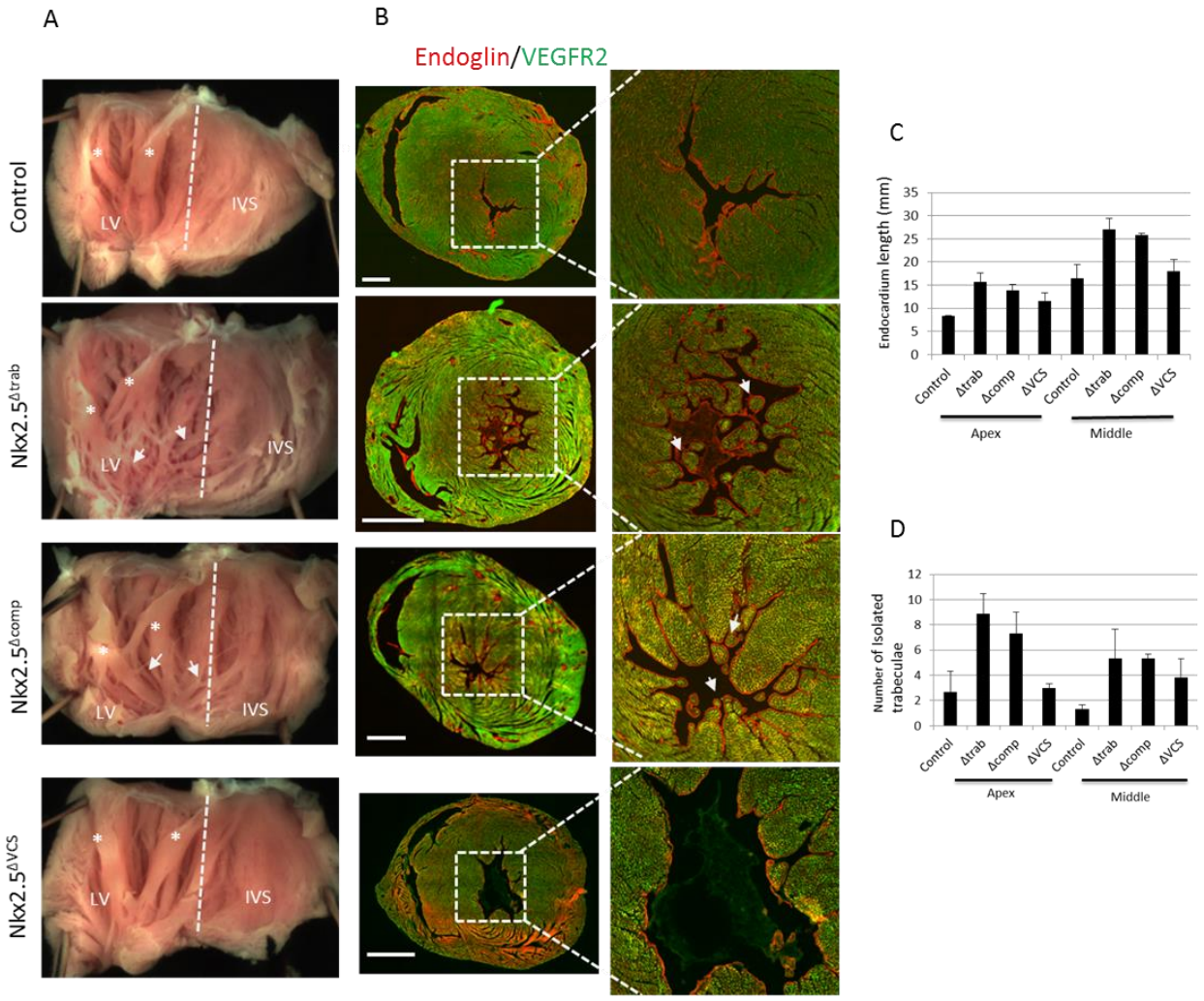
A
B
Endoglin/VEGFR2
Control
Nkx2.5Δtrab
Nkx2.5Δcomp
Nkx2.5ΔVCS
LV
IVS
C
Endocardium length (mm)
Control
Δtrab
Δcomp
ΔVCS
Apex
Middle
D
Number of Isolated trabeculae

Figure 2.

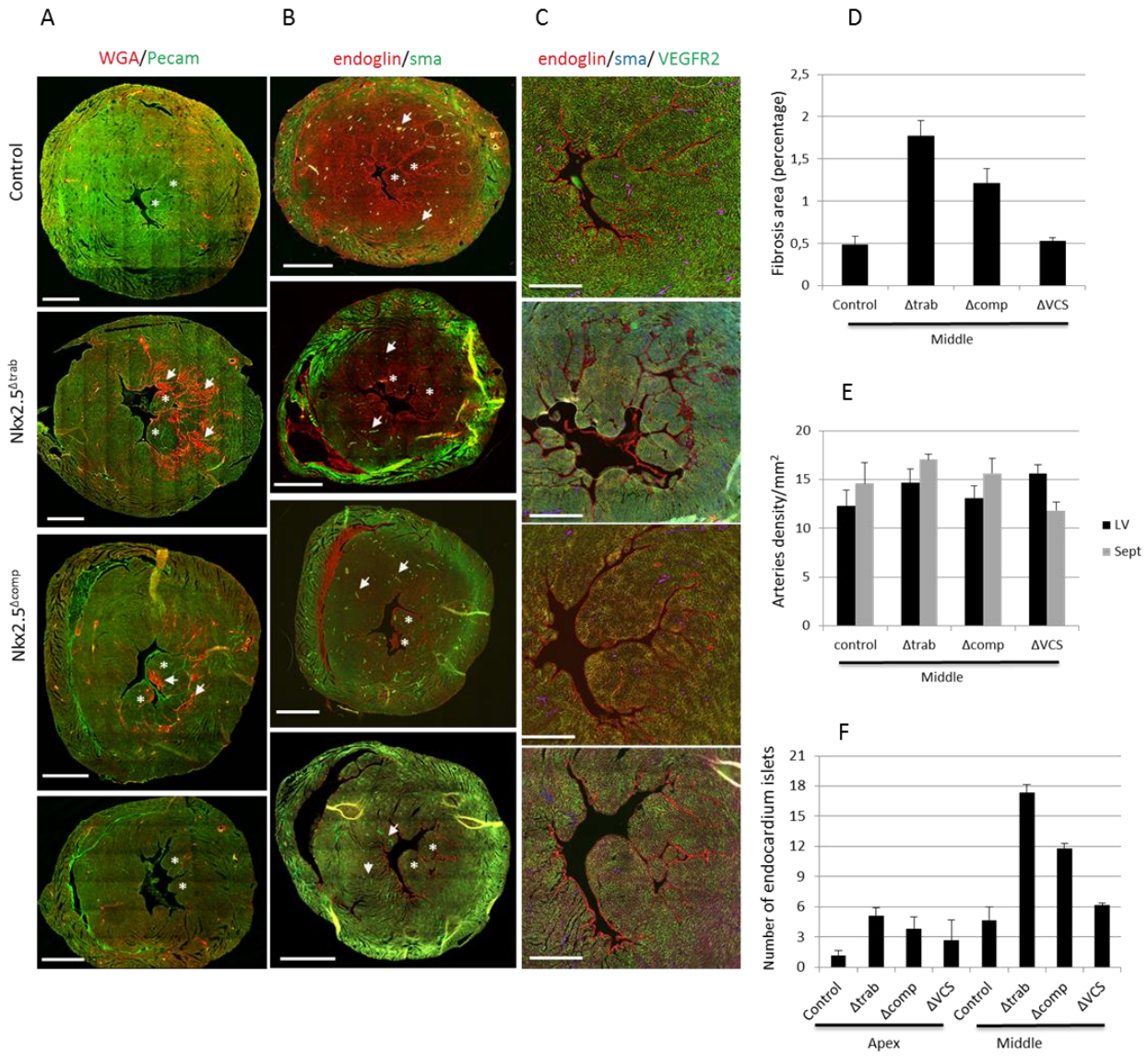
A
B
C
D
WGA/Pecam
endoglin/sma
endoglin/sma/ VEGFR2
Control
Nkx2.5Δtrab
Nkx2.5Δcomp
Fibrosis area (percentage)
2,5
2
1,5
1
0,5
0
Control
Δtrab
Δcomp
ΔVCS
Middle
E
Arteries density/mm2
20
15
10
5
0
control
Δtrab
Δcomp
ΔVCS
Middle
LV
Sept
F
Number of endocardium islets
21
18
15
12
9
6
3
0
Control
Δtrab
Δcomp
ΔVCS
Control
Δtrab
Δcomp
ΔVCS
Apex
Middle

Figure 3.

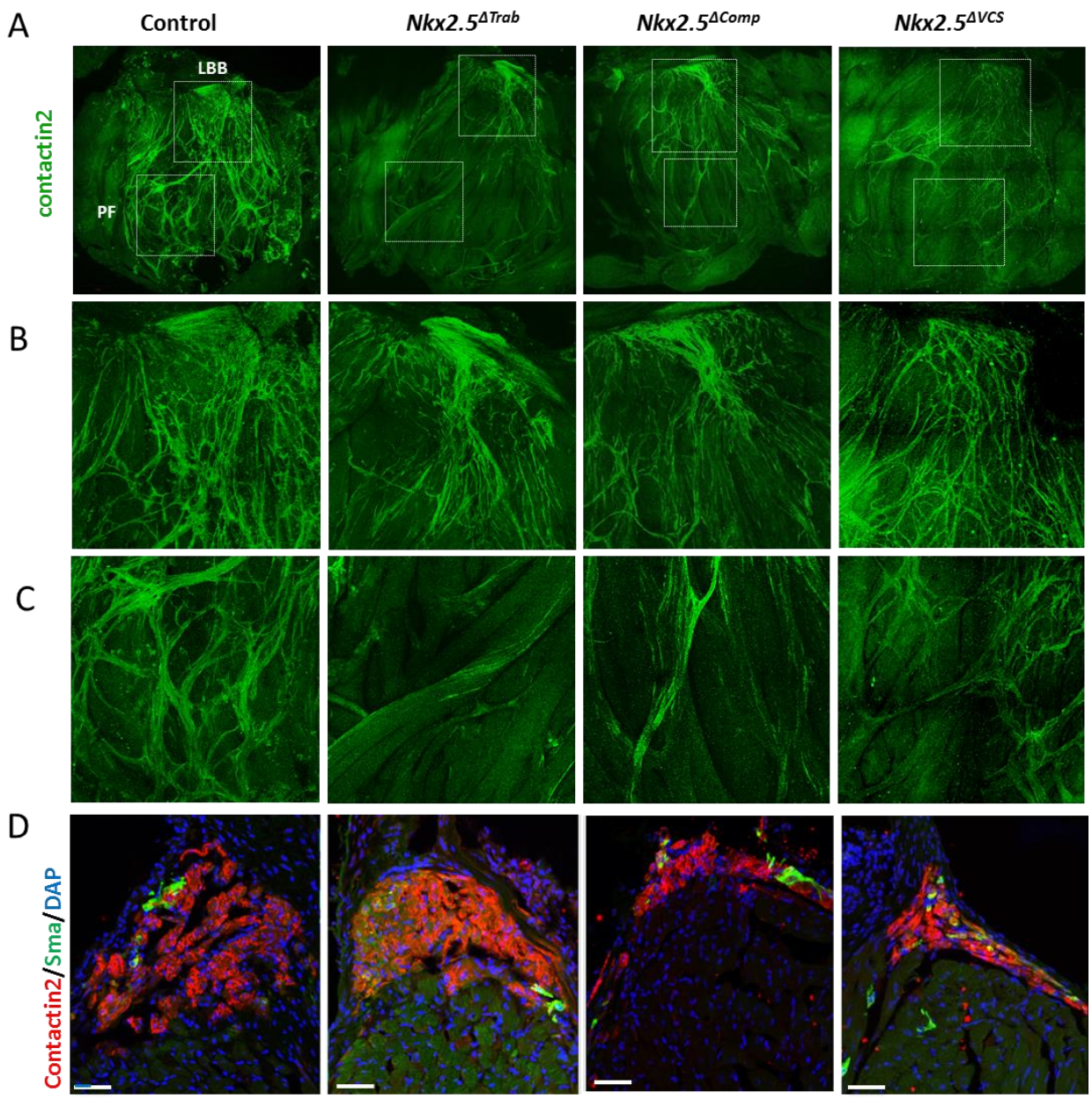
A
Control
Nkx2.5ΔTrab
Nkx2.5ΔComp
Nkx2.5ΔVCS
LBB
PF
contactin2
B
C
D
Contactin2/Sma/DAP

Figure 4.

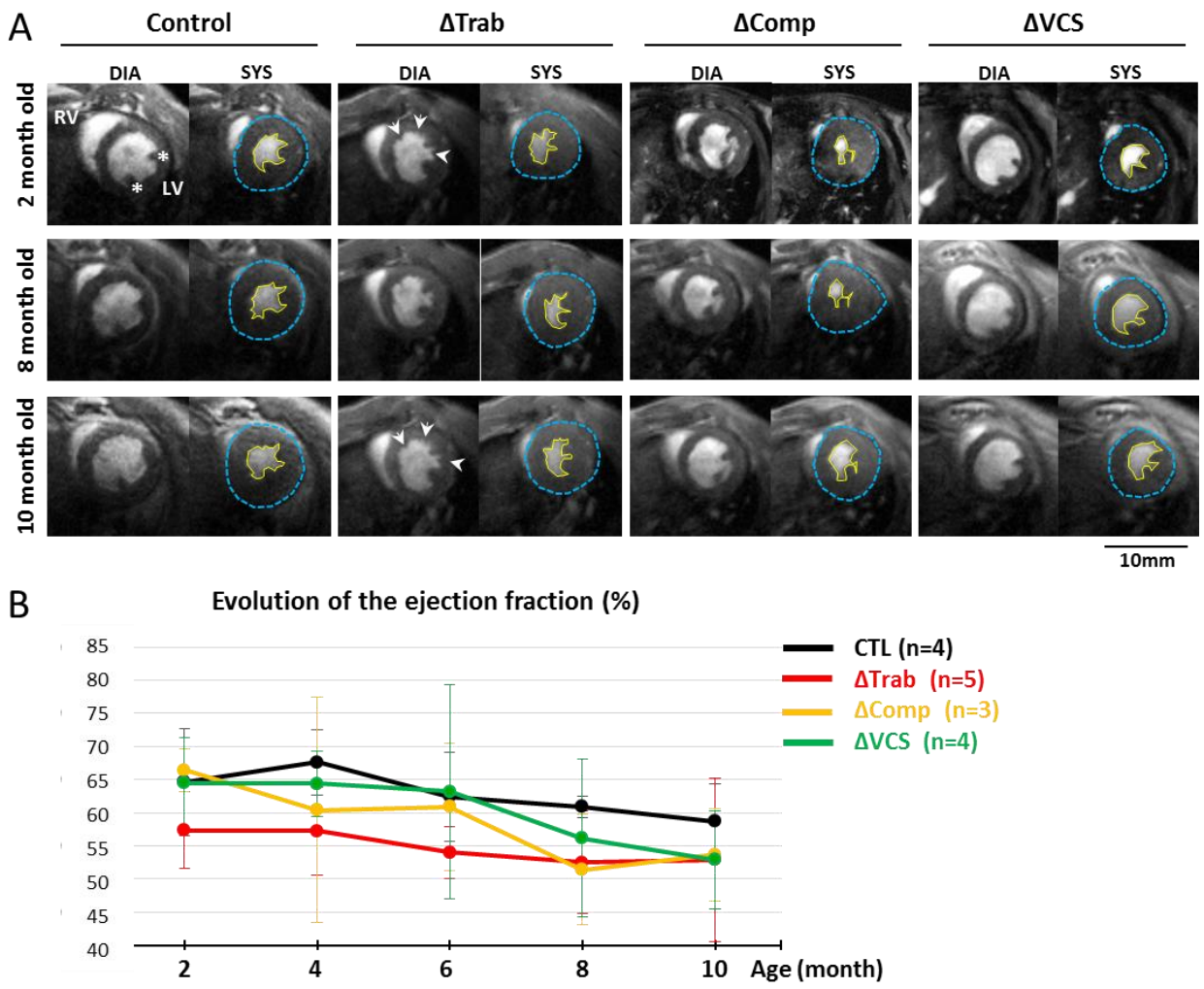
A
Control
ΔTrab
ΔComp
ΔVCS
DIA
SYS
2 month old
8 month old
10 month old
RV
LV
10mm
B
Evolution of the ejection fraction (%)
85
80
75
70
65
60
55
50
45
40
2
4
6
8
10
Age (month)
CTL (n=4)
ΔTrab (n=5)
ΔComp (n=3)
ΔVCS (n=4)

Figure 5.

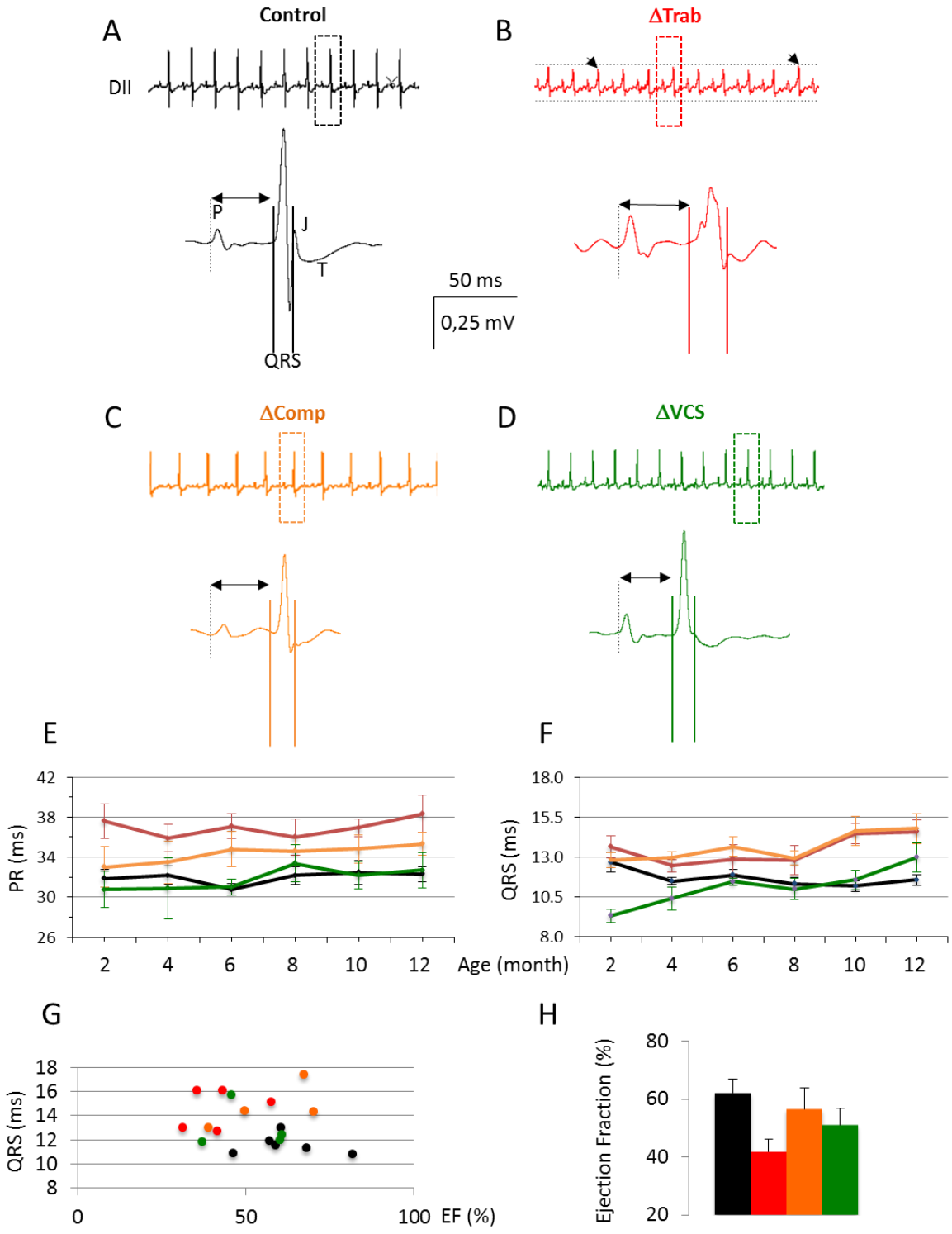
A
Control
DII
P
J
T
QRS
50 ms
0,25 mV
B
ΔTrab
C
ΔComp
D
ΔVCS
E
PR (ms)
Age (month)
F
QRS (ms)
G
QRS (ms)
EF (%)
H
Ejection Fraction (%)

Figure 6.

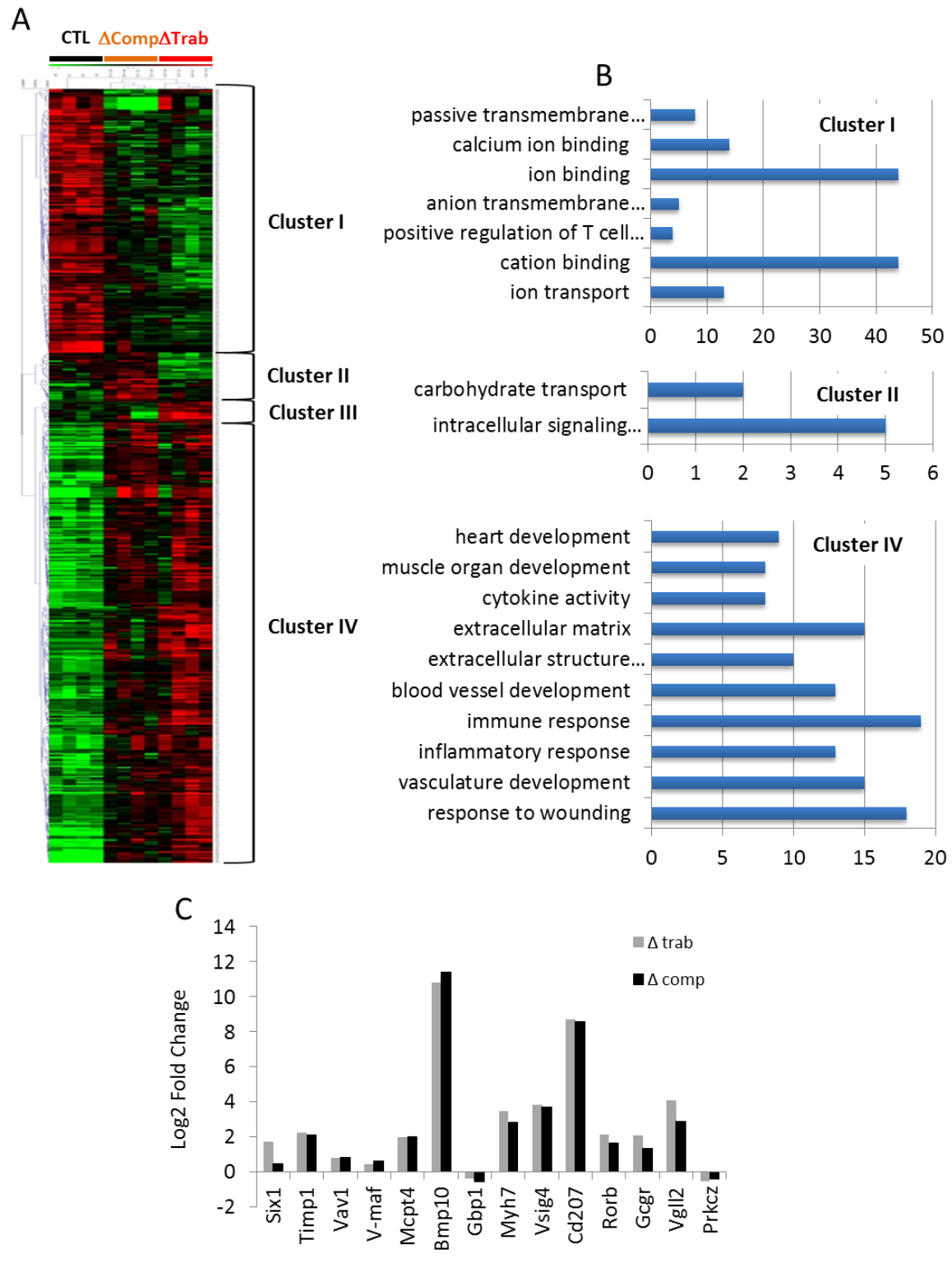
A
CTL
ΔCompΔTrab
Cluster I
Cluster II
Cluster III
Cluster IV
B
Cluster I
passive transmembrane...
calcium ion binding
ion binding
anion transmembrane...
positive regulation of T cell...
cation binding
ion transport
0 10 20 30 40 50
Cluster II
carbohydrate transport
intracellular signaling...
0 1 2 3 4 5 6
Cluster IV
heart development
muscle organ development
cytokine activity
extracellular matrix
extracellular structure...
blood vessel development
immune response
inflammatory response
vasculature development
response to wounding
0 5 10 15 20
C
Log2 Fold Change
14 12 10 8 6 4 2 0 -2
Δ trab
Δ comp
Six1 Timp1 Vav1 V-maf Mcpt4 Bmp10 Gbp1 Myh7 Vsig4 Cd207 Rorb Gcgr Vgll2 Prkcz

Figure 7.

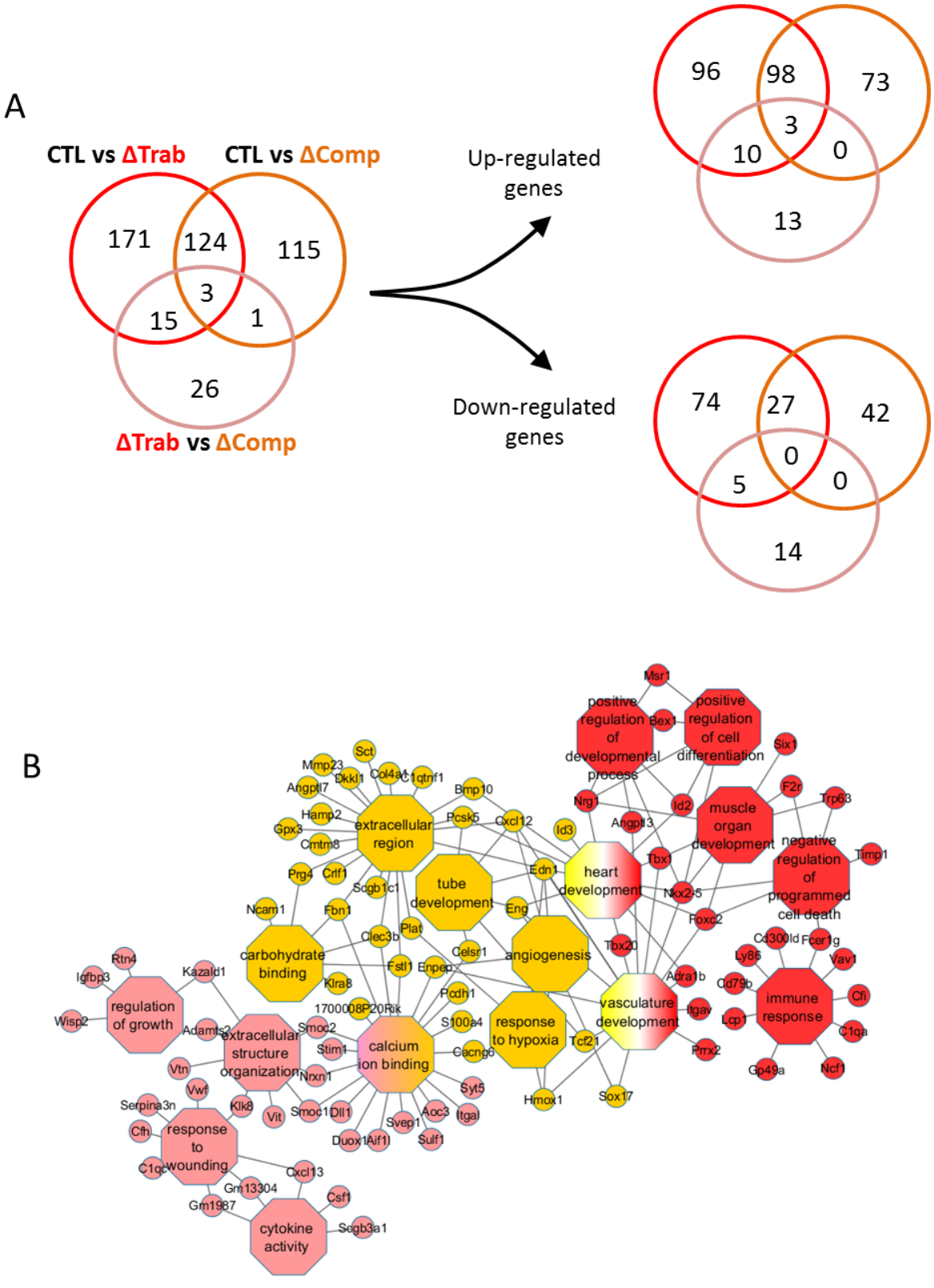
A
CTL vs ΔTrab
CTL vs ΔComp
ΔTrab vs ΔComp
171
124
115
3
15
1
26
Up-regulated genes
Down-regulated genes
96
98
73
3
10
0
13
74
27
42
0
5
0
14
B
extracellular region
tube development
heart development
muscle organ development
negative regulation of programmed cell death
positive regulation of developmental process
positive regulation of cell differentiation
carbohydrate binding
angiogenesis
vasculature development
immune response
regulation of growth
extracellular structure organization
calcium ion binding
response to hypoxia
response to wounding
cytokine activity

Figure 8.

	2 month old				10 month old			
GROUPS:	**CTL**	**ΔTRAB**	**ΔCOMP**	**ΔVCS**	**CTL**	**ΔTRAB**	**ΔCOMP**	**ΔVCS**
Physiological parameters								
N	4	5	4	4	3	5	3	4
Males (%)	75	100	33,3	25	66,7	100	33,3	25
Females (%)	25	0	66,7	75	33,3	0	66,7	75
Body weight (g)	32,6 ± 4	36,2 ± 2	27,5 ± 3	27,8 ± 3	51,8 ± 10	52,4 ± 13	40 ± 6,5	44 ± 2,6
Heart rate (beats/min)	495 ± 71	454 ± 55	443,3 ± 51	446,6 ± 68	570 ± 42	516 ± 61	466,7 ± 57	505 ± 48
Morphological parameters								
EDV (µl)	76,9 ± 15	72,8 ± 7,5	56,3 ± 7,7*	65,3 ± 9,4	92,8 ± 14,2	92,7 ± 16,3	60,4 ± 2,6 *	69,4 ± 11,6 *
ESV (µl)	27,9 ± 10,7	30,9 ± 4,4	19 ± 4,4	23,5 ± 7	38,8 ± 10,3	44,1 ± 15,8	27,9 ± 3	32,2 ± 4,2
LVmass dia (mg)	94,1 ± 17	95,1 ± 9,2	89 ± 8,5	70,3 ± 10 *	126,9 ± 26	128,5 ± 32	87,5 ± 13,1	93,5 ± 18,3
LVmass sys (mg)	117,2 ± 14,3	120,8 ± 14,3	115,7 ± 12,7	99,8 ± 11,8	168,3 ± 26,1	164,2 ± 14,7	119,3 ± 7,8 *	104 ± 24,6 *
sWTn (%)	55 ± 10	43 ± 8	49 ± 4	64 ± 21	49 ± 17	39 ± 15	35 ± 16	27 ± 22
Functional parameters								
EF (%)	65 ± 8	57 ± 5,7	66 ± 3	64 ± 7	58,67 ± 5,7	53 ± 12	54 ± 7	53 ± 7,4
SV (ml)	49 ± 6,4	41,9 ± 3,6	37,3 ± 3,6*	41,8 ± 5,4	54 ± 5	48,5 ± 12,7	32,5 ± 5,6 *	37,2 ± 10,5 *
Normalized morphological parameters								
EDV (µl/g)	2,34 ± 0,21	2,02 ± 0,24*	2,04 ± 0,04 *	2,37 ± 0,45	1,82 ± 0,22	1,8 ± 0,5	1,02 ± 0,93	1,58 ± 0,3
ESV (µl/g)	0,83 ± 0,25	0,85 ± 0,1	0,69 ± 0,08	0,85 ± 0,25	0,74 ± 0,03	0,8 ± 0,51	0,46 ± 0,41	0,73 ± 0,1
LVmass dia (mg/g)	2,87 ± 0,23	2,64 ± 0,35	3,24 ± 0,17 *	2,57 ± 0,52	2,46 ± 0,16	2,54 ± 0,3	1,45 ± 1,26	2,12 ± 0,34
LVmass sys (mg/g)	3,59 ± 0,08	3,34 ± 0,42	4,22 ± 0,4 *	3,66 ± 0,77	3,31 ± 0,46	3,33 ± 0,64	2,0 ± 1,76	2,35 ± 0,45 *

Table 1. Characteristics and volumetric measurements from MRI.

N = number of animals used in this study. **ESV** = End-Systolic volume and **EDV**=End-Diastolic volume, represent the internal volume of the left ventricle chamber at the end of the diastole or systole; **LV mass dia** and **LV mass sys**, represent the mass of the left ventricular wall at the end of the diastole or systole; **sWTn** = systole wall thickening, represents the thickening of the left ventricular wall at the end of the systole compare to the end of the diastole; **EF** = Ejection fraction, represent the percentage of volume measured at the end of the diastole, expulsed at the end of the systole; **SV** = Stroke volume, represent the volume of blood expulsed at the end of the systole. Data are expressed in Mean ±SE *P<0,05.

	2 month old				12 month old			
GROUPS:	**CTL**	**ΔTRAB**	**ΔCOMP**	**ΔVCS**	**CTL**	**ΔTRAB**	**ΔCOMP**	**ΔVCS**
N	6	5	4	4	6	5	4	4
Males (%)	50	100	50	50	50	100	50	50
Females (%)	50	0	50	50	50	0	50	50
Heart rate (beats/min)	608 ± 10	536 ± 14	520 ± 32	546 ± 19	537 ± 8	521 ± 26	491 ± 37	500 ± 32
P (ms)	11,8 ± 1,2	12 ± 1,1	12 ± 0,8	10,6 ± 0,4	10,3 ± 0,4	11,4 ± 0,8	10,6 ± 0,6	12,3 ± 0,5
P (µV)	77 ± 11,9	89,8 ± 13,8	127,6 ± 13,5	95,1 ± 9,3	83,2 ± 7	86,8 ± 9,8	74 ± 11,8	76,9 ± 5
PR (ms)	31,9 ± 0,9	37,6 ± 1,7	33 ± 2	30,8 ± 1,8	32,3 ± 0,8	38,3 ± 1,8	35,3 ± 1,1	32,7 ± 1,7
QRS lead II (ms)	17,7 ± 0,4	22,1 ± 1,3	20,4 ± 1	16,6 ± 0,7	16,9 ± 0,2	20,6 ± 1,4	23,2 ± 1,0	18,8 ± 1,3
QRS lead III (ms)	12,7 ± 0,6	13,6 ± 0,7	12,8 ± 0,5	9,3 ± 0,4	11,6 ± 0,3	14,6 ± 0,7	14,8 ± 0,9	13 ± 0,9
QT (ms)	41,8 ± 1,5	45,6 ± 1,7	43 ± 1,9	45,5 ± 0,8	41,7 ± 0,7	44,1 ± 1,7	47,5 ± 4,6	43,3 ± 2,2
EF (%)	-	-	-	-	62,1 ± 4,8	41,8 ± 4,5	56,5 ± 7,4	51 ± 5,8

Table 2. Three lead surface ECG analysis

N = number of animals used in this study. Values are given as mean ± SEM.

Values for Ejection Fraction (EF) in 12-month old mice were obtained by echography.

3. Result 2: Modulation of *Nkx2.5* expression level by genetic manipulation: impact on ventricular morphology and cardiac function

Introduction

Trabeculae and conduction system development are regulated by several transcription factors including *Nkx2.5*. *Nkx2.5* is a master gene which plays a critical role during heart development across vertebrate species, and it continues to be expressed throughout cardiac development and into adult life (Postma *et al.*, 2011). In human, mutations in the *NKX2.5* gene have resulted in a variety of cardiac anomalies, while *Nkx2.5* knockout mice showed early embryonic lethality, and heterozygotes exhibited an array of cardiac abnormalities such as, scattering of AV bundle, reduced His bundle and AV node cellular density and abnormal levels of gap junction proteins (Chung and Rajakumar, 2016; Postma *et al.*, 2011).

Recent studies indicate that *Nkx2.5* mutant mice may link trabecular development and heart disease. Ventricular restricted *Nkx2.5* deficient mice present hypertrabeculation and cardiac functional defects, including complete heart block, and prolonged PR and QRS time intervals in electrocardiography (ECG) recording (Pashmforoush *et al.*, 2004). Another study shows that *Nkx2.5* missense mutation in the homeodomain presents hypertrabeculation, ventricular noncompaction phenotypes along with diverse cardiac anomalies, including atrioventricular defects (Ashraf *et al.*, 2014). Even if those findings suggest a link between *Nkx2.5* gene and trabeculation, however, the relationship between the level of *Nkx2.5* expression and hypertrabeculation or cardiac anomalies is still unclear. In some studies, *Nkx2.5* mutant mice did not present hypertrabeculation, despite the presence of cardiac anomalies including progressive defects in conduction and contraction in these mice (Briggs *et al*., 2008; Nakashima *et al.*, 2014; Takeda *et al*., 2009; Terada *et al*., 2011). Thus, there is still a remaining question whether a low level of *Nkx2.5* expression can cause cardiac anomalies associated with hypertrabeculation.

Our aim was to study trabeculation and functional characteristics of mutant mice expressing different doses of *Nkx2.5* in order to answer the question whether a low expression of *Nkx2.5* can cause cardiac anomalies or not. We used *Nkx2.5* alleles with different genetic

modifications expressing different levels of *Nkx2.5* (called as *Nkx2.5* dosage mice) to characterize trabeculation and cardiac function. It is important to note that those *Nkx2.5* dosage mice are not knockout mice, but *Nkx2.5* gene expression is variable due to the genetic modification of the *Nkx2.5* allele by the presence or not of *Flox* sequence and *Neo* cassette. This study demonstrates that the lowest levels of *Nkx2.5* expression, approximately 80% and 65%, result in a slightly higher trabeculation, a reduction in number of Purkinje fibers, and a shortening of the PR, QRS, and QT time intervals in ECG. However, no sign of LVNC phenotypes was seen suggesting that reduction levels of *Nkx2.5* expression in the dosage mice is not sufficient to induce phenotypical characteristics observed in LVNC disease.

Material and mothods

Generation of mouse models

Animal procedures were approved by the ethic committee for animal experimentation from French ministry (n° 01055.02). The $Nkx2.5^{Neo/Neo}$ and $Nkx2.5^{Neo/+}$ line was generated by targeted replacement of the two WT alleles or one WT allele with the $Nkx2.5^{Neo}$ construct, a neomycin resistance cassette (*Neo*) flanked by *loxP* sequences, respectively (Furtado *et al*., 2016). The $Nkx2.5^{\Delta Neo/\Delta Neo}$ and $Nkx2.5^{\Delta Neo/+}$ line was generated by deletion of the Neo cassette in two alleles or only one allele of the $Nkx2.5^{Neo}$ construct to form homozygous or heterozygous line. The $Nkx2.5^{lacZ/+}$ mice were generated by targeted replacement of the *Nkx2.5* loci with *β-gal* (*lacZ*) (Meysen *et al.*, 2007).

Macroscopic and histological analyses

Macroscopic examination of the internal surface of the ventricles was previously described (Miquerol *et al*., 2004). For histological studies, adult hearts were dissected, fixed for 4 hours in 4% paraformaldehyde (vol/vol) in PBS, washed in sucrose gradient, then embedded in OCT and cryosectioned. For immunofluorescence, sections were permeabilized in PBS 1X / 0.2% Triton X100 for 20 min and incubated for 1 hour in saturation buffer (PBS 1X / 3% BSA / 0.1% Triton X100). The primary antibodies were incubated overnight in saturation buffer at 4°C. Secondary

antibodies coupled to fluorescent molecules were incubated in saturation buffer and after washes, hearts were observed under a Zeiss apotome microscope.

Antibodies used in this study are specific to GFP (AbD Serotec), Contactin-2 (AF1714 R&D system), endoglin CD105 (MJ7/18-DSHB), VEGFR2 (AF644-R&D SYSTEMS), smooth muscle actin (F3777-SIGMA).

ECG recording

Recording of ECG was performed in lead II and lead III with reference electrode. Mouse was anaesthetized during whole recording time with 1-2% isoflurane in 700 ml O_2 /min via facemask pipe. The surface ECG tracing are filtered using a high pass setting of 0.03s, low pass setting of 120 kHz and recorded in 1 min after few minutes stabilization of the signal. The recorded ECG is analyzed offline using Chart 5 for Window software (v 5.5.6 for Macintosh, AD Instruments) for examining unusually P, QRS, T or J waves morphology and for time-varying intervals. Several values were measured including PR, QRS, QT, and RR. Among those values, only QRS was calculated by lead III meanwhile others were calculated by lead II.

RNA extraction and quantitative RT-PCR

Total RNA was isolated by using TRIzol Reagent (Invitrogen, Life technologies). The RNA extraction procedure follows manufacturer's protocol by Invitrogen (Life technology). In detail, each tissue sample was crashed mechanically and homogenized in 1ml of Trizol reagent, before adding 200 microliters chloroform. After centrifugation, the sample mixture was separated into 3 phases: a lower red phenol – chloroform phase, an interphase, and a colorless aqueous upper phase. The upper aqueous phase was moved into a phase-locked-gel tube and centrifuged in order to absorb remaining organic reagents (phenol, chloroform, salt, etc). The RNA exclusively in the aqueous phase was precipitated by adding 0.5 ml isopropanol. After centrifugation, RNA is often visible and forms a gel-like pellet in the bottom of the eppendorf tube. The RNA pellet was washed by centrifugation with 1 ml of 75% ethanol, and air dried. RNase-free water was used for the resuspension of the RNA pellet before incubating in a 55^{o}C water bath for 10 min. RNA samples were stored at -80 ^{o}C until process.

RNA concentration was then quantified by using the NanoDrop machine (NanoDrop ND-1000, ThermoScientific). The absorbance reading results are converted into concentration (ng/µl), and absorbance ratios of 260/280 and 260/230 are verified. A 260/280 ratio from 1.9 to 2.0 indicates that we had successfully extracted RNA of good purity.

In order to verify RNA integrity, Aligent RNA 6000 Nano kit (Agilent Technologies, Germany) was utilized on Agilent 2100 Bioanalyzer (Agilent technologies, Germany). RNA Integrity was validated based on traditional gel electrophoresis principles. The input RNA concentration was 25 – 500 ng/µL. There are 5 steps including preparing the gel, preparing the gel-dye mix, loading the gel-dye mix, loading the Agilent RNA 6000 nano marker, and loading the ladder and samples according to the manufacturer‟s protocol (Agilent RNA 6000 Nano Kit Quick Start Guide). RNA integrity number (RIN) from 1.8 to 2.0 indicates that we had successfully extracted total RNA without degradation.

To synthesize cDNA, superscript VILO MasterMix was used (Invitrogen, Thermo Fisher Scientific, Netherlands). The reaction was followed the temperature procedure by manufacturer's guidance. Quantitative RT-PCR was performed using SYBR Green PCR master mix (Applied Biosystem, Life technologies, UK). Comparative C_T method (ΔΔCt) was used for quantifying expression of *Nkx2.5* gene in the testing samples normalizing to *RPL32* housekeeping gene.

Results

Variable expression levels of *Nkx2.5* in different alleles

In the way of generating *Nkx2.5* targeted knockout mice, several *Nkx2.5* alleles were created. The genotype of these mutants differs only by the presence at the *Nkx2.5* locus of sequences including *loxP* sites and *Neo* cassette (Figure 1A). Firstly, five groups of mice plus *Nkx2.5* wild-type ($Nkx2.5^{WT}$) were subjected to qPCR analysis to study the level of *Nkx2.5* expression in these different groups. $Nkx2.5^{WT}$ mice were used as control mice with 100% expression. Real time qPCR revealed mRNA expression in hearts from *Nkx2.5* dosage mice as shown in the figure 1B. Heterozygous *Nkx2.5-Neo* deleted mice subsequently called as $Nkx2.5^{\Delta Neo/+}$ had an increase of

25% expression of *Nkx2.5*, while homozygous *Nkx2.5-Neo* deleted mice, which were subsequently designed as $Nkx2.5^{\Delta Neo/\Delta Neo}$ had a quite normal *Nkx2.5* expression as in $Nkx2.5^{WT}$. Heterozygous *Nkx2.5* mice with the insertion of a Neo cassette, or $Nkx2.5^{Neo/+}$, present almost normal expression of *Nkx2.5* like $Nkx2.5^{\Delta Neo/\Delta Neo}$ and $Nkx2.5^{WT}$ groups. However, homozygous *Nkx2.5-Neo* called $Nkx2.5^{Neo/Neo}$ and heterozygous $Nkx2.5^{lacZ/+}$ present a decrease of around 20% and 60% of *Nkx2.5* expression, respectively. It is interesting to note that all these *Nkx2.5* dosage mice are not knockout mice, but the levels of *Nkx2.5* mRNA are variable because of the genetic modifications in these *Nkx2.5* alleles. These results indicate that there is somehow an interaction between the *Neo* cassette and the *Nkx2.5* gene resulting in important changes in *Nkx2.5* expression.

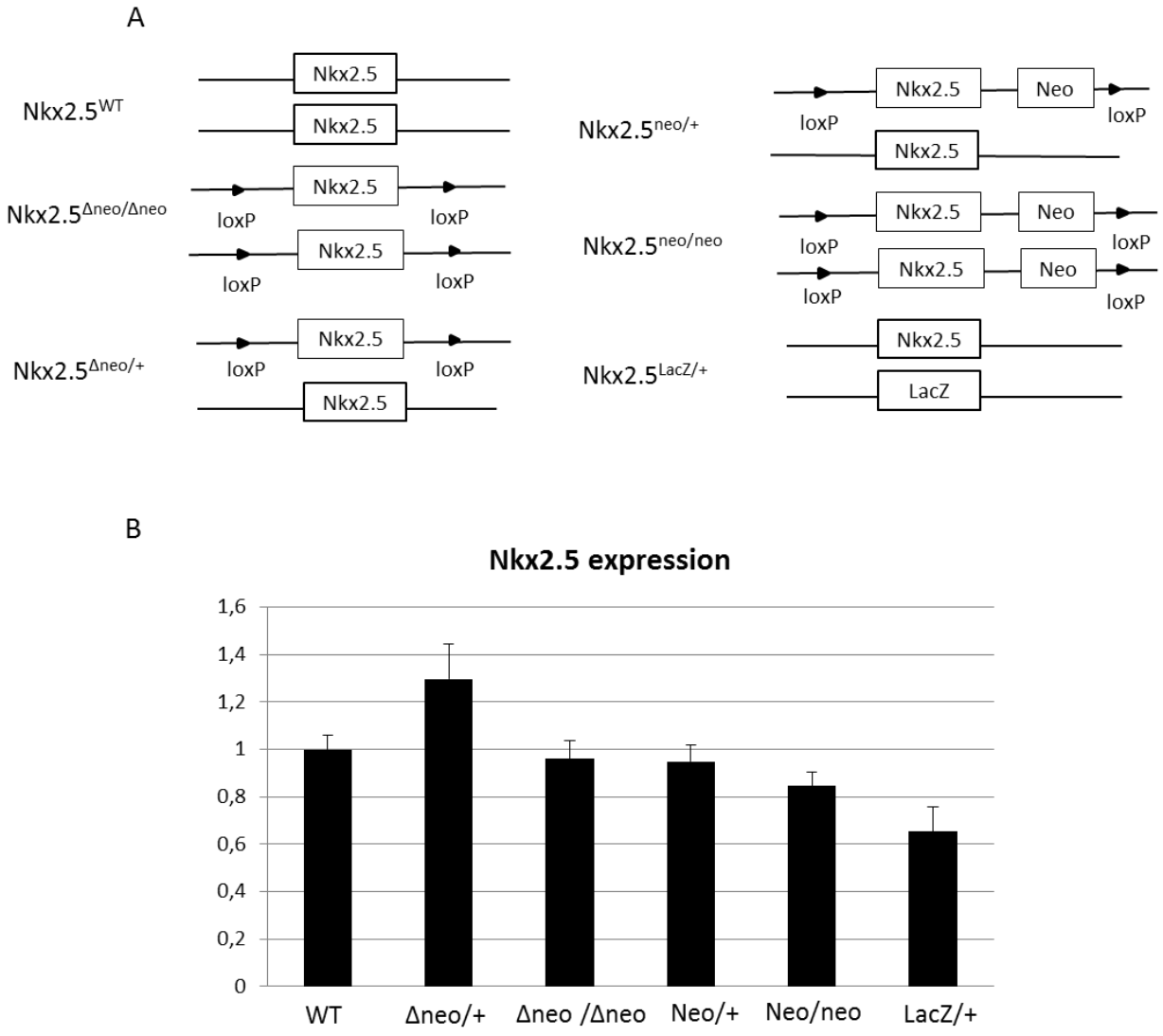

Figure 1. Schematics of *Nkx2.5* gene dosages with differences in mRNA expression level.

(A) Schematics illustration of the *Nkx2.5* dosage mice. Different genetically modification mice were generated in the presence or absence of Neo cassette and loxP sites at *Nkx2.5* locus. (B) Quantification of *Nkx2.5* mRNA expression levels in the left atria from different groups of *Nkx2.5* dosage mice (2-month old) by real time qPCR. Data represent mean plus or minus SEM. N = 4 mice per group.

Variation in expression level of *Nkx2.5* does not result in hypertrabeculation

To study the morphological changes in term of trabeculations in *Nkx2.5* dosage mice, we looked at the anatomy of the LV by dissecting 2-month-old mice. The hearts were opened by cutting along the line from the base to apex in between the two papillary muscles. No hypertrabeculation was observed, but homozygous *Nkx2.5*$^{Neo/Neo}$ and heterozygous *Nkx2.5*$^{lacZ/+}$ mice present more trabeculations (Figure 2A). There was also no anatomical defect in papillary muscle among all groups of mice. These results were confirmed by histological analysis on transverse sections of 2-month-old mice (Figure 2B). Endoglin and VEGFR2 antibodies were used in immunofluorescence experiments to visualize left ventricular trabeculations. By using these specific antibodies, we can distinguish the endocardium layer stained with endoglin from subendocardial endothelial cells stained with VEGFR2 and endoglin antibodies. Hypertrabeculated phenotype was then quantified by measuring the endocardium length and by counting the number of isolated trabeculae at both middle and apex parts of the heart. The results shown in the graphs of figure 2C-D indicate almost no difference in the hypertrabeculated phenotype, except in *Nkx2.5*$^{Neo/Neo}$ mice which present a slight increase in both the length of the endocardium layer and the number of isolated trabeculae. *Nkx2.5*$^{lacZ/+}$ mice show a variable phenotype as demonstrated by the important error bar within the group suggesting an important heterogeneity in the trabeculation phenotype of these mice. To conclude, no sign of obvious hypertrabeculation was found in *Nkx2.5* dosage mice, exception for a slight hypertrabeculated phenotype detected in mice with the lowest level of *Nkx2.5* expression, in the homozygous *Nkx2.5*$^{Neo/Neo}$ and heterozygous Nkx2.5$^{lacZ/+}$ mice.

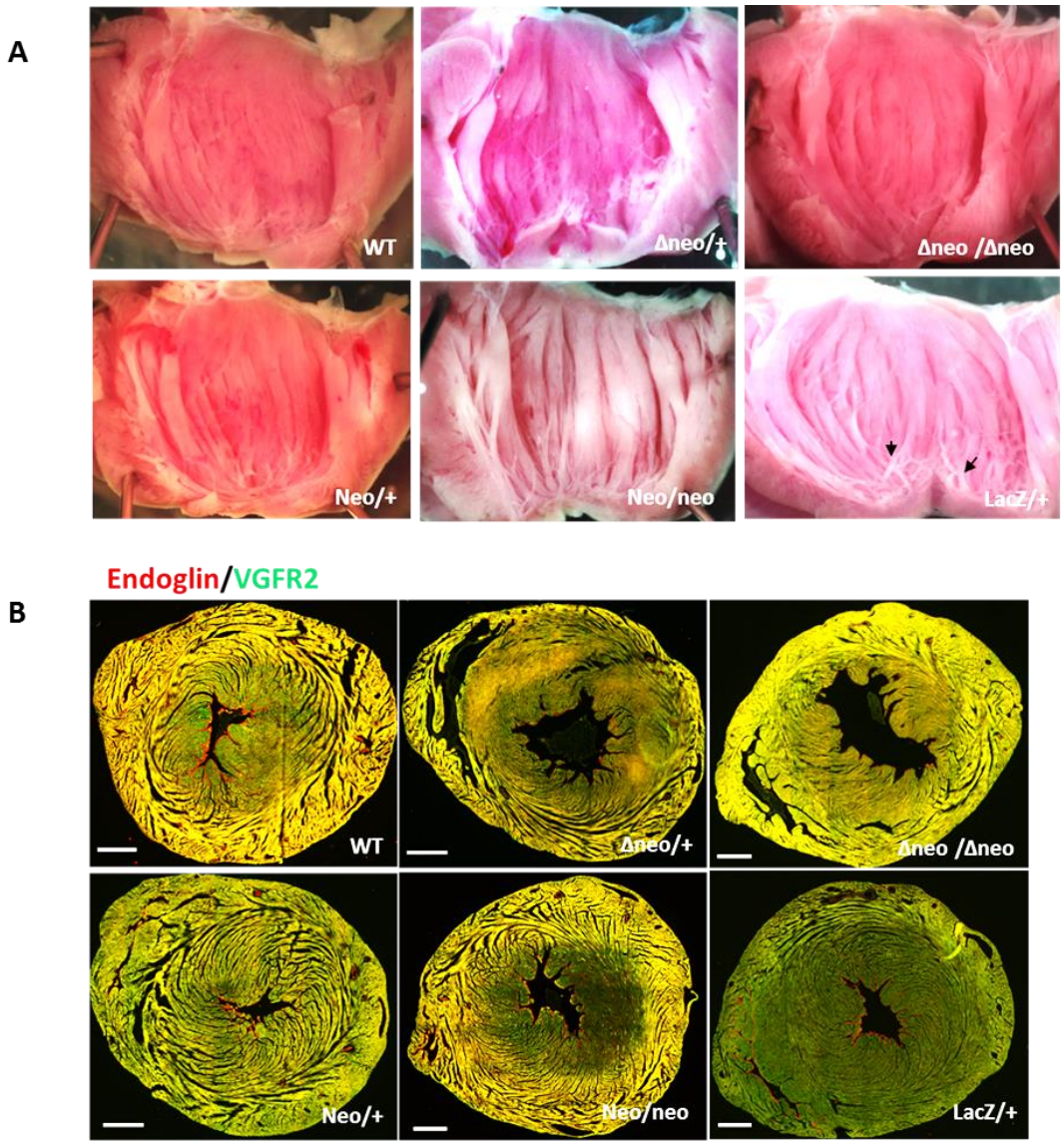
A
WT
Δneo/+
Δneo /Δneo
Neo/+
Neo/neo
LacZ/+
B
Endoglin/VGFR2
WT
Δneo/+
Δneo /Δneo
Neo/+
Neo/neo
LacZ/+
C
Endocardium length (mm)
0
5
10
15
20
25
30
WT
Δneo/+
Δneo/Δneo
Neo/+
Neo/neo
LacZ/+
Middle
Apex
D
Number of isolated trabeculae
0
1
2
3
4
5
6
7
Middle
Apex

Figure 2. Trabecular phenotype of adult *Nkx2.5* gene dosage mice

(A) Anatomical structure of opened left ventricle of 2-month-old mice from 6 different groups of *Nkx2.5* gene dosages. Black arrows indicate trabeculations. (B) Immunofluorescence on transverse sections of 3-month-old mice using endoglin (red) and VEGFR2 (green) antibodies to visualize endocardium and capillary vessels from all 6 groups of *Nkx2.5* dosage mice. Data represent apex sections. Scale bar equal to 500 µm. (C-D) Quantification of hypertrabeculation levels by measuring the total length of the endocardium layer (C) and counting the number of free trabeculae per section (D). These measurements were performed for 3 sections at apex and mid-ventricle in each mouse (N=2). Data are presented as mean ± SD.

Genetic modifications at the *Nkx2.5* locus cause disturbances of the ventricular conduction system

The entire ventricular conduction system (VCS) was visualized by crossing *Cx40-GFP* reporter mice with the *Nkx2.5* dosage mice. By opening the heart to expose the LV cavity, we can see the entire VCS of the LV including the atrioventricular (AV) bundle at the top (Figure 3A). $Nkx2.5^{WT}$ mice present a very dense network of Purkinje fibers forming numerous elliptical structures. We observe a quite similar phenotype in $Nkx2.5^{\Delta Neo/\Delta Neo}$, $Nkx2.5^{\Delta Neo/+}$, and $Nkx2.5^{Neo/+}$ mice with a dense Purkinje fiber network, while there is a strong reduction of Purkinje fibers in $Nkx2.5^{Neo/Neo}$ and $Nkx2.5^{lacZ/+}$ mice. We then performed immunofluorescence experiments with the contactin2 antibody, which stains for conductive cells in order to verify the anatomical phenotype of Purkinje fibers in the dissected hearts. The results showed a decrease in all groups of *Nkx2.5* dosages compared to $Nkx2.5^{WT}$, especially in $Nkx2.5^{lacZ/+}$ mice (Figure 3B). The number of Purkinje fibers was quantified by counting the number of cells with colocalization of contactin2 and Cx40-GFP expression (Figure 3C). $Nkx2.5^{\Delta Neo/\Delta Neo}$ showed a VCS phenotype closest to $Nkx2.5^{WT}$ with a slight decrease of approximately 15% in the middle part. Besides, a dramatic reduction in the number of Purkinje fibers is observed in $Nkx2.5^{Neo/+}$ mice, which is the opposite result observed with *Cx40-GFP* reporter gene in opened hearts suggesting a huge heterogeneity

in this group of mice. A strong decrease in the number of Purkinje fibers was also observed in *Nkx2.5*$^{lacZ/+}$ mice and *Nkx2.5*$^{Neo/Neo}$. Taking all data together, we conclude that a low level of *Nkx2.5* expression could cause hypoplasia of the ventricular conduction system.

A

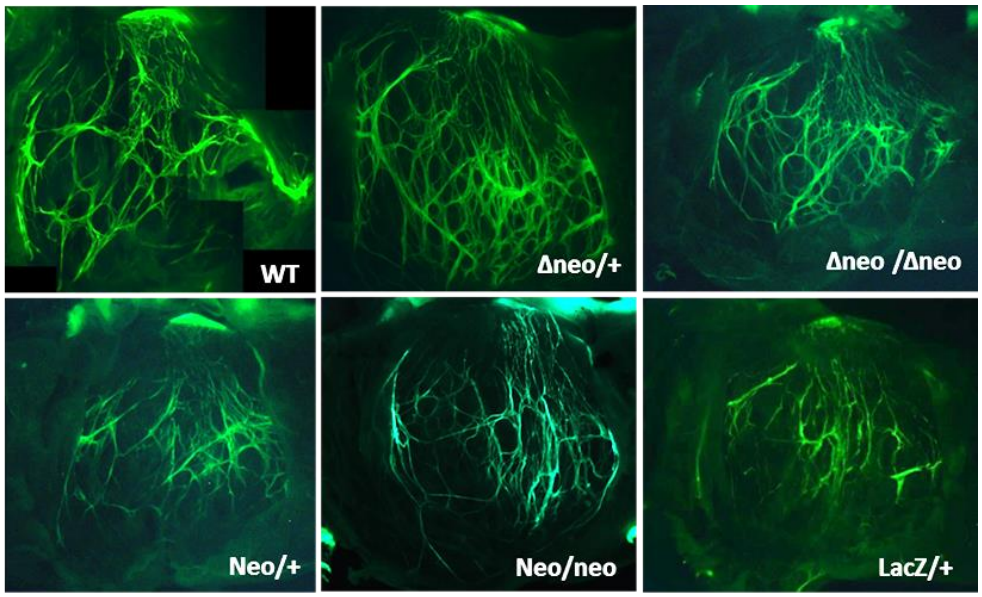
WT
Δneo/+
Δneo /Δneo
Neo/+
Neo/neo
LacZ/+

B

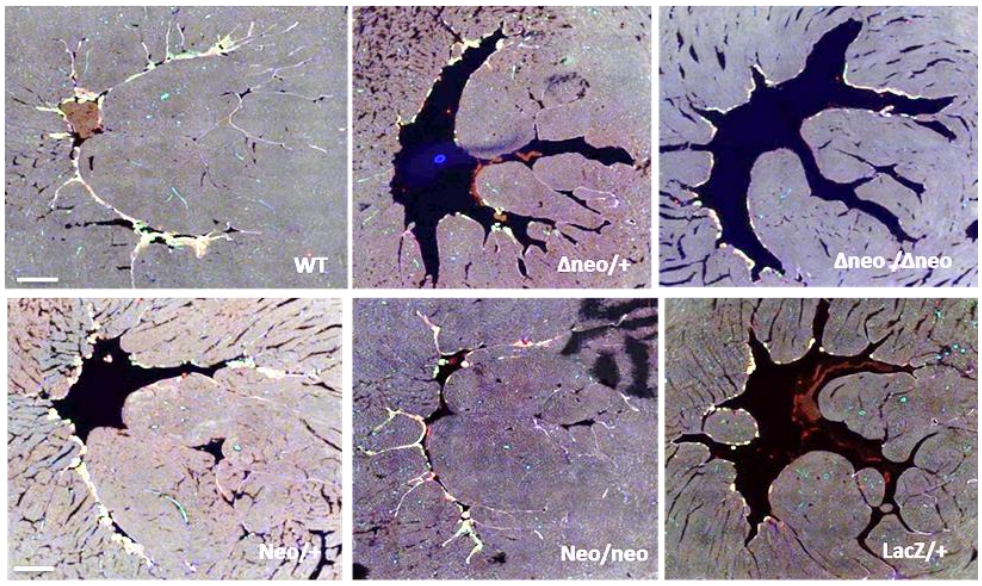
WT
Δneo/+
Δneo /Δneo
Neo/+
Neo/neo
LacZ/+

C

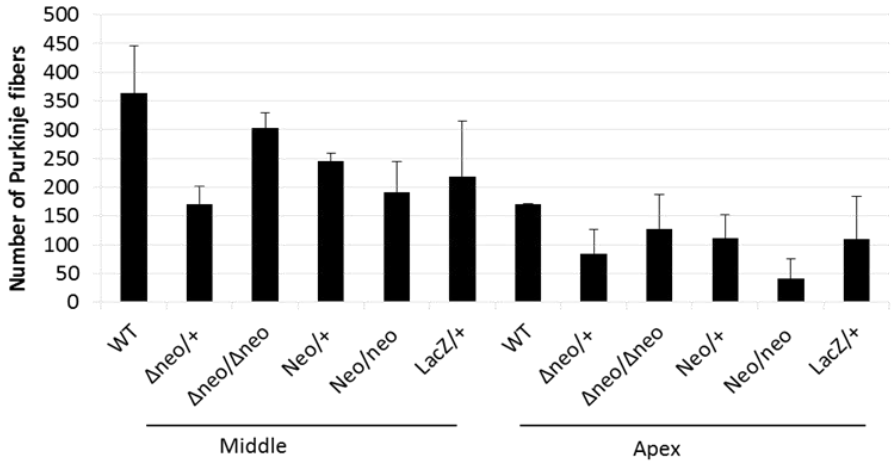
Number of Purkinje fibers
500
450
400
350
300
250
200
150
100
50
0
WT
Δneo/+
Δneo/Δneo
Neo/+
Neo/neo
LacZ/+
WT
Δneo/+
Δneo/Δneo
Neo/+
Neo/neo
LacZ/+
Middle
Apex

Figure 3. Ventricular conduction system defects in low *Nkx2.5* expression level hearts

(A) The Purkinje fiber network observed in fluorescence induced by *Cx40-GFP* reporter gene under the Lumar microscope in all groups of *Nkx2.5* dosage mice. (B) Immunofluorescence with endoglin (white), Contactin 2 (red) and SMA (green) antibodies to delineate Purkinje fibers on transverse sections, which are stained by both Contactin and SMA antibodies at high magnification from mid-ventricle and apex of all groups of *Nkx2.5* dosage mice. (C) Quantification of ventricular conduction system defects by counting the number of Purkinje cells per sections. These measurements were performed for 3 sections at apex and mid-ventricle in each mouse (N=2) at 2-month old. Data are presented as mean ± SD.

Cardiac functional defects in *Nkx2.5* dosage mice

To study the cardiac function of *Nkx2.5* dosage mice, we performed electrocardiography (ECG) to figure out initiation and propagation of the electrical activity through the conduction system. Firstly, no abnormal morphology of ECG pattern was observed (Figure 4). However, mice with low expression of *Nkx2.5* ($Nkx2.5^{lacZ/+}$) present a faster heart rhythm of 578 bpm *versus* 471 bpm in control mice, and shortened PR and QT intervals as shown in the Table 1. PR intervals were unexpectedly prolonged in $Nkx2.5^{\Delta Neo/\Delta Neo}$ mice even this group of mice have a normal expression of *Nkx2.5* gene. The QRS intervals were similar among *Nkx2.5* dosage mice, except in $Nkx2.5^{\Delta Neo/\Delta Neo}$ and $Nkx2.5^{lacZ/+}$, which were higher and lower, respectively. It is difficult to explain why we have defects in ECG in the $Nkx2.5^{\Delta Neo/\Delta Neo}$ mice because its anatomical phenotype of trabeculation and the level of *Nkx2.5* expression are almost normal as in $Nkx2.5^{WT}$. Additionally, the shortened PR and QRS intervals in $Nkx2.5^{lacZ/+}$ mice are opposite with the previous study (Jay *et al*., 2004). Jay and co-workers hypothezised that hypocellular Purkinje network could cause prolongation of the QRS interval because Purkinje cells must depolarize a larger region of working myocardium; however, in our ECG results, shortened QRS interval was observed in the same group of mice with hypoplasia of the VCS ($Nkx2.5^{lacZ/+}$ mice). This explanation of the link between hypocellular Purkinje cells and prolongation of the QRS interval can also not be applied to integrate results of $Nkx2.5^{\Delta Neo/\Delta Neo}$ mice. The other groups of *Nkx2.5* dosage mice did not present any defect in cardiac conduction intervals. In summary, we observed

unexplainable ECG with prolonged PR and QRS intervals in mice with normal trabeculation and level of *Nkx2.5* expression, *Nkx2.5*$^{\Delta Neo/\Delta Neo}$. A shortening of PR and QT intervals in *Nkx2.5*$^{lacZ/+}$ mice which presented a slight increase of trabeculations and a strong hypoplasia of the VCS were observed.

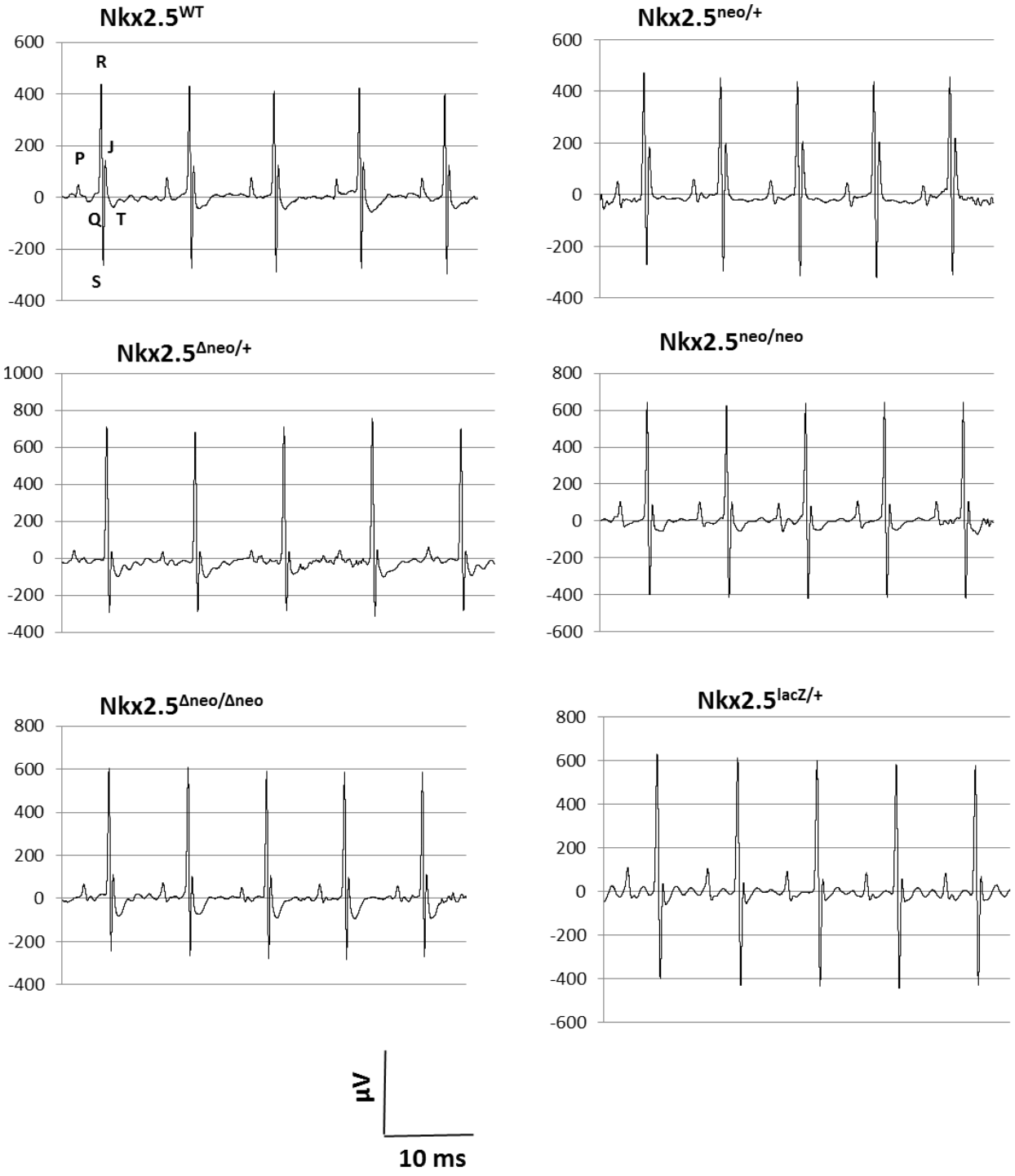

Figure 4. ECG pattern in *Nkx2.5* dosage mice

ECG pattern of 4 cycles for each representative groups of *Nkx2.5* dosage mice. Horizontal axis presents time (ms), and vertical axis presents voltage (μV). ECG were recorded in 2-month old mice.

Table 1. Cardiac conduction intervals in *Nkx2.5* dosage mice.

	Number of mice	HR(bpm)	PR(ms)	QRS(ms)	QT(ms)
$Nkx2.5^{WT}$	9	471 ± 16	32.4 ± 1.5	16.4 ± 0.6	38.4 ± 0.8
$Nkx2.5^{\Delta Neo/+}$	15	498 ± 8	33.7 ± 1.2	16.1 ± 0.5	35 ± 1
$Nkx2.5^{\Delta Neo/\Delta Neo}$	10	467 ± 13	35.9 ± 0.6	22.2 ± 1.1	40 ± 0.5
$Nkx2.5^{Neo/+}$	11	509 ± 12	32.5 ± 0.8	16.9 ± 0.6	39.6 ± 1
$Nkx2.5^{Neo/Neo}$	11	505 ±14	32.2 ± 0.9	17.4 ± 0.7	37.2 ± 0.8
$Nkx2.5^{lacZ/+}$	9	578 ± 13	29 ± 0.8	15.7 ± 0.9	32.8 ± 1.8

ECG intervals were obtained in mice at 2 month-old. Data are presented as mean ± SEM. HR, heart rate; bpm, beats per minute.

Conclusion

This study reveals that *Nkx2.5* gene dosages result in a slight effect on trabeculation in mice with a low expression level of *Nkx2.5* gene, and no hypertrabeculation was observed. Besides, low expression of *Nkx2.5* results in hypoplasia of the ventricular conduction system. However, functional study by ECG showed unexplainable defects in mice with both normal and low *Nkx2.5* expression. Nevertheless, our study shows that a full expression of *Nkx2.5* (100%) is required for the normal phenotypic characteristics of trabeculation and ventricular conduction system.

PART IV. CONCLUSION, DISCUSSION AND PERSPECTIVES

1. Conclusion

This thesis project starts with the generation of novel *Nkx2.5* conditional knockout mice by applying the Flox/loxP system with tamoxifen injection to activate Cre recombination in order to delete *Nkx2.5* allele in atria and trabecular derived cardiomyocytes at embryonic stages when trabeculae arise (at around E10), or start to compact (at around E14), or at neonatal stages (after birth) when the heart has almost finished to compact.

The quantification by qPCR confirms that we were successful in generating three mutant mouse models with differences not only in the level of *Nkx2.5* expression but also in the spatial distribution of this gene in ventricular trabeculae or in the ventricular conduction system. The lowest expression levels of *Nkx2.5* was observed in mice with *Nkx2.5* deletion in the ventricular trabeculae at embryonic stage (*Nkx2.5*$^{\Delta trab}$) or fetal stage (*Nkx2.5*$^{\Delta comp}$), while mice with *Nkx2.5* deletion in the ventricular conduction system at neonatal stage (*Nkx2.5*^{VCS}) showed only a slight reduction of the expression of this gene in comparison to control. Furthermore, quantification of the degree of hypertrabeculation in the left ventricle observed by immunofluorescence experiments indicates that *Nkx2.5* deletion in the ventricular trabeculae at the embryonic stage (*Nkx2.5*$^{\Delta trab}$) presents the most severe phenotype, same remark for disturbances in endocardium fate, as well as a robust existence of fibrosis. The deletion at neonatal stage (*Nkx2.5*$^{\Delta VCS}$) shows the least severe phenotype, meanwhile *Nkx2.5*$^{\Delta comp}$ presents an intermediate phenotype compared to control. In addition, MRI results confirm the presence of numerous trabeculations in mice with *Nkx2.5* deletion at early embryonic stage (*Nkx2.5*$^{\Delta trab}$). Although there is no evolution of trabecular phenotype over time, we observed a progression in the decrease of the ejection fraction, which is a measurement of how much blood the left ventricle pumps out with each contraction, and is an indicator of heart failure. The lower ejection fraction is observed in *Nkx2.5*$^{\Delta trab}$ mice and could be explained by hypertrabeculation level, presence of fibrosis, and defects in the formation of the conduction system or Purkinje fiber network. ECG results also show defects in the cardiac function by elongated PR and QRS intervals in *Nkx2.5*$^{\Delta trab}$ and *Nkx2.5*$^{\Delta comp}$ mice. *Nkx2.5*$^{\Delta trab}$ mice have the longest PR and QRS, whereas *Nkx2.5*$^{\Delta comp}$ mice have longer PR and QRS than control, but less prolonged than in *Nkx2.5*$^{\Delta trab}$ mice. In contrast, *Nkx2.5*$^{\Delta VCS}$ mice present normal PR as control mice from 2 to 12 months. QRS interval in *Nkx2.5*$^{\Delta trab}$ and *Nkx2.5*$^{\Delta comp}$ mice was prolonged compared to control mice with a slow progressive increase.

Nkx2.5$^{\Delta VCS}$ mice present a shortened QRS at 2 and 4 months, but progressive increase to have a normal QRS at 6, 8, and 10 months, and higher QRS at 12 months compared to control mice.

To study molecular pathways involved in the apparition of the pathological phenotypes in LVNC mouse models, we performed microarray experiments in 3 adult groups of 6 month-old, including control mice without tamoxifen injection, mice deleted at embryonic stage (*Nkx2.5*$^{\Delta trab}$), and mice deleted at fetal stage (*Nkx2.5*$^{\Delta comp}$). The results show a clear difference in gene expression profiles between mutants *versus* control. From the heatmap, we divided the gene profiling into four clusters. The cluster 1 presents the profile of genes that are up-regulated in control and down-regulated in both mutants. GO term annotations indicated that the most significant pathways are in cation or ion binding, ion transport, and transporter activity. The cluster 2, the gene profile of down-regulated genes in control and Nkx2.5$^{\Delta trab}$ mice but up-regulated in *Nkx2.5*$^{\Delta comp}$, presents pathways in intracellular signaling cascade and carbohydrate transport. The cluster 3 includes the genes which are down-regulated in control and *Nkx2.5*$^{\Delta comp}$, but up-regulated in *Nkx2.5*$^{\Delta trab}$. However, there is no significant GO term for this cluster. The last one, cluster 4, is the genetic profile of down-regulated genes in control, and up-regulated in *Nkx2.5*$^{\Delta trab}$, and intermediated in *Nkx2.5*$^{\Delta comp}$. This cluster implicated several pathways involved in inflammation or immune response, extracellular matrix, heart development, and vasculature development. Furthermore, Venn diagram showed 313 significant genes differently expressed between *Nkx2.5*$^{\Delta trab}$ *versus* control, 243 genes significantly different between *Nkx2.5*$^{\Delta comp}$ and control, and 45 significantly different genes between both mutants. This transcriptomic study gives us an overview of molecular pathways which are deregulated in each group of *Nkx2.5* mutant mice. It also helps to unravel the molecular mechanisms associated with LVNC in *Nkx2.5* knockout mice and gives helpful explanation for the variable phenotypes observed in these mutant mice.

We also studied 6 groups of *Nkx2.5* gene dosages in relation with the development of trabeculation and conduction system. *Nkx2.5* gene expression varies in these mice from approximately 60% to 130% due to the presence or not of a *Neo* cassette and *loxP* sites in the *Nkx2.5* allele. Quantification by immunofluorescence experiments of the endocardium length and number of free trabeculae indicated that there is no hypertrabeculation in all the groups so that the low expression of *Nkx2.5* by itself does not cause the hypertrabeculation observed in LVNC pathology. However, a low expression of *Nkx2.5* results in hypocellular Purkinje

network, or hypoplasia, in Nkx2.5$^{neo/neo}$ and Nkx2.5$^{lacZ/+}$ mice. Thus, we conclude that *Nkx2.5* gene is required for normal phenotypical characteristics of the ventricular conduction system.

Overall, our study showed that *Nkx2.5* deletion in the ventricular trabeculae and ventricular conduction system at critical steps during trabecular development are suitable mouse models for studying the etiology of LVNC pathology. Besides, we have indicated that the severity of LVNC phenotypes observed in our mouse models depends on the timing when the trabecular disturbances are occuring in embryonic hearts. Additionally, our results show that the group of *Nkx2.5* deleted mice at embryonic stage, when the transition between the trabeculation and compaction step is disturbed, presented the most severe LVNC phenotype of hypertrabeculation and presence of fibrosis. This suggests that LVNC could result from trabecular disturbances in the compaction steps when trabeculations are not completely compacted to form a thick compact layer as in the normal developmental process. Thus, our study provides new insights into the global understanding of LVNC disease.

2. Discussion and perspectives

2.1. Comparison of LVNC phenotypes observed in human patients and in our mouse models

In comparison to LVNC patients, we observed many indications of phenotypical characteristics of LVNC disease in our *Nkx2.5* deleted mice. The anatomic diagnosis of LVNC is based on three criterias, including the presence of prominent trabeculations, multiple deep recesses in the LV, and two-layered appearance of the myocardium: a thick noncompacted and a thin compacted layer (Chin *et al.*, 1990; Ichida, 2009; Jenni *et al*., 2001, 2007; Kohli *et al.*, 2008). In our *Nkx2.5* knockout mouse models, phenotypical characteristics are also the presence of numerous LV trabeculations and deep recesses communicating with the ventricular cavity, so 2 of the 3 diagnostic criterias of LVNC have been found. However, the presence of prominent left ventricular trabeculations is not a strict criteria of LVNC as it can be found also in healthy hearts or in association with other heart diseases, for instance, hypertrophic cardiomyopathy, left ventricular hypertrophy secondary to dilated, valvar or hypertensive cardiomyopathy (Jenni *et al.*, 2001). Additionally, the presence of fibrosis in our mutants is also a common observation in LVNC patients (Burke *et al*., 2005; Hamamichi *et al.*, 2001; Jenni *et al*., 2001; Ker *et al*., 2011; Nucifora *et al.*, 2011). Thus, our *Nkx2.5*-deleted mice share many characteristics with the LVNC patients.

Despite the fact that *Nkx2.5* mutant mice are suitable models for studying LVNC pathology, those mice did not present two-layered myocardium with the ratio of noncompacted/compacted > 2.0 in adult. The presence of two-layered myocardium is the third diagnostic criteria of LVNC in patients. There are two possibilities to explain why our mutant mice did not present the two-layered myocardium like in human. The first point is that the distinction of two-layered myocardium is very difficult to observe in a mouse heart due to its very small size compared to the human heart and also to the low resolution of the imaging techniques used in our study. However, by using immunofluorescence, we were able to quantify hypertrabeculation and show a more important trabecular layer in our mutants. The second point to explain for the absence of a thick noncompacted and a thin compacted layer in the mouse model may come from differences between species. Besides, a severe symptom associated with LVNC, arrhythmia, was not observed in our experimental conditions. We recorded ECG during few minutes and under anesthesia with Isoflurane. It is possible that these resting conditions prevent arrhythmia. One way to answer this question will be to perform a cardiac stress test, using adapted drugs, to increase the cardiac activity. Another possibility will be the telemetric ECGs recording that permits to record ECGs during the normal activity of the mouse during all the day.

All together, even if our LVNC mouse models do not fully phenocopy diagnostic criterias as described in human, they are still representing good models for studying the etiology and molecular pathways of LVNC disease. And the global understanding of LVNC pathology is needed in order to minimize the overestimated or underestimated diagnosis of this disease.

2.2. A link between the three factors: *Nkx2.5* gene, trabecular development and the ventricular conduction system in LVNC disease

Ventricular trabeculae or myocardial projections appear normally in embryonic heart when the vascular circulation system is not yet formed. At fetal stages trabeculae start to compact and this step will finish after birth. Besides, trabecular development is directly linked to the development of the ventricular conduction system (VCS) because trabeculae contain progenitor cells which give rise to the formation of papillary muscles and VCS including Purkinje fibers. Thus, defects in trabecular development may lead to disturbances in the VCS functions and cause LVNC disease.

The transcription factor *Nkx2.5* plays a pivotal role in maintaining the normal function of the cardiac conduction system. *Nkx2.5* mutations have also been found in patients with left ventricular non-compaction (LVNC) (Ashraf *et al.*, 2014; Costa *et al.*, 2013). We showed in the results part 1 that *Nkx2.5* deletion in the ventricular trabeculae results in hypertrabeculation, VCS defects by hypoplasia of the Purkinje network, cardiac conduction defects observed in ECG and MRI results. These phenotypes are presented in LVNC pathology. We also showed in the results part 2 that a reduced expression of *Nkx2.5* does not link to hypertrabeculation. This indicates that deletion of *Nkx2.5* at some critical steps and in specific tissues during trabeculae development, but not a global expression reduction of this gene, results in the hypertrabeculation observed in LVNC. However, both cases of *Nkx2.5* deletion and expression reduction of *Nkx2.5* gene are causing hypoplasia of the VCS. Both results in the part 1 and part 2 suggest the important role of *Nkx2.5* gene in both trabecular and VCS development and functions. *Nkx2.5* knockout mice (the results part 1) presented hypertrabeculation observed in LVNC disease, but expression reduction of *Nkx2.5* in *Nkx2.5* dosage mice (the results part 2) did not result in hypertrabeculation. It means that *Nkx2.5* is critical for trabecular development and absence of this transcription factor (approximately 0% expression) in the trabeculae zone and VCS causes hypertrabeculation and conduction defects. However, a reduction of the expression level of this gene (approximately 40%) in $Nkx2.5^{lacZ/+}$, which is the lowest level in the *Nkx2.5* dosage mice (results part 2), is not sufficient to provoke hypertrabeculation, but suficient to observe a hypoplasia of the VCS. These data suggest that the formation of the mouse VCS is very sensitive to *Nkx2.5* gene dosages while the level of *Nkx2.5* in cardiomyocytes should be lower than 50% to induce hypertrabeculation.

Overall, our study has demonstrated that *Nkx2.5* deletion in the ventricular trabeculae leads to ventricular conduction system defects and presents similar phenotypic characteristics of LVNC pathology. We have also demonstrated that the severity of LVNC phenotypes in our mutants is dependent on the stages when the trabeculae development processes are disturbed. The most severe phenotypes were observed when trabeculae development was disturbed at early embryonic stages. Thus, it could help to understand the origin and heterogeneity observed in the LVNC disease. Our results in the part 2 show that *Nkx2.5* gene dosages in mice with low expression of *Nkx2.5* results in hypoplasia of the VCS but did not cause the hypertrabeculation like in LVNC disease. Thus, disturbances in the ventricular conduction

system as seen by a hypoplasia of the Purkinje network are not always associated with the left ventricular hypertrabeculation.

2.3. Molecular pathways related to phenotypical characteristics observed in LVNC mouse models.

The analysis resulting from microarray experiments give us ideas on the global view of molecular pathways associated with noncompacted cardiomyopathy. From these results, we find out interesting genes specific for each mouse model, that could explain the phenotypical characteristics and cardiac conduction defects observed in the mutant mice. Several interesting points from the transcriptomic analysis are discussed below.

Firstly, the deletion of *Nkx2.5* at embryonic and fetal stages results in the disturbances of normal cardiac development processes, including heart development, vasculature development, tube development, muscle organ development, and blood vessel development as shown in the results part 1. Because *Nkx2.5* is a master gene, which plays a pivotal role in heart development, its deletion at embryonic or fetal stages leads to the disturbances of numerous cardiac development pathways resulting in cardiac malformation and cardiomyopathies. Furthermore, the transcriptomic analysis shows numerous misregulated genes implicating in vasculature and blood vessel development in *Nkx2.5*–deleted mice. Even if there is no significant difference in the density or number of coronary arteries between mutant and control mice, an endocardial phenotype was observed with invaginations of endocardial cells forming endocardial islets where coronary are supposed to form (Figure 3, results part 1).

Secondly, the transcriptomic study reveals disturbances in several extracellular pathways, including extracellular structure organization, extracellular region, and extracellular matrix. The misregulated genes implicated in these pathways could explain the fibrosis phenotype observed in the *Nkx2.5* mutant hearts. The extracellular pathways were found in the cluster 4 of the heatmap (results part 1, figure 7), corresponding to the genes with low expression in control mice and high expression in mice deleted at embryonic stage ($Nkx2.5^{\Delta trab}$) and overexpression but at an intermediate level in $Nkx2.5^{\Delta comp}$ mice. This difference in gene expression profile is in perfect correlation with the level of fibrosis observed in both mutants, which is more severe in mice deleted at early embryonic stage ($Nkx2.5^{\Delta trab}$).

Thirdly, the disturbance in calcium ion binding pathway was found significant in both mutant groups deleted at embryonic and fetal stages. The misregulated genes in this pathway could explain cardiac electrical activity defects observed in ECG and defects in contraction observed in MRI results. Calcium can act in signal transduction resulting from activation of ions channels so that misregulated genes in this pathway could cause defects in cardiac excitation-contraction coupling or heartbeats. Thus, genes implicated in calcium ion and ion channel pathways are important to consider for further studies to explain cardiac functional defects observed in patients.

Fourthly, pathways related to the immune system, including immune response, inflammatory response, response to wounding, and cytokine activity are disturbed in our *Nkx2.5* knockout mice. This result is really interesting because there are only few publications showing inflammatory processes associated with LVNC disease (Jenni et al., 2001). Thus, disturbance of immunity in LVNC hearts could be a very good perspective for future analyses.

Finally, there are few genes known as major misregulated genes in *Nkx2.5*-deficient hearts that were found differentially expressed in our transcriptomic analysis, including *Bmp10*, *Myh7, Nkx2.5* and *Ryr2*. These genes were reviewed in table 4 of the introduction part. Other genes, including known mutations implicated in trabecular morphology (as shown in the table 1), genes associated with LVNC (as in the table 2) or found in *Nkx2.5*-deficient hearts (table 4), and a subset of downstream target genes for *Nkx2.5* (table 5) were also found misregulated in our microarray results but not statistically significant by the statistic methods we have used to screen the significant genes. This could be explained by the strict filtering of 100%, meaning that overexpression of genes in comparison to background is observed in all individuals of each group. After filtering, statistic steps were applied to sort only statistically significant genes using SAM and FDR 5% or p-value ≤ 0.001. However, we did also qPCR for quantification of few genes shown in the table 1, 2 and 4, including *Bmp10*, *Myh7*, *Ryr2*, sarcolipin (*Sln*), *Hcn1*, *Serca2a* (*Atp2a2*), *Scn5a*, *Tnnt2*, *Hcn4*, *HOP*, *ANF* (*Nppa*), *BNP* (*Nppb*), *Irx4*, *MLCK* (*Mylk3*), mink (*Kcne1*), *Cx40*, *Notch1*, and *Dtna*. The results show that those genes are also misregulated in our mutants (data not shown). Thus, for the perspective, we will do other analysis of the microarray experiment using a 75% of filtering and statistic steps by SAM and 5% of FDR, or calculate fold change with p-value ≤ 0.01.

In summary, a schematic diagram is given to summarise several major genes, which are misregulated in our *Nkx2.5* mutant mice tested by qPCR (data not show) (Figure 12). These genes were also reviewed in several publications (Briggs *et al.*, 2008; High and Epstein, 2008; Luxán *et al.*, 2013; Pashmforoush i., 2004; Takeda *et al.*, 2009; Terada *et al.*, 2011; Zhang *et al.*, 2013), and our results confirm their potential role in cardiac malformation and LVNC disease.

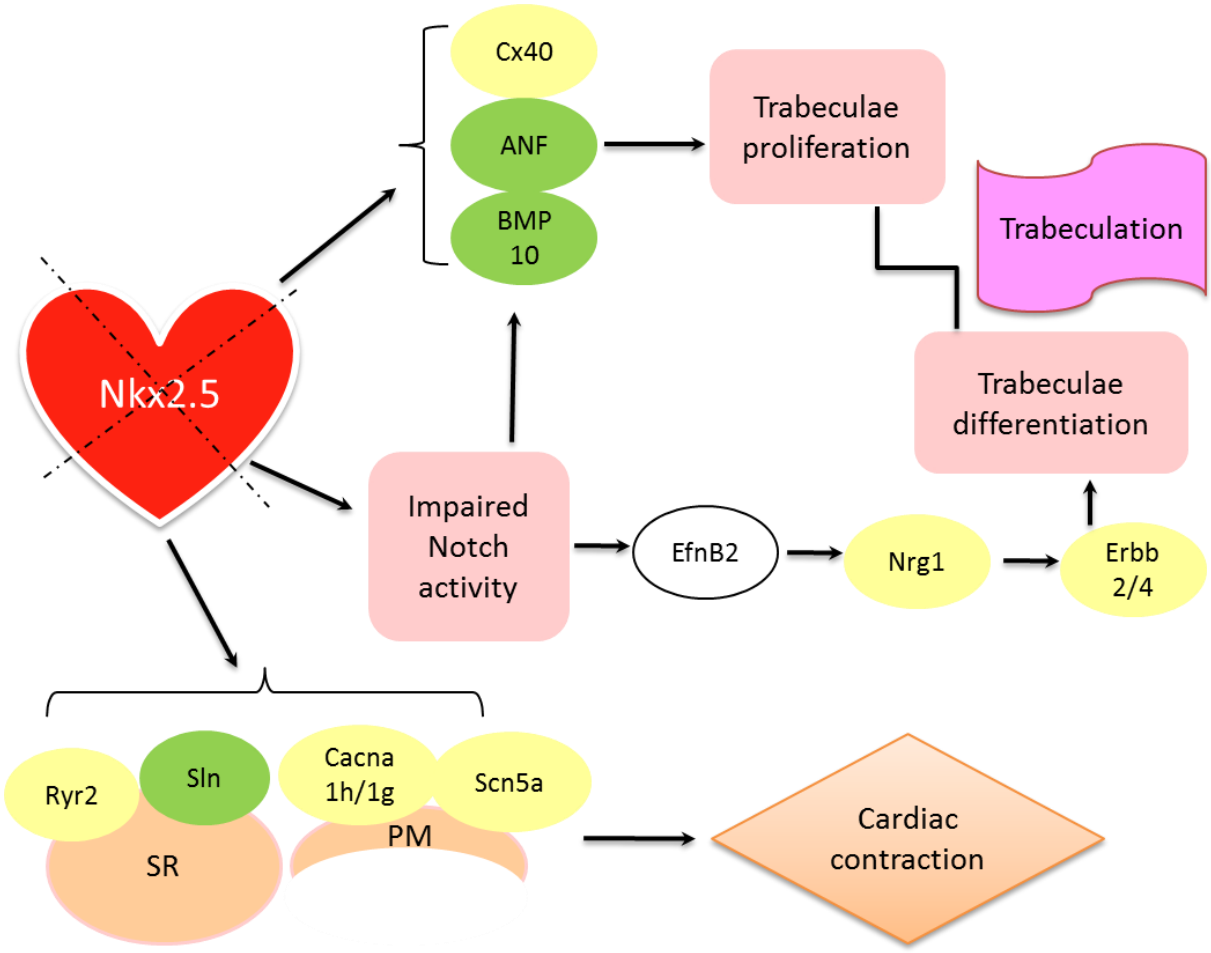

Figure 12. Schematic diagram of misregulated genes and the consequences in *Nkx2.5* deletion mice.

The deletion of Nkx2.5 gene causes misregulation of several genes, including Cx40, ANF, and BMP10 resulting in defects in trabeculae proliferation. Somehow the deletion of Nkx2.5 impairs Notch activity and leads to the misregulation of several genes regulated by the Notch signaling pathway. This causes disturbances in trabeculae differentiation and proliferation. These genes play an important role to control the trabeculae development process, so that the misregulation of these genes disturbs the trabeculation-compaction transition step and maintains trabeculation. Nkx2.5 deletion also causes misregulation in genes implicated in calcium handling and ion channels in the Sarcoplasmic Reticulum (SR) and Plasma Membrane (PM), thus resulting in cardiac contraction defects. Misregulated genes in green are up-regulated, and in yellow are down-regulated. EfnB2, Ephrin B2; Erbbr/4, Erb-B2/4 Receptor Tyrosine Kinase 2/4.

Sources: (High and Epstein, 2008; Luxán et al., 2013; Pashmforoush et al., 2004)

BIBLIOGRAPHY

Aanhaanen, W.T.J., Mommersteeg, M.T.M., Norden, J., Wakker, V., Vries, C. de G., Anderson, R.H., Kispert, A., Moorman, A.F.M., and Christoffels, V.M. (2010). Developmental Origin, Growth, and Three-Dimensional Architecture of the Atrioventricular Conduction Axis of the Mouse Heart. Circ. Res. *107*, 728–736.

Akazawa, H., and Komuro, I. (2005). Cardiac transcription factor Csx/Nkx2-5: Its role in cardiac development and diseases. Pharmacol. Ther. *107*, 252–268.

Arbustini, E., Narula, N., Tavazzi, L., Serio, A., Grasso, M., Favalli, V., Bellazzi, R., Tajik, J.A., Bonow, R.O., Fuster, V., et al. (2014a). The MOGE(S) Classification of Cardiomyopathy for Clinicians. J. Am. Coll. Cardiol. *64*, 304–318.

Arbustini, E., Weidemann, F., and Hall, J.L. (2014b). Left Ventricular Noncompaction. J. Am. Coll. Cardiol. *64*, 1840–1850.

Ashraf, H., Pradhan, L., Chang, E.I., Terada, R., Ryan, N.J., Briggs, L.E., Chowdhury, R., Zárate, M.A., Sugi, Y., Nam, H.-J., et al. (2014). A Mouse Model of Human Congenital Heart Disease High Incidence of Diverse Cardiac Anomalies and Ventricular Noncompaction Produced by Heterozygous Nkx2-5 Homeodomain Missense Mutation. Circ. Cardiovasc. Genet. *7*, 423–433.

Bakker, M.L., Moorman, A.F., and Christoffels, V.M. (2010). The atrioventricular node: origin, development, and genetic program. Trends Cardiovasc. Med. *20*, 164–171.

Bartlett, H., Veenstra, G.J.C., and Weeks, D.L. (2010). Examining the Cardiac NK-2 Genes in Early Heart Development. Pediatr. Cardiol. *31*, 335–341.

Benson, D.W., Silberbach, G.M., Kavanaugh-McHugh, A., Cottrill, C., Zhang, Y., Riggs, S., Smalls, O., Johnson, M.C., Watson, M.S., Seidman, J.G., et al. (1999). Mutations in the cardiac transcription factor NKX2.5 affect diverse cardiac developmental pathways. J. Clin. Invest. *104*, 1567–1573.

Beyer, S., Kelly, R.G., and Miquerol, L. (2011). Inducible Cx40-Cre expression in the cardiac conduction system and arterial endothelial cells. Genesis *49*, 83–91.

Biben, C., and Harvey, R.P. (1997). Homeodomain factor Nkx2-5 controls left/right asymmetric expression of bHLH gene eHand during murine heart development. Genes Dev. *11*, 1357–1369.

Bleyl, S.B., Mumford, B.R., Brown-Harrison, M.-C., Pagotto, L.T., Carey, J.C., Pysher, T.J., Ward, K., and Chin, T.K. (1997). Xq28-linked noncompaction of the left ventricular myocardium: Prenatal diagnosis and pathologic analysis of affected individuals. Am. J. Med. Genet. *72*, 257–265.

von Both, I., Silvestri, C., Erdemir, T., Lickert, H., Walls, J.R., Henkelman, R.M., Rossant, J., Harvey, R.P., Attisano, L., and Wrana, J.L. (2004). Foxh1 Is Essential for Development of the Anterior Heart Field. Dev. Cell *7*, 331–345.

Boukens, B.J., Rivaud, M.R., Rentschler, S., and Coronel, R. (2014). Misinterpretation of the mouse ECG: "musing the waves of Mus musculus." J. Physiol. *592*, 4613–4626.

Briggs, L.E., Takeda, M., Cuadra, A.E., Wakimoto, H., Marks, M.H., Walker, A.J., Seki, T., Oh, S.P., Lu, J.T., Sumners, C., et al. (2008). Perinatal Loss of Nkx2-5 Results in Rapid Conduction and Contraction Defects. Circ. Res. *103*, 580–590.

Bruneau, B.G. (2008). The developmental genetics of congenital heart disease. Nature *451*, 943–948.

Bruneau, B.G., Bao, Z.-Z., Tanaka, M., Schott, J.-J., Izumo, S., Cepko, C.L., Seidman, J.G., and Seidman, C.E. (2000). Cardiac Expression of the Ventricle-Specific Homeobox Gene Irx4 Is Modulated by Nkx2-5 and dHand. Dev. Biol. *217*, 266–277.

Bruneau, B.G., Nemer, G., Schmitt, J.P., Charron, F., Robitaille, L., Caron, S., Conner, D.A., Gessler, M., Nemer, M., Seidman, C.E., et al. (2001). A Murine Model of Holt-Oram Syndrome Defines Roles of the T-Box Transcription Factor Tbx5 in Cardiogenesis and Disease. Cell *106*, 709–721.

Burke, A., Mont, E., Kutys, R., and Virmani, R. (2005). Left ventricular noncompaction: a pathological study of 14 cases. Hum. Pathol. *36*, 403–411.

Captur, G., Syrris, P., Obianyo, C., Limongelli, G., and Moon, J.C. (2015). Formation and Malformation of Cardiac Trabeculae: Biological Basis, Clinical Significance, and Special Yield of Magnetic Resonance Imaging in Assessment. Can. J. Cardiol. *31*, 1325–1337.

Catela, C., Kratsios, P., Hede, M., Lang, F., and Rosenthal, N. (2010). Serum and glucocorticoid-inducible kinase 1 (SGK1) is necessary for vascular remodeling during angiogenesis. Dev. Dyn. *239*, 2149–2160.

Chen, C.Y., and Schwartz, R.J. (1996). Recruitment of the tinman homolog Nkx-2.5 by serum response factor activates cardiac alpha-actin gene transcription. Mol. Cell. Biol. *16*, 6372–6384.

Chen, F., Kook, H., Milewski, R., Gitler, A.D., Lu, M.M., Li, J., Nazarian, R., Schnepp, R., Jen, K., Biben, C., et al. (2002). Hop Is an Unusual Homeobox Gene that Modulates Cardiac Development. Cell *110*, 713–723.

Chen, H., Shi, S., Acosta, L., Li, W., Lu, J., Bao, S., Chen, Z., Yang, Z., Schneider, M.D., Chien, K.R., et al. (2004). BMP-10 is essential for maintaining cardiac growth during murine cardiogenesis. Dev. Camb. Engl. *131*, 2219–2231.

Cheng, G., Litchenberg, W.H., Cole, G.J., Mikawa, T., Thompson, R.P., and Gourdie, R.G. (1999). Development of the cardiac conduction system involves recruitment within a multipotent cardiomyogenic lineage. Development *126*, 5041–5049.

Chin, T.K., Perloff, J.K., Williams, R.G., Jue, K., and Mohrmann, R. (1990). Isolated noncompaction of left ventricular myocardium. A study of eight cases. Circulation *82*, 507–513.

Christoffels, V.M., and Moorman, A.F.M. (2009). Development of the Cardiac Conduction System Why Are Some Regions of the Heart More Arrhythmogenic Than Others? Circ. Arrhythm. Electrophysiol. *2*, 195–207.

Chung, I.-M., and Rajakumar, G. (2016). Genetics of Congenital Heart Defects: The NKX2-5 Gene, a Key Player. Genes *7*.

Costa, M.W., Guo, G., Wolstein, O., Vale, M., Castro, M.L., Wang, L., Otway, R., Riek, P., Cochrane, N., Furtado, M., et al. (2013). Functional characterization of a novel mutation in

NKX2-5 associated with congenital heart disease and adult-onset cardiomyopathy. Circ. Cardiovasc. Genet. *6*, 238–247.

Dawson, D.K., McLernon, D.J., Raj, V.J., Maceira, A.M., Prasad, S., Frenneaux, M.P., Pennell, D.J., and Kilner, P.J. (2014). Cardiovascular Magnetic Resonance Determinants of Left Ventricular Noncompaction. Am. J. Cardiol. *114*, 456–462.

Dobrzynski, H., Anderson, R.H., Atkinson, A., Borbas, Z., D'Souza, A., Fraser, J.F., Inada, S., Logantha, S.J.R.J., Monfredi, O., Morris, G.M., et al. (2013). Structure, function and clinical relevance of the cardiac conduction system, including the atrioventricular ring and outflow tract tissues. Pharmacol. Ther. *139*, 260–288.

Doetschman, T., and Azhar, M. (2012). Cardiac-Specific Inducible and Conditional Gene Targeting in Mice. Circ. Res. *110*, 1498–1512.

Durocher, D., Chen, C.Y., Ardati, A., Schwartz, R.J., and Nemer, M. (1996). The atrial natriuretic factor promoter is a downstream target for Nkx-2.5 in the myocardium. Mol. Cell. Biol. *16*, 4648–4655.

Elliott, D.A., Kirk, E.P., Yeoh, T., Chandar, S., McKenzie, F., Taylor, P., Grossfeld, P., Fatkin, D., Jones, O., Hayes, P., et al. (2003). Cardiac homeobox gene NKX2-5 mutations and congenital heart diseaseAssociations with atrial septal defect and hypoplastic left heart syndrome. J. Am. Coll. Cardiol. *41*, 2072–2076.

Elliott, P., Andersson, B., Arbustini, E., Bilinska, Z., Cecchi, F., Charron, P., Dubourg, O., Kühl, U., Maisch, B., McKenna, W.J., et al. (2008). Classification of the cardiomyopathies: a position statement from the european society of cardiology working group on myocardial and pericardial diseases. Eur. Heart J. *29*, 270–276.

Finsterer, J., Stöllberger, C., and Feichtinger, H. (2002). Histological Appearance of Left Ventricular Hypertrabeculation/Noncompaction. Cardiology *98*, 162–164.

Funke-Kaiser, H., Lemmer, J., Langsdorff, C. v, Thomas, A., Kovacevic, S.D., Strasdat, M., Behrouzi, T., Zollmann, F.S., Paul, M., and Orzechowski, H.-D. (2003). Endothelin-converting enzyme-1 is a downstream target of the homeobox transcription factor Nkx2-5. FASEB J.

Furtado, M.B., Nim, H.T., Boyd, S.E., and Rosenthal, N.A. (2016). View from the heart: cardiac fibroblasts in development, scarring and regeneration. Dev. Camb. Engl. *143*, 387–397.

Gassmann, M., Casagranda, F., Orioli, D., Simon, H., Lai, C., Klein, R., and Lemke, G. (1995). Aberrant neural and cardiac development in mice lacking the ErbB4 neuregulin receptor. Nature *378*, 390–394.

Gati, S., Rajani, R., Carr-White, G.S., and Chambers, J.B. (2014). Adult Left Ventricular Noncompaction. JACC Cardiovasc. Imaging *7*, 1266–1275.

Goldmuntz, E., Geiger, E., and Benson, D.W. (2001). NKX2.5 mutations in patients with tetralogy of fallot. Circulation *104*, 2565–2568.

Gourdie, R.G., Mima, T., Thompson, R.P., and Mikawa, T. (1995). Terminal diversification of the myocyte lineage generates Purkinje fibers of the cardiac conduction system. Dev. Camb. Engl. *121*, 1423–1431.

Greener, I.D., Tellez, J.O., Dobrzynski, H., Yamamoto, M., Graham, G.M., Billeter, R., and Boyett, M.R. (2009). Ion Channel Transcript Expression at the Rabbit Atrioventricular Conduction Axis. Circ. Arrhythm. Electrophysiol. *2*, 305–315.

Grego-Bessa, J., Luna-Zurita, L., Monte, G. del, Bolós, V., Melgar, P., Arandilla, A., Garratt, A.N., Zang, H., Mukouyama, Y., Chen, H., et al. (2007). Notch Signaling is Essential for Ventricular Chamber Development. Dev. Cell *12*, 415–429.

Gros, D., Dupays, L., Alcoléa, S., Meysen, S., Miquerol, L., and Théveniau-Ruissy, M. (2004). Genetically modified mice: tools to decode the functions of connexins in the heart-new models for cardiovascular research. Cardiovasc. Res. *62*, 299–308.

Grothoff, M., Pachowsky, M., Hoffmann, J., Posch, M., Klaassen, S., Lehmkuhl, L., and Gutberlet, M. (2012). Value of cardiovascular MR in diagnosing left ventricular non-compaction cardiomyopathy and in discriminating between other cardiomyopathies. Eur. Radiol. *22*, 2699–2709.

Guo, L., Lynch, J., Nakamura, K., Fliegel, L., Kasahara, H., Izumo, S., Komuro, I., Agellon, L.B., and Michalak, M. (2001). COUP-TF1 Antagonizes Nkx2.5-mediated Activation of the Calreticulin Gene during Cardiac Development. J. Biol. Chem. *276*, 2797–2801.

Gutierrez-Roelens, I., Sluysmans, T., Gewillig, M., Devriendt, K., and Vikkula, M. (2002). Progressive AV-block and anomalous venous return among cardiac anomalies associated with two novel missense mutations in the CSX/NKX2-5 Gene. Hum. Mutat. *20*, 75–76.

Hamamichi, Y., Ichida, F., Hashimoto, I., Uese, K.H.K., Miyawaki, T., Tsukano, S., Ono, Y., Echigo, S., and Kamiya, T. (2001). Isolated noncompaction of the ventricular myocardium: Ultrafast computed tomography and magnetic resonance imaging. Int. J. Cardiovasc. Imaging *17*, 305–314.

Hershberger, R.E., and Morales, A. (1993). LMNA-Related Dilated Cardiomyopathy. In GeneReviews(®), R.A. Pagon, M.P. Adam, H.H. Ardinger, S.E. Wallace, A. Amemiya, L.J. Bean, T.D. Bird, C.-T. Fong, H.C. Mefford, R.J. Smith, et al., eds. (Seattle (WA): University of Washington, Seattle), p.

Hertig, C.M., Kubalak, S.W., Wang, Y., and Chien, K.R. (1999). Synergistic Roles of Neuregulin-1 and Insulin-like Growth Factor-I in Activation of the Phosphatidylinositol 3-Kinase Pathway and Cardiac Chamber Morphogenesis. J. Biol. Chem. *274*, 37362–37369.

Hertzberg, E.L. (2000). Gap Junctions (Elsevier).

High, F.A., and Epstein, J.A. (2008). The multifaceted role of Notch in cardiac development and disease. Nat. Rev. Genet. *9*, 49–61.

Hoedemaekers, Y.M., Caliskan, K., Majoor-Krakauer, D., Laar, I. van de, Michels, M., Witsenburg, M., Cate, F.J. ten, Simoons, M.L., and Dooijes, D. (2007). Cardiac β-myosin heavy chain defects in two families with non-compaction cardiomyopathy: linking non-compaction to hypertrophic, restrictive, and dilated cardiomyopathies. Eur. Heart J. *28*, 2732–2737.

Hussein, A., Karimianpour, A., Collier, P., and Krasuski, R.A. (2015). Isolated Noncompaction of the Left Ventricle in Adults. J. Am. Coll. Cardiol. *66*, 578–585.

Ichida, F. (2009). Left ventricular noncompaction. Circ. J. *73*, 19–26.

Ichida, F., Tsubata, S., Bowles, K.R., Haneda, N., Uese, K., Miyawaki, T., Dreyer, W.J., Messina, J., Li, H., Bowles, N.E., et al. (2001). Novel Gene Mutations in Patients With Left Ventricular Noncompaction or Barth Syndrome. Circulation *103*, 1256–1263.

Ikeda, U., Minamisawa, M., and Koyama, J. (2015). Isolated left ventricular non-compaction cardiomyopathy in adults. J. Cardiol. *65*, 91–97.

Ikeda, Y., Hiroi, Y., Hosoda, T., Utsunomiya, T., Matsuo, S., Ito, T., Inoue, J., Sumiyoshi, T., Takano, H., Nagai, R., et al. (2002). Novel Point Mutation in the Cardiac Transcription Factor *CSX/NKX2.5* Associated With Congenital Heart Disease. Circ. J. *66*, 561–563.

James, T.N. (2003). Structure and function of the sinus node, AV node and his bundle of the human heart: part II--function. Prog. Cardiovasc. Dis. *45*, 327–360.

Jay, P.Y., Harris, B.S., Maguire, C.T., Buerger, A., Wakimoto, H., Tanaka, M., Kupershmidt, S., Roden, D.M., Schultheiss, T.M., O'Brien, T.X., et al. (2004). Nkx2-5 mutation causes anatomic hypoplasia of the cardiac conduction system. J. Clin. Invest. *113*, 1130–1137.

Jenni, R., Oechslin, E., Schneider, J., Jost, C., and Kaufmann, P. (2001). Echocardiographic and pathoanatomical characteristics of isolated left ventricular non-compaction: a step towards classification as a distinct cardiomyopathy. Heart *86*, 666–671.

Jenni, R., Oechslin, E.N., and van der Loo, B. (2007). Isolated ventricular non-compaction of the myocardium in adults. Heart *93*, 11–15.

Jongbloed, M.R.M., Vicente Steijn, R., Hahurij, N.D., Kelder, T.P., Schalij, M.J., Gittenberger-de Groot, A.C., and Blom, N.A. (2012). Normal and abnormal development of the cardiac conduction system; implications for conduction and rhythm disorders in the child and adult. Differ. Res. Biol. Divers. *84*, 131–148.

Joung, B., Ogawa, M., Lin, S.-F., and Chen, P.-S. (2009). The Calcium and Voltage Clocks in Sinoatrial Node Automaticity. Korean Circ. J. *39*, 217–222.

Ker, L Du Toit-Prinsloo, WFP Van Heerden, and G Saayman (2011). Subendocardial Fibrosis in Left Ventricular Hypertrabeculation-Cause or Consequence? Clin. Med. Insights Cardiol. 13.

Kim, Y., and Nirenberg, M. (1989). Drosophila NK-homeobox genes. Proc. Natl. Acad. Sci. U. S. A. *86*, 7716–7720.

Klaassen, S., Probst, S., Oechslin, E., Gerull, B., Krings, G., Schuler, P., Greutmann, M., Hürlimann, D., Yegitbasi, M., Pons, L., et al. (2008). Mutations in Sarcomere Protein Genes in Left Ventricular Noncompaction. Circulation *117*, 2893–2901.

Kohli, S.K., Pantazis, A.A., Shah, J.S., Adeyemi, B., Jackson, G., McKenna, W.J., Sharma, S., and Elliott, P.M. (2008). Diagnosis of left-ventricular non-compaction in patients with left-ventricular systolic dysfunction: time for a reappraisal of diagnostic criteria? Eur. Heart J. *29*, 89–95.

Kokubo, H., Miyagawa-Tomita, S., Nakazawa, M., Saga, Y., and Johnson, R.L. (2005). Mouse hesr1 and hesr2 genes are redundantly required to mediate Notch signaling in the developing cardiovascular system. Dev. Biol. *278*, 301–309.

Kreuzberg, M.M., Willecke, K., and Bukauskas, F.F. (2006). Connexin-Mediated Cardiac Impulse Propagation: Connexin 30.2 Slows Atrioventricular Conduction in Mouse Heart. Trends Cardiovasc. Med. *16*, 266–272.

Kurian, T., Ambrosi, C., Hucker, W., Fedorov, V.V., and Efimov, I.R. (2010). ANATOMY AND ELECTROPHYSIOLOGY OF THE HUMAN AV NODE. Pacing Clin. Electrophysiol. PACE *33*, 754–762.

Lakatta, E.G., and DiFrancesco, D. (2009). What keeps us ticking: a funny current, a calcium clock, or both? J. Mol. Cell. Cardiol. *47*, 157–170.

Lee, Y., Shioi, T., Kasahara, H., Jobe, S.M., Wiese, R.J., Markham, B.E., and Izumo, S. (1998). The Cardiac Tissue-Restricted Homeobox Protein Csx/Nkx2.5 Physically Associates with the Zinc Finger Protein GATA4 and Cooperatively Activates Atrial Natriuretic Factor Gene Expression. Mol. Cell. Biol. *18*, 3120–3129.

Liu, G., Iden, J.B., Kovithavongs, K., Gulamhusein, R., Duff, H.J., and Kavanagh, K.M. (2004). In vivo temporal and spatial distribution of depolarization and repolarization and the illusive murine T wave. J. Physiol. *555*, 267–279.

Lofiego, C., Biagini, E., Pasquale, F., Ferlito, M., Rocchi, G., Perugini, E., Bacchi-Reggiani, L., Boriani, G., Leone, O., Caliskan, K., et al. (2007). Wide spectrum of presentation and variable outcomes of isolated left ventricular non-compaction. Heart *93*, 65–71.

Luxán, G., Casanova, J.C., Martínez-Poveda, B., Prados, B., D'Amato, G., MacGrogan, D., Gonzalez-Rajal, A., Dobarro, D., Torroja, C., Martinez, F., et al. (2013). Mutations in the NOTCH pathway regulator MIB1 cause left ventricular noncompaction cardiomyopathy. Nat. Med. *19*, 193–201.

Lyons, I., Parsons, L.M., Hartley, L., Li, R., Andrews, J.E., Robb, L., and Harvey, R.P. (1995). Myogenic and morphogenetic defects in the heart tubes of murine embryos lacking the homeo box gene Nkx2-5. Genes Dev. *9*, 1654–1666.

Marionneau, C., Couette, B., Liu, J., Li, H., Mangoni, M.E., Nargeot, J., Lei, M., Escande, D., and Demolombe, S. (2005). Specific pattern of ionic channel gene expression associated with pacemaker activity in the mouse heart. J. Physiol. *562*, 223–234.

Maron, B.J., Towbin, J.A., Thiene, G., Antzelevitch, C., Corrado, D., Arnett, D., Moss, A.J., Seidman, C.E., and Young, J.B. (2006). Contemporary Definitions and Classification of the Cardiomyopathies An American Heart Association Scientific Statement From the Council on Clinical Cardiology, Heart Failure and Transplantation Committee; Quality of Care and Outcomes Research and Functional Genomics and Translational Biology Interdisciplinary Working Groups; and Council on Epidemiology and Prevention. Circulation *113*, 1807–1816.

McCright, B., Lozier, J., and Gridley, T. (2002). A mouse model of Alagille syndrome: Notch2 as a genetic modifier of Jag1 haploinsufficiency. Development *129*, 1075–1082.

Meysen, S., Marger, L., Hewett, K.W., Jarry-Guichard, T., Agarkova, I., Chauvin, J.P., Perriard, J.C., Izumo, S., Gourdie, R.G., Mangoni, M.E., et al. (2007). Nkx2.5 cell-autonomous gene

function is required for the postnatal formation of the peripheral ventricular conduction system. Dev. Biol. *303*, 740–753.

Milano, A., Vermeer, A.M.C., Lodder, E.M., Barc, J., Verkerk, A.O., Postma, A.V., van der Bilt, I.A.C., Baars, M.J.H., van Haelst, P.L., Caliskan, K., et al. (2014). HCN4 Mutations in Multiple Families With Bradycardia and Left Ventricular Noncompaction Cardiomyopathy. J. Am. Coll. Cardiol. *64*, 745–756.

Miquerol, L., and Kelly, R.G. (2013). Organogenesis of the vertebrate heart. Wiley Interdiscip. Rev. Dev. Biol. *2*, 17–29.

Miquerol, L., Meysen, S., Mangoni, M., Bois, P., Rijen, H.V.M. van, Abran, P., Jongsma, H., Nargeot, J., and Gros, D. (2004). Architectural and functional asymmetry of the His–Purkinje system of the murine heart. Cardiovasc. Res. *63*, 77–86.

Miquerol, L., Moreno-Rascon, N., Beyer, S., Dupays, L., Meilhac, S.M., Buckingham, M.E., Franco, D., and Kelly, R.G. (2010). Biphasic development of the mammalian ventricular conduction system. Circ. Res. *107*, 153–161.

Miquerol, L., Beyer, S., and Kelly, R.G. (2011). Establishment of the mouse ventricular conduction system. Cardiovasc. Res. *91*, 232–242.

Mommersteeg, M.T.M., Hoogaars, W.M.H., Prall, O.W.J., de Gier-de Vries, C., Wiese, C., Clout, D.E.W., Papaioannou, V.E., Brown, N.A., Harvey, R.P., Moorman, A.F.M., et al. (2007). Molecular pathway for the localized formation of the sinoatrial node. Circ. Res. *100*, 354–362.

Monfredi, O., Dobrzynski, H., Mondal, T., Boyett, M.R., and Morris, G.M. (2010). The anatomy and physiology of the sinoatrial node--a contemporary review. Pacing Clin. Electrophysiol. PACE *33*, 1392–1406.

Monserrat, L., Hermida-Prieto, M., Fernandez, X., Rodríguez, I., Dumont, C., Cazón, L., Cuesta, M.G., Gonzalez-Juanatey, C., Peteiro, J., Álvarez, N., et al. (2007). Mutation in the alpha-cardiac actin gene associated with apical hypertrophic cardiomyopathy, left ventricular non-compaction, and septal defects. Eur. Heart J. *28*, 1953–1961.

Moorman, A., Webb, S., Brown, N.A., Lamers, W., and Anderson, R.H. (2003). Development of the heart:(1) formation of the cardiac chambers and arterial trunks. Heart *89*, 806–814.

Müller, J.G., Thompson, J.T., Edmonson, A.M., Rackley, M.S., Kasahara, H., Izumo, S., McQuinn, T.C., Menick, D.R., and O'Brien, T.X. (2002). Differential Regulation of the Cardiac Sodium Calcium Exchanger Promoter in Adult and Neonatal Cardiomyocytes by Nkx2.5 and Serum Response Factor. J. Mol. Cell. Cardiol. *34*, 807–821.

Nakashima, Y., Yanez, D.A., Touma, M., Nakano, H., Jaroszewicz, A., Jordan, M.C., Pellegrini, M., Roos, K.P., and Nakano, A. (2014). Nkx2-5 Suppresses the Proliferation of Atrial Myocytes and Conduction SystemNovelty and Significance. Circ. Res. *114*, 1103–1113.

Nandi, S.S., and Mishra, P.K. (2015). Harnessing fetal and adult genetic reprograming for therapy of heart disease. J. Nat. Sci. *1*, 71.

Nucifora, G., Aquaro, G.D., Pingitore, A., Masci, P.G., and Lombardi, M. (2011). Myocardial fibrosis in isolated left ventricular non-compaction and its relation to disease severity. Eur. J. Heart Fail. *13*, 170–176.

Pashmforoush, M., Lu, J.T., Chen, H., St Amand, T., Kondo, R., Pradervand, S., Evans, S.M., Clark, B., Feramisco, J.R., Giles, W., et al. (2004). Nkx2-5 pathways and congenital heart disease: loss of ventricular myocyte lineage specification leads to progressive cardiomyopathy and complete heart block. Cell *117*, 373–386.

Petersen, S.E., Selvanayagam, J.B., Wiesmann, F., Robson, M.D., Francis, J.M., Anderson, R.H., Watkins, H., and Neubauer, S. (2005). Left Ventricular Non-Compaction. J. Am. Coll. Cardiol. *46*, 101–105.

Postma, A.V., Christoffels, V.M., and Bezzina, C.R. (2011). Developmental aspects of cardiac arrhythmogenesis. Cardiovasc. Res. *91*, 243–251.

Reecy, J.M., Li, X., Yamada, M., DeMayo, F.J., Newman, C.S., Harvey, R.P., and Schwartz, R.J. (1999). Identification of upstream regulatory regions in the heart-expressed homeobox gene Nkx2-5. Development *126*, 839–849.

Risebro, C.A., and Riley, P.R. (2006). Formation of the Ventricles. Sci. World J. *6*, 1862–1880.

Rivkees, S.A., Chen, M., Kulkarni, J., Browne, J., and Zhao, Z. (1999). Characterization of the Murine A1 Adenosine Receptor Promoter, Potent Regulation by GATA-4 and Nkx2.5. J. Biol. Chem. *274*, 14204–14209.

Roberts, W.C., Karia, S.J., Ko, J.M., Grayburn, P.A., George, B.A., Hall, S.A., Kuiper, J.J., and Meyer, D.M. (2011). Examination of Isolated Ventricular Noncompaction (Hypertrabeculation) as a Distinct Entity in Adults. Am. J. Cardiol. *108*, 747–752.

Sasse-Klaassen, S., Gerull, B., Oechslin, E., Jenni, R., and Thierfelder, L. (2003). Isolated noncompaction of the left ventricular myocardium in the adult is an autosomal dominant disorder in the majority of patients. Am. J. Med. Genet. A. *119A*, 162–167.

Schott, J.J., Benson, D.W., Basson, C.T., Pease, W., Silberbach, G.M., Moak, J.P., Maron, B.J., Seidman, C.E., and Seidman, J.G. (1998). Congenital heart disease caused by mutations in the transcription factor NKX2-5. Science *281*, 108–111.

Schram, G., Pourrier, M., Melnyk, P., and Nattel, S. (2002). Differential Distribution of Cardiac Ion Channel Expression as a Basis for Regional Specialization in Electrical Function. Circ. Res. *90*, 939–950.

Sedmera, D., and McQuinn, T. (2008). Embryogenesis of the Heart Muscle. Heart Fail. Clin. *4*, 235–245.

Sedmera, D., Pexieder, T., Hu, N., and Clark, E.B. (1997). Developmental changes in the myocardial architecture of the chick. Anat. Rec. *248*, 421–432.

Sen-Chowdhry, S., and McKenna, W.J. (2008). Left ventricular noncompaction and cardiomyopathy: cause, contributor, or epiphenomenon?: Curr. Opin. Cardiol. *23*, 171–175.

Shan, L., Makita, N., Xing, Y., Watanabe, S., Futatani, T., Ye, F., Saito, K., Ibuki, K., Watanabe, K., Hirono, K., et al. (2008). SCN5A variants in Japanese patients with left ventricular noncompaction and arrhythmia. Mol. Genet. Metab. *93*, 468–474.

Shin, C.H., Liu, Z.-P., Passier, R., Zhang, C.-L., Wang, D.-Z., Harris, T.M., Yamagishi, H., Richardson, J.A., Childs, G., and Olson, E.N. (2002). Modulation of Cardiac Growth and Development by HOP, an Unusual Homeodomain Protein. Cell *110*, 725–735.

Shiojima, I., Komuro, I., Oka, T., Hiroi, Y., Mizuno, T., Takimoto, E., Monzen, K., Aikawa, R., Akazawa, H., Yamazaki, T., et al. (1999). Context-dependent Transcriptional Cooperation Mediated by Cardiac Transcription Factors Csx/Nkx-2.5 and GATA-4. J. Biol. Chem. *274*, 8231–8239.

Shou, W., Aghdasi, B., Armstrong, D.L., Guo, Q., Bao, S., Charng, M.-J., Mathews, L.M., Schneider, M.D., Hamilton, S.L., and Matzuk, M.M. (1998). Cardiac defects and altered ryanodine receptor function in mice lacking FKBP12. Nature *391*, 489–492.

Stöllberger, C., Finsterer, J., and Blazek, G. (2002). Left ventricular hypertrabeculation/noncompaction and association with additional cardiac abnormalities and neuromuscular disorders. Am. J. Cardiol. *90*, 899–902.

Takeda, M., Briggs, L.E., Wakimoto, H., Marks, M.H., Warren, S.A., Lu, J.T., Weinberg, E.O., Robertson, K.D., Chien, K.R., and Kasahara, H. (2009). Slow progressive conduction and contraction defects in loss of Nkx2–5 mice after cardiomyocyte terminal differentiation. Lab. Investig. J. Tech. Methods Pathol. *89*, 983–993.

Tanaka, M., Chen, Z., Bartunkova, S., Yamasaki, N., and Izumo, S. (1999). The cardiac homeobox gene Csx/Nkx2.5 lies genetically upstream of multiple genes essential for heart development. Development *126*, 1269–1280.

Temple, I.P., Inada, S., Dobrzynski, H., and Boyett, M.R. (2013). Connexins and the atrioventricular node. Heart Rhythm *10*, 297–304.

Terada, R., Warren, S., Lu, J.T., Chien, K.R., Wessels, A., and Kasahara, H. (2011). Ablation of Nkx2-5 at mid-embryonic stage results in premature lethality and cardiac malformation. Cardiovasc. Res. *91*, 289–299.

Thuny, F., Jacquier, A., Jop, B., Giorgi, R., Gaubert, J.-Y., Bartoli, J.-M., Moulin, G., and Habib, G. (2010). Assessment of left ventricular non-compaction in adults: Side-by-side comparison of

cardiac magnetic resonance imaging with echocardiography. Arch. Cardiovasc. Dis. *103*, 150–159.

Udeoji, D.U., Philip, K.J., Morrissey, R.P., Phan, A., and Schwarz, E.R. (2013). Left ventricular noncompaction cardiomyopathy: updated review. Ther. Adv. Cardiovasc. Dis. *7*, 260–273.

Ueyama, T., Kasahara, H., Ishiwata, T., Nie, Q., and Izumo, S. (2003a). Myocardin Expression Is Regulated by Nkx2.5, and Its Function Is Required for Cardiomyogenesis. Mol. Cell. Biol. *23*, 9222–9232.

Ueyama, T., Kasahara, H., Ishiwata, T., Yamasaki, N., and Izumo, S. (2003b). Csm, a Cardiac-specific Isoform of the RNA Helicase Mov10l1, Is Regulated by Nkx2.5 in Embryonic Heart. J. Biol. Chem. *278*, 28750–28757.

Vatta, M., Mohapatra, B., Jimenez, S., Sanchez, X., Faulkner, G., Perles, Z., Sinagra, G., Lin, J.-H., Vu, T.M., Zhou, Q., et al. (2003). Mutations in Cypher/ZASP in patients with dilated cardiomyopathy and left ventricular non-compaction. J. Am. Coll. Cardiol. *42*, 2014–2027.

Vincent, S.D., and Buckingham, M.E. (2010). Chapter One - How to Make a Heart: The Origin and Regulation of Cardiac Progenitor Cells. In Current Topics in Developmental Biology, P. Koopman, ed. (Academic Press), pp. 1–41.

Virágh, S., and Challice, C.E. (1980). The development of the conduction system in the mouse embryo heart. Dev. Biol. *80*, 28–45.

Wang, H.U., Chen, Z.-F., and Anderson, D.J. (1998). Molecular Distinction and Angiogenic Interaction between Embryonic Arteries and Veins Revealed by ephrin-B2 and Its Receptor Eph-B4. Cell *93*, 741–753.

Weerd, J.H. van, and Christoffels, V.M. (2016). The formation and function of the cardiac conduction system. Development *143*, 197–210.

Xu, Q., Dewey, S., Nguyen, S., and Gomes, A.V. (2010). Malignant and benign mutations in familial cardiomyopathies: Insights into mutations linked to complex cardiovascular phenotypes. J. Mol. Cell. Cardiol. *48*, 899–909.

Yang, J., Bücker, S., Jungblut, B., Böttger, T., Cinnamon, Y., Tchorz, J., Müller, M., Bettler, B., Harvey, R., Sun, Q.-Y., et al. (2012). Inhibition of Notch2 by Numb/Numblike controls myocardial compaction in the heart. Cardiovasc. Res. *96*, 276–285.

Zhang, W., Chen, H., Qu, X., Chang, C.-P., and Shou, W. (2013). Molecular mechanism of ventricular trabeculation/compaction and the pathogenesis of the left ventricular noncompaction cardiomyopathy (LVNC): AMERICAN JOURNAL OF MEDICAL GENETICS PART C (SEMINARS IN MEDICAL GENETICS). Am. J. Med. Genet. C Semin. Med. Genet. *163*, 144–156.

Zou, Y., Evans, S., Chen, J., Kuo, H.C., Harvey, R.P., and Chien, K.R. (1997). CARP, a cardiac ankyrin repeat protein, is downstream in the Nkx2-5 homeobox gene pathway. Development *124*, 793–804.